VOLUME 32 JANUARY 1954 NUMBER 1

Canadian Journal of Physics

Editor: G. M. VOLKOFF

Associate Editors:

L. G. ELLIOTT, *Atomic Energy of Canada, Ltd., Chalk River*
J. S. FOSTER, *McGill University*
L. LEPRINCE-RINGUET, *Ecole Polytechnique, Paris*
D. W. R. McKINLEY, *National Research Council*
B. W. SARGENT, *Queen's University*
F. E. SIMON, *Clarendon Laboratory, University of Oxford*
W. H. WATSON, *University of Toronto*

Published by THE NATIONAL RESEARCH COUNCIL
OTTAWA CANADA

CANADIAN JOURNAL OF PHYSICS

(Formerly Section A, Canadian Journal of Research)

The CANADIAN JOURNAL OF PHYSICS is published monthly by the National Research Council of Canada under the authority of the Chairman of the Committee of the Privy Council on Scientific and Industrial Research. The National Research Council publishes also: *Canadian Journal of Biochemistry and Physiology, Canadian Journal of Botany, Canadian Journal of Chemistry, Canadian Journal of Technology, Canadian Journal of Zoology.*

Matters of general policy concerning the Council's journals are the responsibility of a joint Editorial Board consisting of: the Editors of the journals; members representing the National Research Council of Canada and the Royal Society of Canada and two other scientific societies; and two ex-officio members.

EDITORIAL BOARD

Editors of the Journals

D. L. Bailey, *University of Toronto*
J. B. Collip, *University of Western Ontario*
E. H. Craigie, *University of Toronto*
G. A. Ledingham, *National Research Council*
Léo Marion, *National Research Council*
G. M. Volkoff, *University of British Columbia*

Representatives of the National Research Council

C. W. Argue (Chairman), *University of New Brunswick*
G. E. Hall, *University of Western Ontario*
T. Thorvaldson, *University of Saskatchewan*
W. H. Watson, *University of Toronto*

Representatives of Societies

D. L. Bailey, *University of Toronto*
Royal Society of Canada
E. H. Craigie, *University of Toronto*
Royal Society of Canada
H. G. Thode, *McMaster University*
Chemical Institute of Canada
T. Thorvaldson, *University of Saskatchewan*
Royal Society of Canada
G. M. Volkoff, *University of British Columbia*
Royal Society of Canada
Canadian Association of Physicists

Ex officio

Léo Marion (Editor-in-Chief)
National Research Council
H. H. Saunderson
National Research Council

Manuscripts should be addressed to:

Dr. Léo Marion,
Editor-in-Chief,
Canadian Journal of Physics,
National Research Council,
Ottawa 2, Canada.

Subscriptions, renewals, and orders for back numbers should be addressed to:

Division of Administration,
National Research Council,
Ottawa 2, Canada.

Subscription rate: $4.00 a year, single numbers: 50 cents. Remittances should be made payable to the Receiver General of Canada, credit National Research Council.

VOLUME 32 1954

Canadian Journal of Physics

Editor: G. M. VOLKOFF

Associate Editors:
L. G. ELLIOTT, *Atomic Energy of Canada, Ltd., Chalk River*
J. S. FOSTER, *McGill University*
L. LEPRINCE-RINGUET, *Ecole Polytechnique, Paris*
D. W. R. McKINLEY, *National Research Council*
B. W. SARGENT, *Queen's University*
F. E. SIMON, *Clarendon Laboratory, University of Oxford*
W. H. WATSON, *University of Toronto*

Published by THE NATIONAL RESEARCH COUNCIL
OTTAWA CANADA

Canadian Journal of Physics

Issued by THE NATIONAL RESEARCH COUNCIL OF CANADA

VOLUME 32 JANUARY 1954 NUMBER 1

CLAUSIUS-MOSOTTI EQUATION FOR CERTAIN TYPES OF ANISOTROPIC CRYSTALS[1]

BY H. E. J. NEUGEBAUER

ABSTRACT

The Clausius-Mosotti equation is derived for crystals whose particles are anisotropic and arranged in any lattice provided that all the particles are of the same type and provided that the principal axes of their tensors of polarizability are parallel to each other. The formulas are of special interest for artificial dielectrics used as lens material for microwave frequencies. They explain experimental results.

The Clausius-Mosotti equation (CME) establishes a relation between the dielectric constant ϵ of a substance, the polarizability α, and the density N of its particles. Derivations for crystals of a cubic lattice and for amorphous substances are well known.

van Santen and Opechowski (6) have derived a generalized equation for crystals containing particles of different types provided their polarizabilities are independent of the direction of the field. Jonker and van Santen (2) showed that this equation was not sufficient to explain the essential properties of barium titanate. Slater (4) completed the CME for this substance taking into account the mobility of the titanium ion.

The present publication gives a different generalization. It is mainly characterized by the assumption that the polarizabilities of the particles depend on the direction of the field so that, except for very special cases, the crystal is anisotropic, i.e. its dielectric constant depends also on the direction of the field. Further assumptions are that all particles are alike, that the principal axes of the tensors of polarizability are oriented parallel to each other, and that the particles are not too closely packed. These assumptions will be specified later.

The new equations can be applied, in the first place, to artificial dielectrics used as lens material for microwave frequencies. Another application can be made to crystals of chemical elements.

In the following sections the term "anisotropic particle" is used when the polarizability of the particle is a tensor, the term "anisotropic crystal" is used when the dielectric constant is a tensor. The anisotropy of the crystal is due to the anisotropy of the particles or to the structure of the crystal lattice, or in general, to both of them.

[1] *Manuscript received in original form December 11, 1952, and as revised, August 5, 1953. Contribution from Eaton Electronics Research Laboratory, McGill University, Montreal, P.Q.*

1. ISOTROPIC PARTICLES IN A CUBIC LATTICE

By giving a short review of how the CME usually is derived for crystals with cubic structure and isotropic particles we lay the foundation for the following section on anisotropic crystals.

If a field $\mathbf{E}_{dip}$ is acting on one of the particles, a dipole

[1] $$\mathbf{p} = \alpha \mathbf{E}_{dip}$$

is produced.

The field in the dielectric is $\mathbf{E}$. By definition

[2] $$\mathbf{D} = \epsilon \mathbf{E} = \mathbf{E} + 4\pi \mathbf{P}$$

or

[3] $$4\pi \mathbf{P} = (\epsilon - 1) \cdot \mathbf{E}.$$

If there are N particles per unit volume, then

[4] $$\mathbf{P} = N\mathbf{p}.$$

From [1], [3], and [4],

[5] $$4\pi N \alpha \mathbf{E}_{dip} = (\epsilon - 1)\mathbf{E}.$$

Once the relation between $\mathbf{E}_{dip}$ and $\mathbf{E}$ is known, ϵ can be computed from [5] as a function of α and N.

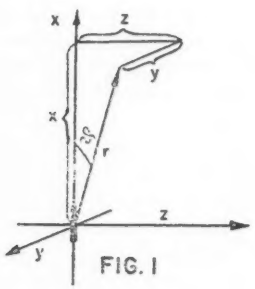

FIG. 1

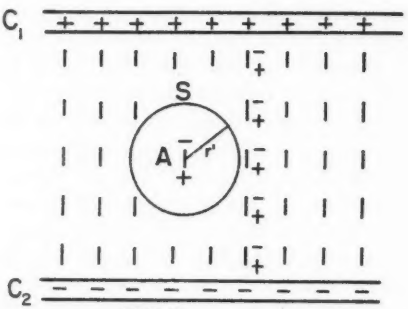

FIG. 2

The field E_x, E_y, E_z produced at the point x, y, z, by a dipole p parallel to the direction x (Fig. 1) is

[6] $$E_x = -p(r^{-3} - 3x^2 r^{-5}) = -pr^{-3}(1 - 3\cos^2\theta),$$

[7] $$E_y = -p\,xyr^{-5},$$

[8] $$E_z = -p\,xzr^{-5}$$

$$(r^2 = x^2 + y^2 + z^2).$$

In an isotropic crystal the directions of $\mathbf{p}$ and $\mathbf{E}$ are the same. If nothing is mentioned to the contrary the field $\mathbf{E}$ will be considered parallel to the x-axis of a rectangular coordinate system.

Fig. 2 represents a dielectric between the two condenser plates C_1 and C_2. The field produced by the electric charges on C_1 and C_2 is $\mathbf{D}$. The average field $\mathbf{E}$ between C_1 and C_2 is modified by the dipoles such that

[9] $$\mathbf{E} = \mathbf{D} - 4\pi\mathbf{P}.$$

To find $\mathbf{E}_{dip}$ which, in general, is different from $\mathbf{E}$, a sphere S is drawn with its center in a particle A. The radius r' of the sphere is chosen to be large compared to the average distance b between two neighboring dipoles. The distance l between the plus and the minus charge of one particle must be small compared to b, allowing the physical dipoles of finite size to be replaced by point dipoles and allowing moments of higher order to be neglected.

The field $\mathbf{E}_{dip}$ acting on the particle at A is the sum of three terms:

[10] $$\mathbf{E}_{dip} = \mathbf{D} + \mathbf{E}' + \mathbf{E}''$$

where $\mathbf{D}$ is the field of the charges on the condenser plates C_1 and C_2.

$\mathbf{E}'$ is the field of the dipoles within S.

$\mathbf{E}''$ is the field of all the other dipoles.

We assume a coordinate system like that of Fig. 1 with its origin at the point A of Fig. 2. The coordinates of any dipole within the sphere may be x_k, y_k, z_k. The field at A due to this dipole is

$$E_x = -p(r_k^{-3} - 3x_k^2 r_k^{-5}).$$

The field of all the dipoles inside the sphere is

$$E_x' = -p\sum_k (r_k^{-3} - 3x_k^2 r_k^{-5}).$$

Under the assumption that the particles are arranged in a cubic lattice, then for geometrical reasons:

$$\sum_k (r_k^{-3} - 3x_k^2 r_k^{-5}) = \sum_k (r_k^{-3} - 3y_k^2 r_k^{-5}) = \sum_k (r_k^{-3} - 3z_k^2 r_k^{-5}).$$

The sum of these three terms is zero because of $x_k^2 + y_k^2 + z_k^2 = r_k^2$. Therefore,

[11] $$\mathbf{E}' = 0$$

The dipoles outside S can be dealt with as though they fill the space uniformly at a density of N dipoles per unit volume because their distances from A are large compared to the distance between two neighboring dipoles. One easily obtains

[12] $$\mathbf{E}'' = -4\pi\mathbf{P} + \tfrac{4}{3}\pi\mathbf{P}.$$

From [10], [11], [12]:

[13] $$\mathbf{E}_{dip} = \mathbf{D} + 0 - 4\pi\mathbf{P} + \tfrac{1}{3}4\pi\mathbf{P} = \mathbf{E} + \tfrac{1}{3}4\pi\mathbf{P}.$$

Using [3] gives

[14] $$\mathbf{E}_{dip} = \mathbf{E} + \tfrac{1}{3}(\epsilon - 1)\,\mathbf{E} = \tfrac{1}{3}(\epsilon + 2)\,\mathbf{E}.$$

From [5] and [14] we find:

$$\frac{4\pi\alpha N}{3} = \frac{\epsilon - 1}{\epsilon + 2}. \tag{15}$$

This is the Clausius-Mosotti equation (CME) which can also be written:

$$\epsilon = \frac{1 + \frac{2}{3}4\pi\alpha N}{1 - \frac{1}{3}4\pi\alpha N}. \tag{16}$$

2. ANISOTROPIC CRYSTALS

In this section the assumption of isotropy is dropped. Both the polarizability and the dielectric constant are tensors. Even if the field is applied in such a direction that the polarization **P** is parallel to **E**, the field $\mathbf{E}_{dip}$ acting on a particle may have components normal to **E**.

In any anisotropic dielectric there exist three mutually perpendicular directions x, y, z such that:

$$D_x = \epsilon_x E_x, \qquad D_y = \epsilon_y E_y, \qquad D_z = \epsilon_z E_z. \tag{17}$$

We assume a dielectric with only one type of particles whose polarizability is given by

$$\begin{aligned} p_x &= \alpha_{xx}E_{dip,x} + \alpha_{xy}E_{dip,y} + \alpha_{xz}E_{dip,z}, \\ p_y &= \alpha_{yx}E_{dip,x} + \alpha_{yy}E_{dip,y} + \alpha_{yz}E_{dip,z}, \\ p_z &= \alpha_{zx}E_{dip,x} + \alpha_{zy}E_{dip,y} + \alpha_{zz}E_{dip,z}. \end{aligned} \tag{18}$$

If the field is applied in the direction x:

$$D_y = D_z = E_y = E_z = 0.$$

From [3] it follows that:

$$P_y = [(\epsilon_y - 1)/4\pi]E_y = 0; \quad P_z = [(\epsilon_z - 1)/4\pi]E_z = 0 \text{ and from [4]}$$

$$p_y = P_y/N = 0, \qquad p_z = P_z/N = 0. \tag{19}$$

The dipoles have no component in the y- or z-direction. The field $\mathbf{E}_{dip}$ may or may not have components in these directions.

Again the field $\mathbf{E}_{dip}$ is computed by drawing a sphere S and splitting $\mathbf{E}_{dip}$ into three terms, $\mathbf{E}_{dip} = \mathbf{D} + \mathbf{E}' + \mathbf{E}''$. As before we find

$$(D + E'')_x = E_x + \tfrac{1}{3}4\pi P_x, \quad (D + E'')_y = 0, \quad (D + E'')_z = 0. \tag{20}$$

$\mathbf{E}'$ can be computed from [6], [7], [8]:

$$\begin{aligned} E_x' &= -p_x A_x, \\ E_y' &= -p_x B_{xy}, \\ E_z' &= -p_x B_{xz}, \end{aligned} \tag{21}$$

with

$$\left.\begin{aligned} A_x &= \sum_k (r_k^{-3} - 3x_k^2 r_k^{-5}) \\ B_{xy} &= 3\sum_k x_k y_k r_k^{-5} \\ B_{xz} &= 3\sum_k x_k z_k r_k^{-5} \end{aligned}\right\} \tag{22}$$

the sums are extended over all dipoles within the sphere S (Fig. 2) except the dipole at the center

Introducing [10], [20], [21], and [19] into [18] gives

$$
\begin{aligned}
p_x &= \alpha_{xx}(E_x + \tfrac{1}{3}4\pi P_x - p_x A_x) - \alpha_{xy}p_z B_{xy} - \alpha_{xz}p_z B_{xz},\\
0 &= \alpha_{yx}(E_x + \tfrac{1}{3}4\pi P_x - p_x A_x) - \alpha_{yy}p_z B_{xy} - \alpha_{yz}p_z B_{xz},\\
0 &= \alpha_{zx}(E_x + \tfrac{1}{3}4\pi P_x - p_x A_x) - \alpha_{zy}p_z B_{xy} - \alpha_{zz}p_z B_{xz}.
\end{aligned} \tag{23}
$$

From [3] and [4]

$$
E_x + \tfrac{1}{3}4\pi P_x = \frac{4\pi N(\epsilon_x + 2)}{3(\epsilon_x - 1)}\, p_x = L_x p_x, \tag{24}
$$

with

$$
L_x = \frac{4\pi N}{3}\,\frac{\epsilon_x + 2}{\epsilon_x - 1}. \tag{25}
$$

Substitution of [24] reduces [23] to:

$$
\begin{aligned}
1 &= \alpha_{xx}(L_x - A_x) - \alpha_{xy}B_{xy} - \alpha_{xz}B_{xz},\\
0 &= \alpha_{yx}(L_x - A_x) - \alpha_{yy}B_{xy} - \alpha_{yz}B_{xz},\\
0 &= \alpha_{zx}(L_x - A_x) - \alpha_{zy}B_{xy} - \alpha_{zz}B_{xz}.
\end{aligned} \tag{26}
$$

From these equations $L_x - A_x$ can be computed:

$$
L_x - A_x = (\alpha_{yy}\alpha_{zz} - \alpha_{yz}\alpha_{zy})/|\alpha_{ik}|. \tag{27}
$$

Also B_{xy} and B_{xz} can be computed from [26].

Six more equations result from [26] by interchanging the x, y, and z directions. If B_{xy}, B_{xz}, and B_{yz} are computed from them as well, we find:

$$
\alpha_{xy} = \alpha_{yx}, \qquad \alpha_{xz} = \alpha_{zx}, \qquad \alpha_{yz} = \alpha_{zy}.
$$

Therefore

$$
L_x - A_x = (\alpha_{yy}\alpha_{zz} - \alpha_{yz}^2)/|\alpha_{ik}|. \tag{28}
$$

Using the abbreviation

$$
A_x + (\alpha_{yy}\alpha_{zz} - \alpha_{yz}^2)/|\alpha_{ik}| = 1/\beta_x, \tag{29}
$$

we find from [25] and [28]:

$$
\frac{(\epsilon_x - 1)}{(\epsilon_x + 2)} = \frac{4\pi N\beta_x}{3} \quad \text{or} \tag{30}
$$

$$
\epsilon_x = \frac{1 + \frac{2}{3}4\pi N\beta_x}{1 - \frac{1}{3}4\pi N\beta_x}. \tag{31}
$$

This is the generalization of the CME [15] and [16] for anisotropic dielectrics with one type of particles.

β_x may be called "apparent polarizability." It contains the effect of the crystal structure represented by A_x and the effect of the particles' anisotropy represented by $|\alpha_{ik}|/(\alpha_{yy}\alpha_{zz} - \alpha_{yz}^2)$.

The effect of the crystal structure can be eliminated by adding [28] to the two other equations resulting from [28] when x is replaced by y and z. Since

$$
A_x + A_y + A_z = \sum [3r_k^{-3} - 3(x_k^2 + y_k^2 + z_k^2)r_k^{-5}] = 3\sum (r_k^{-3} - r_k^{-3}) = 0, \tag{32}
$$

we find:

$$\frac{\epsilon_x + 2}{\epsilon_x - 1} + \frac{\epsilon_y + 2}{\epsilon_y - 1} + \frac{\epsilon_z + 2}{\epsilon_z - 1} = \frac{9}{4\pi NA} \tag{33}$$

with

$$A = 3|\alpha_{ik}|/(\alpha_{xx}\alpha_{yy} + \alpha_{xx}\alpha_{zz} + \alpha_{yy}\alpha_{zz} - \alpha_{xy}^2 - \alpha_{xz}^2 - \alpha_{yz}^2). \tag{34}$$

Equation [33] may also be called a generalization of the CME [15] for anisotropic dielectrics, A being a kind of average polarizability.

Remark 1

If the main axes of the tensor of polarizability are parallel to those of the tensor of dielectric constant,

$$\alpha_{yz} = \alpha_{xz} = \alpha_{xy} = 0,$$

then

$$\frac{1}{\beta_x} = A_x + \frac{1}{\alpha_x}, \tag{35}$$

$$\frac{1}{A} = \frac{1}{3}\left(\frac{1}{\alpha_{xx}} + \frac{1}{\alpha_{yy}} + \frac{1}{\alpha_{zz}}\right).$$

If the particles are isotropic, $\alpha_{xx} = \alpha_{yy} = \alpha_{zz} = \alpha$, so that the anisotropy of the crystal results from its structure alone, then

$$\frac{1}{\beta_x} = A_x + \frac{1}{\alpha} \qquad A = \alpha. \tag{36}$$

Equation [36] can also be obtained from van Santen and Opechowski's (6) equation when the latter is specialized for one type of particles.

Remark 2

Another special case is an isotropic dielectric with anisotropic particles: $\epsilon_x = \epsilon_y = \epsilon_z = \epsilon$.

From [30] follows: $\beta_x = \beta_y = \beta_z = \beta$.

[33] reduces to

$$\frac{\epsilon + 2}{\epsilon - 1} = \frac{3}{4\pi NA}. \tag{37}$$

[30] reduces to

$$\frac{\epsilon + 2}{\epsilon - 1} = \frac{3}{4\pi N\beta}. \tag{38}$$

Comparing [37] with [38], $\beta = A$, or with [29] and [34], gives

$$A_x = (\alpha_{xx}\alpha_{yy} + \alpha_{xx}\alpha_{zz} - 2\alpha_{yy}\alpha_{zz} - \alpha_{xy}^2 - \alpha_{xz}^2 + 2\alpha_{yz}^2)/3|\alpha_{ik}|. \tag{39}$$

[39] is the condition that an isotropic dielectric consists of anisotropic particles. Since, usually, the α_{ik} are functions of the frequency of the applied electric field, [39] can be fulfilled only for one special frequency.

If, however, the dielectric and the particles are isotropic, equation [39] becomes $A_x = 0$ and correspondingly $A_y = A_z = 0$.

Remark 3

The meaning of equations like [39] may seem to be uncertain because the sphere S limiting the sums [22] has not been defined in a completely distinct manner. However, A_x, B_{xy}, . . . are mainly determined by those terms for which r_k is small, whereas the sum of the terms with larger r_k rapidly tends to zero. Therefore, the uncertainty can be removed by extending the sums to infinity.

3. APPLICATION TO AN ARTIFICIAL DIELECTRIC

An artificial dielectric may consist of thin circular metal disks arranged as in Fig. 2. Their thickness may be denoted by t, their radius by ρ. If $t \ll \rho$ and if the flat particles lie parallel to the $x-y$ plane, then

$$\alpha_x = \alpha_y = 4\rho^2/3\pi, \quad \alpha_z = \tfrac{1}{3}\rho^2 t, \tag{40}$$

$$\alpha_{yz} = \alpha_{xz} = \alpha_{xy} = 0.$$

These are the limiting values for the polarizabilities of an oblate ellipsoid of vanishing thickness t. The particles may be arranged in a rectangular lattice with their centers at $x_n = an$, $y_m = bm$, $z_q = cq$ $(n, m, q = 0, 1, 2, \ldots)$.

If the lattice constants a, b, c are the same in all three directions, the structural contribution to the anisotropy of the crystal is zero, $A_x = A_y = A_z = 0$ and $\beta_x = \alpha_x$, $\beta_y = \alpha_y$, $\beta_z = \alpha_z$.

As a numerical example we choose $a = b = 10$, $c = 3.1623$. The term A_z has been computed from [22] for three different radii, r', of spheres S (Fig. 2):

$$\begin{aligned} A_z &= -0.13982 \text{ for } r' = 20, \\ A_z &= -0.13737 \text{ for } r' = 40, \\ A_z &= -0.13759 \text{ for } r' = 50. \end{aligned} \tag{41}$$

The fact that the three values obtained for A_z are almost the same confirms that the near neighbors of a particle contribute predominantly to the value of A_z.

From [32] and [41],

$$A_x = A_y = +0.06880. \tag{42}$$

We assume particles of radius $\rho = 2$ and thickness $t = 0.02$. The polarizabilities are computed from [40]:

$$\begin{aligned} \alpha_x &= \alpha_y = 3.395, \\ \alpha_z &= 0.0267. \end{aligned} \tag{43}$$

From [35]

$$\begin{aligned} \beta_x &= \beta_y = 2.753, \\ \beta_z &= 0.0268. \end{aligned}$$

This result confirms Süsskind's (5) statement based on Cohn's (1) experiments that the dielectric constant ϵ_x is smaller than could be expected from the

CME if $c < a = b$ and that it approaches the values predicted by the CME if c/a tends to unity.

When the formulas are applied to the magnetic field it must be borne in mind that the polarizabilities are negative. It follows from measurements of Peppiatt (3) that in this case also the theory is in agreement with experiments.

ACKNOWLEDGMENTS

This research forms part of a project on microwave optics, supported at McGill University by the United States Air Force through its Cambridge Research Center.

The author is greatly indebted to Prof. G. A. Woonton for several discussions of the matter.

REFERENCES

1. COHN, S. B. J. Applied Phys. 21: 674. 1950.
2. JONKER, G. H. and VAN SANTEN, J. H. Science, 109: 632. 1949.
3. PEPPIATT, H. J. Ph. D. Thesis, McGill University, Montreal, Que. 1953.
4. SLATER, J. C. Phys. Rev. 78: 748. 1950.
5. SÜSSKIND, C. J. Brit. Inst. Radio Engrs. 12: 49. 1952.
6. VAN SANTEN, J. H. and OPECHOWSKI, W. Physica, 14: 545. 1948.

SPECTRUM OF THE AlC MOLECULE[1]

By P. B. Zeeman[2]

ABSTRACT

An extensive system of bands in the visible and near infrared regions of the spectrum has been observed in emission when aluminum is present in a King Furnace. These bands have been attributed to the AlC molecule. No metallic carbide spectrum has been described before. A vibrational analysis of the bands has been made. The values $\omega_e' = 278.79_5$ and $\omega_e'' = 350.01_1$ kaysers were obtained.

INTRODUCTION

While exposures were made of the violet AlH band system with a King Furnace as source, a new band system was observed in the visible region of the spectrum. The system consists of a number of remarkably long sequences. The bands are degraded to the red.

EXPERIMENTAL

(1) *The King Furnace*

The King Furnace used was designed by the writer and built at the N.R.C. Laboratories, Ottawa. Some ideas on the design were obtained from previous workers (1, 3).

In Fig. 1 the furnace is shown in section. The graphite tube which served as furnace element was clamped at its ends by two split graphite cones. These cones fitted into two brass cones which were cooled by water running through an outer jacket, care being taken to avoid the formation of "dead spaces" in the running water. The brass cones were hard soldered to brass flanges. These flanges were bolted to a brass cylinder, which housed the insulation materials.

The thermal insulation of the furnace element consisted of a layer of Norton's Zirconia D Insulation Grain (or granulated charcoal) followed by a layer of Johns Manville 3 X Firecrete castable refractory. These insulation materials formed two concentric layers and were bounded on the inside by a graphite tube and on the outside by a perforated steel cylinder. This thick-walled "insulation cylinder" formed a unit of its own and could slide into the main brass cylinder.

To assemble the furnace the "insulation cylinder" was first put into position inside the main brass cylinder. The flanges carrying the brass cones were then bolted to the main cylinder. A graphite furnace element could now be inserted through the central opening of the furnace and its ends clamped into position by means of the split graphite cones. These graphite cones were held firmly in position by means of two steel plates which pressed against the outside surfaces

[1] *Manuscript received July 14, 1953.*

The work described in the present paper was carried out by the writer while he was holding a postdoctorate fellowship at the National Research Council Laboratories, Ottawa, Ontario, Canada. The manuscript was written at the Merensky Institute for Physics, Stellenbosch, South Africa. Issued as N.R.C. publication No. 3101.

[2] *Merensky Institute for Physics, University of Stellenbosch, South Africa.*

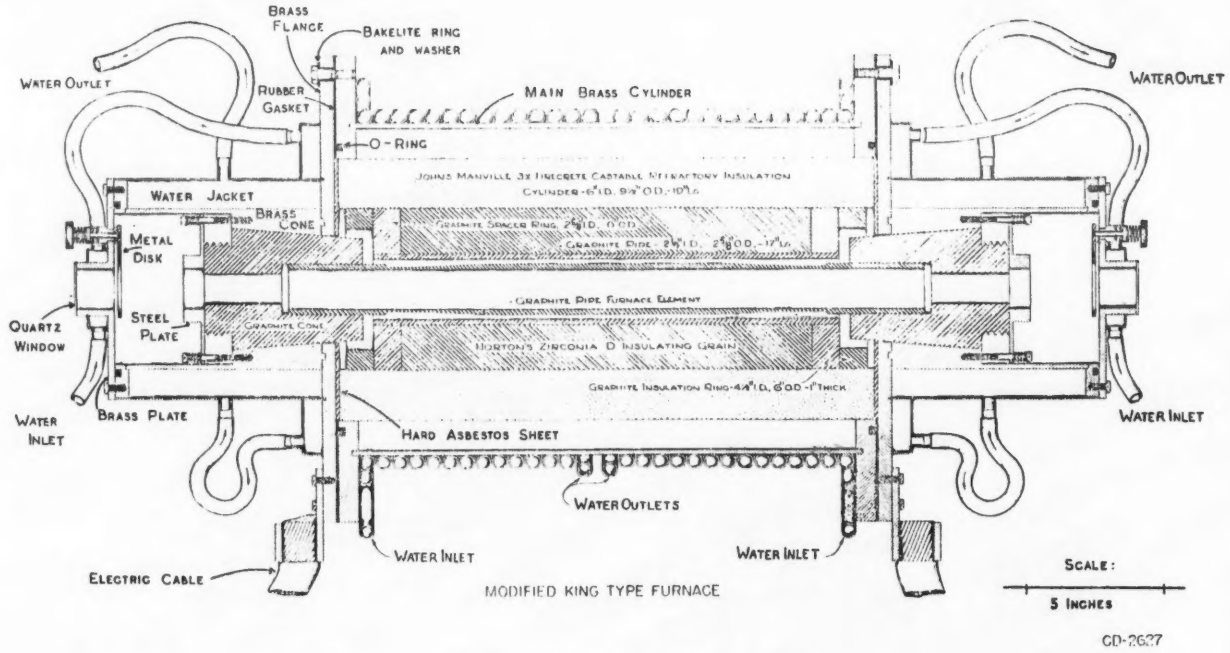

FIG. 1. Sectional drawing of the King Furnace.

of the cones as shown in Fig. 1. The graphite cones were threaded at the outside end to take a pull-out device. A burnt-out tube could be replaced in about fifteen minutes, provided the furnace was cold.

The outer ends of the brass cones mentioned above were closed by means of two brass plates bolted against O-rings to the walls of the cones. Quartz windows were waxed to the central portions of these plates and were cooled by running water. Two metal disks could be rotated in front of the windows to prevent the deposit of evaporating materials. This precaution was found necessary especially when a tube was heated for the first time.

The power for the furnace was supplied by a 25 kva. step-down transformer with a large Variac in the primary circuit for control of the temperature. The secondary terminals were connected to the flanges carrying the brass cones. Electrical insulation between the brass flanges and the main cylinder was obtained by means of bakelite rings and washers and rubber gaskets as shown in the figure.

The graphite furnace element was tapered as shown in the figure to obtain a longer region of uniform temperature. The furnace was designed for absorption work in which a long path is advantageous. The life of a tube below 2600°C. is several weeks; but it decreases to perhaps one day at 2800°C. and to about an hour at 3000°C. This decrease of lifetime is due to the rapid evaporation of graphite at the elevated temperatures. The life of a tube also depends on the pressure inside the furnace and the type of gas with which the furnace is filled.

(2) *Technique for Exciting Carbide Spectra*

It was found that when substances like silicon, boron, and aluminum were placed inside the graphite furnace element their carbides were formed at elevated temperatures. Accordingly the graphite tube either burned through or became nonconducting to a large extent. In either case the furnace element became useless. In order to avoid this, a second and shorter graphite tube was inserted as a liner inside the tube which served as the furnace element. The substance of interest was placed inside the liner which turned into the corresponding carbide when the furnace was heated. In this way a carbide liner was made *in situ*. Commercial carbide liners were found unsuitable because the cement which held such carbide tubes together distilled off at elevated temperatures, with the result that the tubes crumbled away.

While experimenting with aluminum in an aluminum carbide liner in a hydrogen atmosphere the violet AlH bands were observed with extreme intensity. Besides the AlH bands a new system of closely spaced bands was observed in the visible region. Under low dispersion the bands appear single-headed, but in the third order some band heads split into very close doublets. The bands are degraded to the red and form very long sequences.

(3) *Evidence in Favor of AlC as the Emitter of the New System*

The following experiments were carried out in order to discover the carrier of the new spectrum. A new graphite liner was outgassed in a vacuum at 2300°C. The furnace was then filled with hydrogen to a pressure of 50 cm.

On raising the temperature to 2150°C. the new spectrum did not appear. When aluminum was placed inside the liner in the hydrogen atmosphere the new bands appeared strongly at 2150°C. With aluminum in the liner, the new bands also appeared in a helium and an argon atmosphere at 2150°C., but only very weakly in a nitrogen atmosphere. This might be due to the rapid formation of aluminum nitride at the high temperatures. The aluminum used was in the form of a wire. This wire was supplied for aluminizing mirror surfaces and was of a high degree of purity.

The above experiments indicate that aluminum is essential for obtaining the bands. In the next experiments carbon was introduced under controlled conditions. A zirconium oxide liner was carefully outgassed in a vacuum at a high temperature. Aluminum was then inserted into the liner and the furnace filled with argon at a pressure of 50 cm. At 2150°C. some AlO bands were observed, but not the new spectrum. A short piece of specpure carbon rod was then placed inside the liner as well as fresh aluminum, and the furnace was again filled with argon. At 2150°C. the new bands were developed strongly. The above experiments indicate that the new bands are only excited when aluminum and carbon are present in the furnace liner. Hence AlC is the most likely emitter.

VIBRATIONAL ANALYSIS

The bands were photographed in the first, second, and third orders of the 21-ft. grating spectrograph at Ottawa. This concave grating has 15,000 lines per in. The spectrum of an iron arc was used as the comparison spectrum. For the vibrational analysis first order exposures taken on III F plates were measured on a Gaertner comparator. In Table I the Deslandres table of the new band system is given. The intensities and spacings of the bands are such that the (0,0) band could easily be recognized. The long sequences also simplified the construction of the Deslandres table. In Fig. 2 a spectrogram showing some of the bands is reproduced.

In order to evaluate the vibrational constants use was made of the expressions for $\Delta G_{v+\frac{1}{2}}$ and $\Delta^2 G_{v+1}$ given by Herzberg (2). Putting $\omega_0 z_0 = \omega_e z_e = 0$ we obtain the following relations:

$$[1] \qquad \Delta G_{v+\frac{1}{2}} = (\omega_0 - \omega_0 x_0 + \omega_0 y_0) - (2\omega_0 x_0 - 3\omega_0 y_0)\, v + 3\omega_0 y_0 v^2$$

and

$$[2] \qquad \Delta^2 G_{v+1} = -(2\omega_0 x_0 - 6\omega_0 y_0) + 6\omega_0 y_0 v.$$

Hence a graph of $\Delta^2 G_{v+1}$ against v should give a straight line with slope $6\omega_0 y_0$. Using this graphical method, the values $\omega_0' y_0' = -0.010_4$ and $\omega_0'' y_0'' = -0.010_5$ kayser were obtained.

By rearranging equation [1] it can be seen that a graph of $(\Delta G_{v+\frac{1}{2}} - 3\omega_0 y_0 v^2)$ against v should give a straight line with intercept $(\omega_0 - \omega_0 x_0 + \omega_0 y_0)$ and slope $(2\omega_0 x_0 - 3\omega_0 y_0)$. Such a graph is plotted in Fig. 3 for the lower state using $\omega_0'' y_0''$ already obtained. It yields $\omega_0'' = 347.98$ and $\omega_0'' x_0'' = 2.038$ kaysers. In a similar manner one obtains for the upper state $\omega_0' = 277.96$ and $\omega_0' x_0' = 0.846$ kaysers.

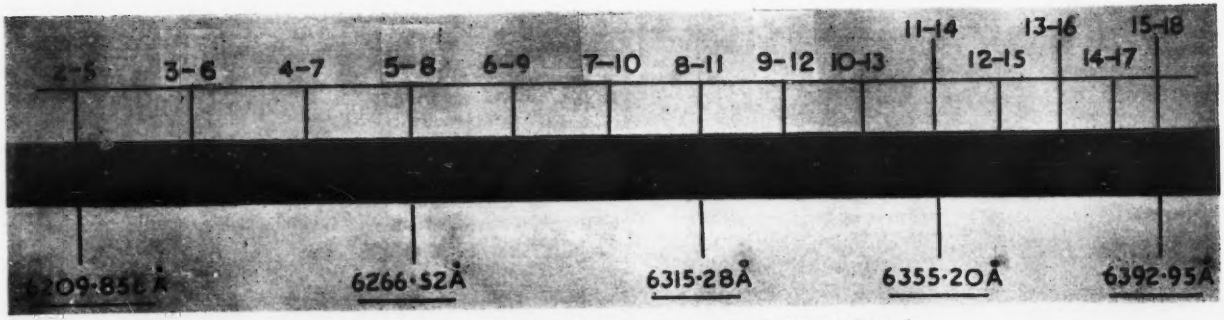

FIG. 2. Spectrogram of part of the sequence $\Delta v = -3$ of the AlC bands.

TABLE I

DESLANDRES TABLE OF THE VISIBLE AlC BANDS (BAND HEADS, KAYSERS)

v'' / v'	0	1	2	3	4	5	6	7	8	9
0	17234.05	16887.96	16546.13	—	—	—	—	—	—	—
1	17511.17	—	16823.20	16485.64	16152.48	—	—	—	—	—
2	—	17440.39	—	16761.04	16427.78	16098.98	—	—	—	—
3	—	—	17371.84	—	16701.34	16372.41	16048.27	—	—	—
4	—	—	—	—	—	—	16319.94	15998.73	—	—
5	—	—	—	—	—	—	—	16268.47	15953.51	—
6	—	—	—	—	—	—	—	—	16221.23	15909.70
7	—	—	—	—	—	—	—	—	—	16175.48

v'' / v'	9	10	11	12	13	14	15	16	17	18
7	16175.48	15868.79	15566.77	15270.03	—	—	—	—	—	—
8	—	16132.57	15830.24	15533.37	15241.21	—	—	—	—	—
9	—	—	—	15794.88	15502.22	15215.35	—	—	—	—
10	—	—	—	—	15761.41	15473.76	15192.96	—	—	—
11	—	—	—	—	—	15730.53	15448.68	—	—	—
12	—	—	—	—	—	—	15703.07	15426.03	—	—
13	—	—	—	—	—	—	—	15678.72	15406.87	—
14	—	—	—	—	—	—	—	—	15657.10	15389.96
15	—	—	—	—	—	—	—	—	—	15638.04

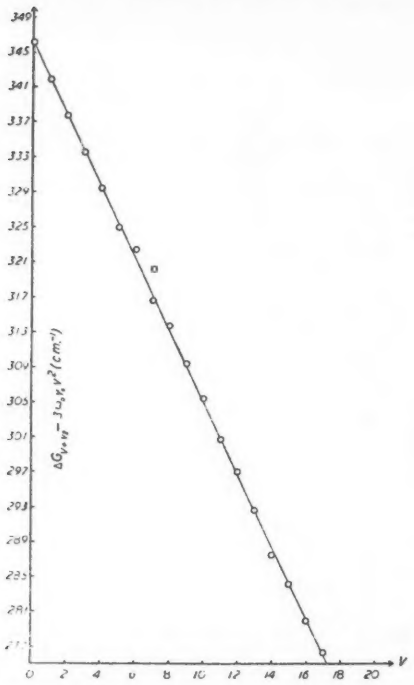

FIG. 5. Graphical determination of ω_0 and $\omega_0 x_0$ for the lower state of the observed AlC bands.

Using these vibrational constants one finds that the heads of the AlC bands can be represented by

[3] $$\nu_{\text{head}} = 17234.0_5 + (277.96\,v' - 0.846\,v'^2 - 0.010_4\,v'^3) - (347.98\,v'' - 2.038\,v''^2 - 0.010_5\,v''^3).$$

In order to obtain the dissociation energy of the lower state, $\Delta G_{v+\frac{1}{2}}$ was plotted against v and extrapolated. A plot of $\Delta G_{v+\frac{1}{2}}$ against G_v was also made. The results obtained are rather uncertain, but D_0 is estimated at 1.6 ± 0.2 ev.

TABLE II

VIBRATIONAL CONSTANTS OF THE AlC MOLECULE IN THE UPPER AND LOWER STATES OF THE VISIBLE BAND SYSTEM

Constant	Lower state	Upper state
ν_e		17269.3_6 kaysers
ν_{00}		17234.0_5 kaysers
ω_e	350.01 kaysers	278.80 kaysers
ω_0	347.98 kaysers	277.96 kaysers
$\omega_e x_e$	2.022 kaysers	0.831 kaysers
$\omega_0 x_0$	2.038 kaysers	0.846 kaysers
$\omega_e y_e = \omega_0 y_0$	-0.010_5 kaysers	-0.010_4 kaysers
k_v	$5.993_4 \times 10^4$ dynes/cm.	$3.802_6 \times 10^4$ dynes/cm.

ROTATIONAL ANALYSIS

The (0,0), (0,1), and (1,0) bands were photographed in the third order on high contrast plates. These are the only bands which are not badly masked by the overlapping of adjacent bands. Each band has two heads of about equal intensity, very close together. Groups of lines regularly spaced seem to form series, but the lines in each group are not sufficiently resolved to establish the number of branches in each band. The second difference of these groups of lines is very small, about 0.033 kayser. Thus far a complete rotational analysis could not be carried out and it is therefore not possible to ascertain what type of transition the band system represents.

CONCLUSION

In view of the fact that the bands have been observed in thermal emission, the two electronic states involved in the new bands must be low-lying states and it appears quite probable that the lower state is the ground state of the AlC molecule. On the other hand, it is difficult to account for such a small value of the vibrational frequency in the ground state of AlC when that of AlO or AlF in their respective ground states is about twice as large. For an unambiguous assignment to AlC, an investigation of the isotope effect would be desirable. However, the experimental evidence for AlC presented above seems fairly conclusive. Work under still higher resolution will be required in order to obtain a satisfactory rotational analysis of this band system and to determine the nature of the upper and lower states.

ACKNOWLEDGMENTS

The writer wishes to thank the National Research Council of Canada for the fellowship awarded to him. The writer also wishes to thank Dr. G. Herzberg who suggested the problem, for his guidance and valuable suggestions in the course of the work.

REFERENCES

1. BREWER, L., GILLES, P. W., and JENKINS, F. A. J. Chem. Phys. 16: 797. 1948.
2. HERZBERG, G. Molecular spectra and molecular structure. Vol. I. Spectra of diatomic molecules. D. Van Nostrand Company, Inc., New York. 1950. p. 96.
3. KING, A. S. Trans. Am. Electrochem. Soc. 56: 97. 1929.

BIREFRINGENCE IN CRYSTALS AND IN THE IONOSPHERE[1]

By C. H. M. Turner

ABSTRACT

Propagation of plane electromagnetic waves in a homogeneous ionized gas in a uniform magnetic field is compared with the propagation of light in an optically inactive birefringent crystal. It is well known that propagation in a crystal may be described by using a system of real orthogonal axes for which the dielectric constant is given by a diagonal matrix. This paper shows that propagation of plane waves in the ionosphere may be described in a similar manner, the medium having an effective dielectric constant given by a diagonal matrix, provided that a system of "complex" orthogonal axes is used for the description of the components of the field vectors. This set of component axes (which is quite different from and not to be confused with coordinate axes) is equivalent to resolving the field vectors into components parallel to the magnetic field and two contrarotating *circular* components in a plane perpendicular to the magnetic field. An expression giving the velocity of each of the two modes of propagation in a given direction and expressions for the amplitude of each component of the field vectors are obtained (equations 43 and 44). Provided that one accepts the concept of a complex velocity of propagation, the results hold when electron collisions are included. When electron collisions are neglected, it is possible to form a double-sheeted surface, called the normal velocity surface, which is of some assistance in visualizing the manner in which the velocity of propagation of the plane waves in each mode changes with direction.

1. INTRODUCTION

A comparison of double refraction in crystals and in the ionosphere has been made by Lange-Hesse (6). Using the theory of crystal optics he showed that a plane wave in an optically inactive anisotropic crystal was characterized by two velocities of propagation, thus explaining the birefringence of the medium. He then obtained corresponding equations for the propagation of plane waves in a collision-free homogeneous ionized gas in a uniform magnetic field and compared them with those obtained for the crystal. A similarity existed since principal axes of coordinates could be found for both media (relative to which the effective dielectric constant could be written in its simplest form as a diagonal matrix). A similarity also existed since both media were birefringent—but the details of the birefringency were very dissimilar. For example, it might be thought that the ionized gas in the magnetic field could be regarded as a medium with physical properties which are symmetrical about an axis parallel to the magnetic field, so that the gas might be expected to have properties similar to those shown by crystals with an electrical axis of symmetry (uniaxial crystals). In actual fact the properties are quite different, since firstly, each mode of propagation is linearly polarized in a crystal, but is elliptically polarized in the ionosphere; and secondly along the axis of symmetry the velocities of the two modes of propagation are equal in a (uniaxial) crystal but are not equal in the ionosphere.

It is believed that propagation in the ionosphere could be more closely compared with propagation in optically active anisotropic media, than with optically

[1] *Manuscript received March 31, 1953.*

Contribution from the Defence Research Telecommunications Establishment, Radio Physics Laboratory, Ottawa, Canada. Work performed under Defence Research Board project number D48-95-11-01. Substance of a paper presented in brief form at the 1953 Congress of the Canadian Association of Physicists.

inactive anisotropic media, since elliptical polarization is always associated with each of the two modes of propagation in the latter. However the interpretation of the physical characteristics of propagation in an optically inactive anisotropic medium is simpler than that for an optically active anisotropic medium. In the present investigation therefore, like Lange-Hesse we will still carry out a comparison of propagation in the ionosphere with that in an optically inactive crystal, but introduce the added complication of damping due to collisions of electrons with other particles. It is found that in the ionosphere (regarded as a slowly varying medium) the propagation of a plane wave is always characterized by three components of the field vectors, one of which is linearly polarized along the direction of the uniform magnetic field and the other two circularly polarized in the planes perpendicular to the magnetic field.

Throughout this paper the rationalized m.k.s. system of units, the time factor $e^{+j\omega t}$, and the representation of plane waves by the factor $e^{+j\omega[t-(\mathbf{n}.\mathbf{r})/v]} = e^{+j\omega[t-(\alpha x_1+\beta x_2+\gamma x_3)/v]}$ are used. The derivation of the effective dielectric constant is given in Appendix A, and a list of symbols in Appendix B.

2. PROPAGATION IN ANISOTROPIC MEDIA

It is well known that the field vectors representing an electromagnetic field satisfy the equations (Ref. 14, p. 23)

[1:2] $$\nabla \times \mathbf{E} = -\frac{\partial \mathbf{B}}{\partial t}: \quad \nabla \cdot \mathbf{B} = 0,$$

[3:4] $$\nabla \times \mathbf{H} = \mathbf{J} + \frac{\partial \mathbf{D}}{\partial t}: \quad \nabla \cdot \mathbf{D} = \rho.$$

In a crystal

[5] $$\mathbf{B} = \mu_0 \mathbf{H},$$

[6] $$\mathbf{J} = 0,$$

and

[7] $$\mathbf{D} = \epsilon_c \epsilon_0 \mathbf{E},$$

where μ_0, ϵ_0 are the permeability and permittivity of free space and are independent of the directions of $(\mathbf{B}, \mathbf{H})$ or $(\mathbf{D}, \mathbf{E})$ respectively, and ϵ_c, the relative permittivity of the crystal, is a tensor.

In the ionosphere, which will be considered as an ionized gas in a uniform magnetic field,

[8] $$\mathbf{B} = \mu_0 \mathbf{H},$$

[9] $$\mathbf{J} = \sigma \mathbf{E},$$

[10] $$\mathbf{D} = \epsilon_0 \mathbf{E},$$

where the only new constant σ, the conductivity of the medium, is a tensor.

From an examination of the set of equations 5, 6, 7 and the set 8, 9, 10, there would appear to be no connection between the propagation of electromagnetic waves in the two media. But by introducing the effective displacement vector, $\tilde{\mathbf{D}}$, and by writing

$$\frac{\partial \tilde{\mathbf{D}}}{\partial t} = \mathbf{J} + \frac{\partial \mathbf{D}}{\partial t} \tag{11}$$

in equation 3 some similarity is apparent, since for *both* media one now has

$$\nabla \times \mathbf{E} = -\partial \mathbf{B}/\partial t, \tag{12}$$

$$\nabla \times \mathbf{H} = \partial \tilde{\mathbf{D}}/\partial t, \tag{13}$$

and since divcurl $\equiv 0$, one also has

$$\nabla \cdot \tilde{\mathbf{D}} = 0. \tag{14}$$

The equations 12, 13, 14 are, of course, true for any medium. Next since the field vectors have a time factor $e^{+j\omega t}$, one obtains from 12, 13, 14

$$\nabla \times \mathbf{E} = -j\omega \mathbf{B} = -j\omega\mu_0 \mathbf{H}, \tag{15}$$

$$\nabla \times \mathbf{H} = +j\omega \tilde{\mathbf{D}}, \tag{16}$$

$$\nabla \cdot \tilde{\mathbf{D}} = 0. \tag{17}$$

Then using 11 one observes that in a crystal

$$\tilde{\mathbf{D}} = \mathbf{D} = (\epsilon_c \epsilon_0)\,\mathbf{E} \tag{18}$$

and in the ionosphere

$$\tilde{\mathbf{D}} = \frac{\mathbf{J}}{j\omega} + \mathbf{D} = \left(\frac{\sigma}{j\omega} + \epsilon_0\right)\mathbf{E}, \tag{19}$$

where $(\epsilon_c \epsilon_0)$ and $[(\sigma/j\omega) + \epsilon_0]$ are tensors. These constitutive equations 18 and 19 are the key to the properties of the two media.*

If we restrict the mode of propagation to plane waves, then each of the vector field components will contain the factor

$$e^{j\omega[t-(\mathbf{s}\cdot\mathbf{r})/v]} = e^{j\omega[t-(\alpha x_1+\beta x_2+\gamma x_3)/v]}, \tag{20}$$

where $\mathbf{r}$ is the vector from the origin to a point in the field, and $\mathbf{s}$ is a unit vector perpendicular to the planes of constant phase, so that with respect to any set of orthogonal axes $Oxyz$, the direction cosines of $\mathbf{s}$ are (α, β, γ). The phase velocity is v, and as will be seen shortly it is dependent on the direction $\mathbf{s}$. Using 20, equations 15, 16, 17 become

$$\frac{1}{v}(\mathbf{s} \times \mathbf{E}) = \mu_0 \mathbf{H}, \tag{21}$$

$$-\frac{1}{v}(\mathbf{s} \times \mathbf{H}) = \tilde{\mathbf{D}}, \tag{22}$$

$$\mathbf{s} \cdot \tilde{\mathbf{D}} = 0, \tag{23}$$

and eliminating $\mathbf{H}$,

$$\tilde{\mathbf{D}} = -\frac{1}{\mu_0 v^2}(\mathbf{s} \times \mathbf{s} \times \mathbf{E}) = \frac{1}{\mu_0 v^2}[\mathbf{E} - \mathbf{s}(\mathbf{s} \cdot \mathbf{E})]. \tag{24}$$

**Some authors prefer the use of the polarization vector* $\mathbf{P}$ *in equation 19, which would then be written* $\tilde{\mathbf{D}} = \mathbf{P} + \epsilon_0 \mathbf{E}$. *See footnote to equation A-4.*

Some important features of the propagation are seen immediately from these equations (Fig. 1), for it is evident that **H**, **s**, and $\tilde{\mathbf{D}}$ form a right orthogonal system, and that **E** is in the plane of **s** and $\tilde{\mathbf{D}}$ (Ref. 9, p. 372).

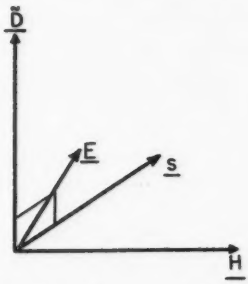

FIG. 1. Instantaneous position of the effective displacement, electric, and magnetic field vectors $\tilde{\mathbf{D}}$, **E**, and **H** in anisotropic media with respect to direction of propagation **s**. (Note that **H**, **s**, and $\tilde{\mathbf{D}}$ form an orthogonal set.)

In an anisotropic crystal $\tilde{\mathbf{D}}$ is identical to the displacement vector **D**, and in the ionosphere it is an effective displacement vector.

Next, equations 21, 22, and 23 will be used to discover more about the velocity of propagation v, and the relationships between the components of the field vectors (E_1, E_2, E_3), (H_1, H_2, H_3), and (D_1, D_2, D_3). Propagation in a nonconducting anisotropic crystal will be studied first, and then a comparative study made of propagation in an ionized gas in a uniform magnetic field.

3. PROPAGATION IN NONCONDUCTING ANISOTROPIC CRYSTALS

It is well known that in a nonconducting anisotropic crystal it is possible to orient an orthogonal system of axes $O(x, y, z)$ so that **D** and **E** are connected by a diagonal matrix containing real elements, i.e.

$$[25] \qquad \begin{bmatrix} \epsilon_x & 0 & 0 \\ 0 & \epsilon_y & 0 \\ 0 & 0 & \epsilon_z \end{bmatrix} \begin{bmatrix} \epsilon_0 E_x \\ \epsilon_0 E_y \\ \epsilon_0 E_z \end{bmatrix} = \begin{bmatrix} D_x \\ D_y \\ D_z \end{bmatrix} = \begin{bmatrix} \tilde{D}_x \\ \tilde{D}_y \\ \tilde{D}_z \end{bmatrix}.$$

The axes Ox, Oy, Oz are then called the principal electric axes of the crystal.

Using 24, and 18, one obtains

$$[26] \qquad \mathbf{s}\,(\mathbf{s}\,.\,\mathbf{E}) = \mathbf{E} - \mu_0 v^2 \tilde{\mathbf{D}}$$

and resolving this into its vector components (using 25) one finds

$$[27] \qquad \begin{cases} \alpha(\mathbf{s}\,.\,\mathbf{E}) = \left(\dfrac{1}{\epsilon_x \epsilon_0} - \mu_0 v^2\right) \tilde{D}_x, \\ \beta(\mathbf{s}\,.\,\mathbf{E}) = \left(\dfrac{1}{\epsilon_y \epsilon_0} - \mu_0 v^2\right) \tilde{D}_y, \\ \gamma(\mathbf{s}\,.\,\mathbf{E}) = \left(\dfrac{1}{\epsilon_z \epsilon_0} - \mu_0 v^2\right) \tilde{D}_z. \end{cases}$$

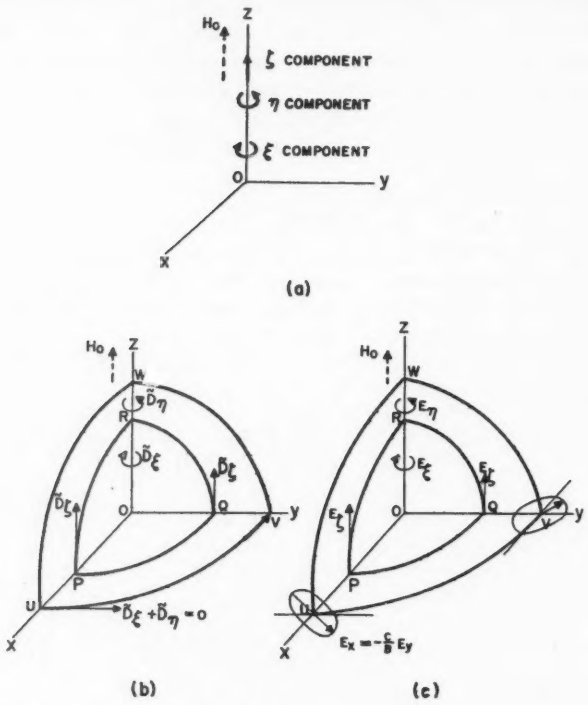

FIG. 4. Basic features of propagation in ionosphere.

(*a*) Principal components of electromagnetic field vectors.

(*b*) The normal velocity surfaces, and the polarization of the effective displacement vector for propagation of plane waves along cardinal axes *Ox*, *Oy*, and *Oz*.

(*c*) Polarization of the electric vector for propagation of plane waves along *Ox*, *Oy*, and *Oz*,

$$v_\xi = OR, \quad v_\zeta = OP = OQ,$$
$$v_\eta = OW, \quad v_\epsilon = OU = OV.$$

3. The two modes of propagation are propagated independently, and the existence of one does not require the existence of the other. (Coupling between the two modes does exist, however, when the ionized gas is not homogeneous, Ref. 11.)

4. For the hollow cone which includes all directions of propagation inclined at a constant angle to the direction of the magnetic field, the velocities of the two modes of propagation are constant (equation 43), and hence on this cone (equation 44) the (ζ) components of the field vectors parallel to the magnetic field remain unchanged in amplitude and phase, and the two circularly polarized (ξ and η) components of the field vector change in phase but not in amplitude.

4.4 *Normal Velocity Surfaces*

A normal velocity surface is a surface such that the radius vector to it from the origin is everywhere proportional to the phase velocity of the plane waves propagated in the direction of the radius vector (see section 3).

Corresponding to the normal velocity surface for a crystal, shown in Fig. 2, there is a normal velocity surface for propagation in an ionized gas in a uniform magnetic field. As for a crystal, it is a double sheet, one octant of which is shown in Fig. 4(*b*) or 4(*c*).

These figures give a true physical representation of phase velocity in any direction when the collision frequency is negligible, for, using the relationships given in appendix B, 30, 31, 32, 33, it may be shown that when the frequency of the propagated wave (ω) and the critical frequency (ω_c) satisfy

(i) $0 < \omega_c^2/\omega < \omega + \omega_0$, then $v_\xi < v_\zeta < v_4 < v_\eta$ (Figs. 4(*b*) and 4(*c*)),

or (ii) $\omega_c^2/\omega < \omega < -\omega_0$, then $v_\eta < v_4 < v_\xi < v_\zeta$.

Since the velocity v_ζ is independent of the strength of the uniform magnetic field, the sheet *PQR* corresponds to the so-called 'ordinary' mode of propagation, and the sheet *UVW* to the extraordinary mode (Ref. 10). The arrows attached to, and around the axes in Figs. 4(*b*) and 4(*c*) give the polarization of the effective displacement vector and of the electric vector respectively for electromagnetic plane waves propagated in the direction of the axes.

These directions of polarization of the effective displacement vector are obtained from equation 44*a* after using equation 39 to express ($\mathbf{s} \cdot \mathbf{E}$) in terms of $\tilde{D}_\xi, \tilde{D}_\eta, \tilde{D}_\zeta$; similarly, the directions of polarization of the electric vector are obtained from equation 44*b*. It will be seen that, for propagation along the magnetic field, the ordinary mode *OR* possesses only the ξ circular component, and the extraordinary mode *OW* possesses only the η circular component. For propagation perpendicular to the magnetic field the ordinary mode *OQ* or *OP* possesses only the linear component. However the extraordinary mode *OV* or *OU* possesses only the two circular components which, being equal in amplitude ($\tilde{D}_\xi \pm \tilde{D}_\eta = 0$), degenerate into a linear component as shown in Fig. 4*b*. It is interesting to recall Fig. 1, in which it was pointed out that **E**, in general, has a component in the direction of propagation. It may be noticed (Fig. 4(*c*)) that this component of **E** in the direction of propagation vanishes for both modes of propagation along the uniform magnetic field, and for the ordinary mode of propagation perpendicular to the uniform magnetic field, but does exist for the extraordinary mode of propagation perpendicular to the uniform magnetic field. The polarization of the current vector **J** is similar to that illustrated in Fig. 4*c* for **E**.

From the expressions 30–33 of appendix B, which are dependent on the value of $\omega_c^2 = Ne^2/\epsilon_0 m$ (and therefore on the electron density) it will be seen that the shape of the normal velocity double sheet must change as a wave is propagated through the ionosphere. The nature of this change in shape of the sheet may be followed with the help of Figs. 5(*a*) and 5(*b*) (similar to the diagrams in References 1, 2, and 11) which show the variation in $(c/v)^2$ (or square of the refractive index) with ω_c^2 for both modes and for any direction of propagation but neglect

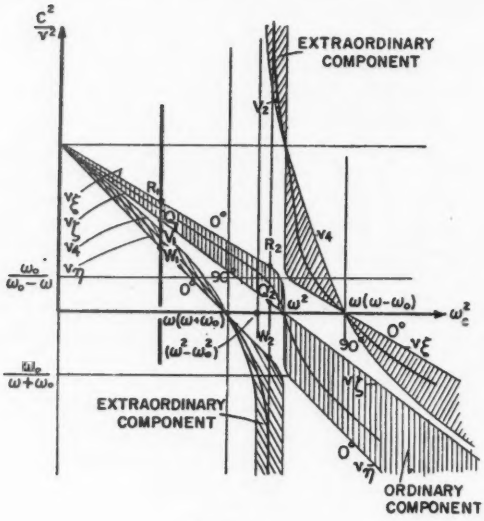

Fig. 5a

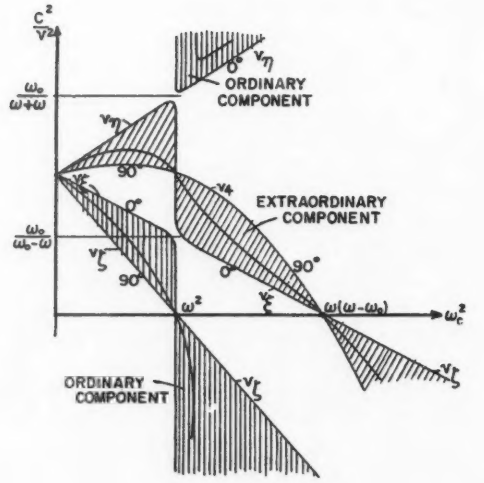

Fig. 5b

FIG. 5. Variation in (refractive index)^2 with (critical frequency)^2 for plane waves whose direction of propagation is inclined at any angle to the direction of the magnetic field. (Note that collision frequency has been neglected and that $\omega_0 = eB/m$ is negative for electrons.) (*a*) $\omega > (-\omega_0)$. (*b*) $\omega < (-\omega_0)$.

collisions. For example, when the frequency of propagation is greater than the gyrofrequency ($\omega > -\omega_0$), Fig. 5(*a*) must be used, and on it a line such as $R_1 Q_1 V_1 W_1$ gives the characteristics of the propagation in any direction at a point in the ionosphere having the critical frequency given by the intercept of $R_1 Q_1 V_1 W_1$ with the abscissa. The velocities corresponding to the strips $R_1 Q_1$ and $W_1 V_1$ in Fig. 5*a* give the velocity variations in the ordinary and extraordinary modes (OR to OQ) and OW to OV, Figs. 4(*b*, *c*) as the direction of propagation changes from along to perpendicular to the direction of the uniform magnetic field. As one ascends through the ionosphere, the critical frequency initially increasing, the line $R_1 Q_1 V_1 W_1$ moves to the right, and the normal velocity double sheets change their shape accordingly. For instance the line $V_2 R_2 Q_2 W_2$ corresponds to a normal velocity double sheet whose section by a plane through the direction of the magnetic field is shown in Fig. 6. It will be

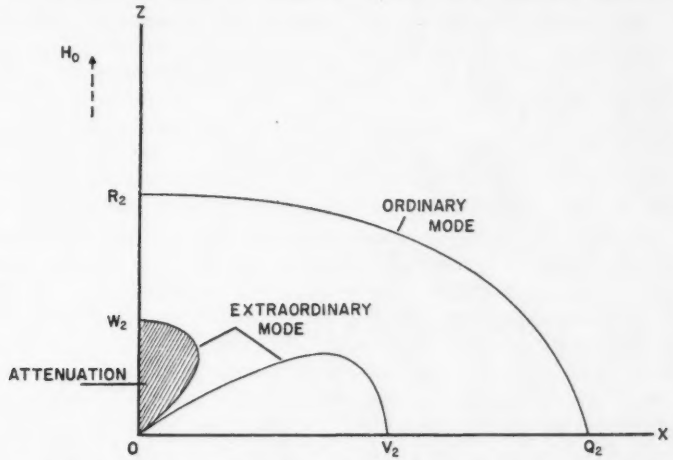

FIG. 6. Section of the normal velocity surface at a point in the ionosphere where the critical frequency corresponds to $V_2 R_2 Q_2 W_2$ (Fig. 5(*a*)). Note attenuation corresponding to negative values of c^2/v^2.

observed that either mode may be the inner or outer sheet depending on the critical frequency (i.e. electron density) and also that when $(c/v)^2$ is imaginary (as at W_2) the attenuation which it represents may also be illustrated (as in the shaded section).

5. CONCLUSIONS

The propagation of plane electromagnetic waves in a homogeneous ionized gas in a uniform magnetic field has been compared with that in optically inactive nonabsorbing anisotropic crystals.

It has been confirmed that normal velocity surfaces (consisting of two sheets, one corresponding to each mode of propagation) may be drawn for both media. In optically inactive crystals it is well known that these surfaces generally meet

at four singular points, defining two optical axes along which plane waves associated with each mode are propagated with equal phase velocities. It has been shown that in the ionosphere, when collisions are neglected, these surfaces do not meet at any point, and, in a given direction, the velocities of propagation associated with each mode are in general different.

It has also been established that for propagation in the ionosphere even when electron collisions are included, the electromagnetic field vectors are very simply related to each other by diagonal matrix transformations, if the field vectors are resolved into three special components, the first of which is linearly polarized along the direction of the earth's magnetic field, and the second and third of which are two contrarotating circularly polarized components lying in the plane perpendicular to the magnetic field. Here we differ from Lange-Hesse (6) who reported that for a collision-free ionosphere the second and third components were elliptically polarized. We also differ from Saha and Banerjea (Ref. 12, equation 22) who, without reference to propagation in crystals, had suggested three components similar to ours, but implied that they travelled with three different velocities. The latter authors made no reference to the diagonal matrix property.

Apart from the simplicity of the diagonal matrix transformation connecting the field vectors when they are resolved in the special manner suggested above, one also obtains a simple picture of the polarization of the field vectors when the plane electromagnetic wave is propagated along or perpendicular to the magnetic field. From the general expressions in equation 44, the directions of polarization of (say) the **E**-vector shown in Fig. 4(*c*), for propagation in the direction of any of the axes and for either mode, are simply obtained.

As the plane wave passes through the ionosphere, the electron density, and hence the critical frequency ω_c, changes. Provided the ionosphere may still be regarded as a slowly varying medium, the concept of normal velocity surfaces still holds but these surfaces change their shape in conformity with the characteristics obtained by previous authors and illustrated in Fig. 5.

APPENDIX A

The Conductivity and Effective Dielectric Constant Matrix for an Ionized Gas in a Uniform Magnetic Field

This matrix has been obtained previously by several authors (Ref. 3; and Ref. 12, equations 5 and 12). Its derivation is repeated here, following Hines (Ref. 4), but using the m.k.s. nomenclature in order to provide a convenient reference for the form of the effective dielectric constant matrix

$$\epsilon_i = \begin{bmatrix} B & C & 0 \\ -C & B & 0 \\ 0 & 0 & A \end{bmatrix}$$

given in equation 30.

The equation of motion of a charged particle of mass m and charge e in a constant magnetic field H_0 is

[A-1] $$m\dot{\mathbf{V}} = e\mathbf{E} + e\mu_0 [\mathbf{V} \times (\mathbf{H}_0 + \mathbf{H})] - \nu m\mathbf{V}$$

where $\mathbf{V}$ = velocity,

$\mathbf{E}$ and $\mathbf{H}$ = electric and magnetic field (due to the electromagnetic radiation),

ν = collision frequency,

μ_0 = permeability of free space.

If we now assume that the field vectors associated with the electromagnetic radiation have a common factor

[A-2] $$e^{j\omega[t-(\alpha u_1+\beta u_2+\gamma u_3)/v]}$$

so that the radiation is a plane wave with phase velocity v and direction of propagation defined by direction cosines (α, β, γ) in the right orthogonal system of axes $O(u_1, u_2, u_3)$, then the term containing H is usually neglected since it is small compared with that containing E provided $|V|/v \ll 1$. Hence A-1 is generally written

[A-3] $$\mathbf{E} = \frac{1}{e}(m\dot{\mathbf{V}} + \nu m\mathbf{V}) - \mu_0 \mathbf{V} \times \mathbf{H}_0.$$

It is usual to consider only the motion of electrons, since the velocity of other (heavier) charged particles is much smaller. Hence the current $\mathbf{J} = Ne\mathbf{V}$, where N is the electron density, is related to the electric field by the expression*

[A-4] $$\mathbf{E} = \frac{m}{Ne^2}(\dot{\mathbf{J}} + \nu\mathbf{J}) + \frac{\mu_0}{Ne}\mathbf{H}_0 \times \mathbf{J}.$$

Now if

ϵ_0 = permittivity of free space,

$$\omega_c^2 = \frac{Ne^2}{\epsilon_0 m},$$

$$a = (j\omega + \nu),$$

$$\text{and } \omega_0, \omega_1, \omega_2, \omega_3 = \frac{e\mu_0 H_0}{m}, \frac{e\mu_0 H_1}{m}, \frac{e\mu_0 H_2}{m}, \frac{e\mu_0 H_3}{m},$$

where (H_1, H_2, H_3) are the components of $\mathbf{H}_0$ parallel to the coordinate axes $O(u_1, u_2, u_3)$, then one obtains from A-4

[A-5] $$\epsilon_0\mathbf{E} = \frac{am\epsilon_0}{Ne^2}\mathbf{J} + \frac{m\epsilon_0}{Ne^2}\left(\frac{e\mu_0\mathbf{H}_0}{m} \times \mathbf{J}\right).$$

[A-6] $$= \frac{1}{\omega_c^2}\left\{a\mathbf{J} + \omega_0 \cdot \frac{\mathbf{H}_0}{H_0} \times \mathbf{J}\right\}.$$

[A-7] $$= \frac{1}{\omega_c^2}\begin{bmatrix} a & -\omega_3 & \omega_2 \\ \omega_3 & a & -\omega_1 \\ -\omega_2 & +\omega_1 & a \end{bmatrix}\mathbf{J}.$$

*If the movement of electric charges is considered in terms of displacement rather than velocity, one could appropriately use the polarization vector $\mathbf{P}$ where $\mathbf{J} = \partial\mathbf{P}/\partial t$.

From this, as is also evident from equation A-3, the effect of the collisions changes the conductivity tensor from $\sigma(j\omega)$ to $\sigma(j\omega + \nu)$. Then inverting equation A-7, the conductivity tensor is given by

$$[A\text{-}8] \qquad \mathbf{J} = \frac{\omega_c^2 \epsilon_0}{a(a^2 + \omega_0^2)} \begin{bmatrix} a^2 + \omega_1^2 & \omega_1\omega_2 + a\omega_3 & \omega_1\omega_3 - a\omega_2 \\ \omega_1\omega_2 - a\omega_3 & a^2 + \omega_2^2 & \omega_2\omega_3 + a\omega_1 \\ \omega_1\omega_3 + a\omega_2 & \omega_2\omega_3 - a\omega_1 & a^2 + \omega_3^2 \end{bmatrix} \mathbf{E}.$$

If now, special coordinate axes $O(x, y, z)$ are chosen so that the Oz axis lies along the direction of the earth's magnetic field, then $\omega_3 = \omega_0$ and $\omega_1 = \omega_2 = 0$ so that

$$[A\text{-}9] \qquad \mathbf{J} = \frac{\omega_c^2 \epsilon_0}{a(a^2 + \omega_0^2)} \begin{bmatrix} a^2 & a\omega_0 & 0 \\ -a\omega_0 & a^2 & 0 \\ 0 & 0 & a^2 + \omega_0^2 \end{bmatrix} \mathbf{E}.$$

Hence the effective displacement vector $\tilde{\mathbf{D}}$ and the electric field vector $\mathbf{E}$ related by equation 19 are connected by the expression

$$[19] \qquad \tilde{\mathbf{D}} = \left(\frac{\sigma}{j\omega} + \epsilon_0\right) \mathbf{E}$$

$$[A\text{-}10] \qquad = \epsilon_0 \begin{bmatrix} 1 + \dfrac{a\omega_c^2}{j\omega(a^2 + \omega_0^2)} & \dfrac{\omega_c^2\omega_0}{j\omega(a^2 + \omega_0^2)} & 0 \\ -\dfrac{\omega_c^2\omega_0}{j\omega(a^2 + \omega_0^2)} & 1 + \dfrac{a\omega_c^2}{j\omega(a^2 + \omega_0^2)} & 0 \\ 0 & 0 & 1 + \dfrac{\omega_c^2}{j\omega a} \end{bmatrix} \mathbf{E}$$

which may be written in the form quoted in equation 30, namely

$$[A\text{-}11] \qquad \tilde{\mathbf{D}} = \epsilon_0 \begin{bmatrix} B & C & 0 \\ -C & B & 0 \\ 0 & 0 & A \end{bmatrix}$$

APPENDIX B

Reference List of Symbols, etc.

1. $\mathbf{E}$, $\mathbf{D}$, $\tilde{\mathbf{D}}$, $\mathbf{H}$, $\mathbf{B}$, $\mathbf{J}$—complex electric, displacement, effective displacement, magnetic, induction, and current density field vectors; each contains the plane wave factor $e^{+j\omega[t-(\alpha u_1+\beta u_2+\gamma u_3)/v]}$.
2. ρ—electric charge density.
3. $(\alpha, \beta, \gamma) \equiv \mathbf{s}$—direction cosines of and unit vector in the direction of propagation of the plane wave.
4. v, ω—phase velocity and angular frequency of the plane wave.
5. $O(u_1, u_2, u_3)$—any system of right orthogonal axes.
6. $O(x, y, z)$—a system of right orthogonal real axes. In the crystal these are the principal electric axes, and in the ionized gas Oz is parallel to the uniform magnetic field.

7. $O(\xi, \eta, \zeta)$—the system of right orthogonal complex component axes (complex principal electric axes) of the ionized gas in the uniform magnetic field.
8. μ_0, ϵ_0—permeability, permittivity of free space.
9. ϵ_c, ϵ_i—dielectric constant, or permittivity relative to free space of crystal and ionosphere respectively; these are matrices.
10. σ—conductivity. In the ionosphere this is a matrix.
11. $\nabla \equiv \mathbf{u}_1 \dfrac{\partial}{\partial u_1} + \mathbf{u}_2 \dfrac{\partial}{\partial u_2} + \mathbf{u}_3 \dfrac{\partial}{\partial u_3}$ where $\mathbf{u}_1, \mathbf{u}_2, \mathbf{u}_3$ are unit vectors parallel to the coordinate axes.
12. (E_x, E_y, E_z), etc.—complex components of the field vectors $\mathbf{E}$, etc. resolved in the directions of the real axes Ox, Oy, Oz.
13. (E_ξ, E_η, E_ζ), etc.—complex components of the field vectors $\mathbf{E}' = \mathbf{E}$, etc., resolved in the directions of the complex 'component' axes $O\xi$, $O\eta$, $O\zeta$.
14. $(\epsilon_x, \epsilon_y, \epsilon_z)$—principal dielectric constants of crystal.
15. (v_x, v_y, v_z)—velocities associated with principal dielectric constants of crystal.
16. v_1, v_2—phase velocities of the two modes propagated in the direction (α, β, γ).
17. $\tilde{\mathbf{D}}_1, \mathbf{D}_1, \mathbf{E}_1, \mathbf{H}_1; \tilde{\mathbf{D}}_2, \mathbf{D}_2, \mathbf{E}_2, \mathbf{H}_2$—field vectors associated with each mode of propagation.
18. $\epsilon_i = \begin{bmatrix} B & C & 0 \\ -C & B & 0 \\ 0 & 0 & A \end{bmatrix}$ matrix of the effective dielectric constant in the ionosphere in the $O(x, y, z)$ system of components.
19. $\epsilon_i' = \begin{bmatrix} B + jC & 0 & 0 \\ 0 & B - jC & 0 \\ 0 & 0 & A \end{bmatrix} \equiv \begin{bmatrix} \epsilon_\xi & 0 & 0 \\ 0 & \epsilon_\eta & 0 \\ 0 & 0 & \epsilon_\zeta \end{bmatrix}$ matrix of the dielectric constant in the $O(\xi, \eta, \zeta)$ system of components.
20. (v_ξ, v_η, v_ζ)—velocities associated with principal dielectric constants of ionized gas in uniform magnetic field, given by $v_\xi^2 = 1/\epsilon_\xi \epsilon_0 \mu_0$, etc. When there are no collisions these components are real or imaginary, and when there are collisions they are complex.
21. $B = 1 + \dfrac{a\omega_c^2}{j\omega(a^2 + \omega_0^2)}$.
22. $C = \dfrac{\omega_c^2 \omega_0}{j\omega(a^2 + \omega_0^2)}$.
23. $A = 1 + (\omega_c^2/j\omega a)$.
24. $\omega_c^2 = Ne^2/\epsilon_0 m$.
25. $\omega_0 = e\mu_0 H_0/m$ (this is $\pm ve$ for $\pm ve$ particles respectively).
26. $a = j\omega + \nu$.
27. m, e—mass and charge of electron.
28. N—electron density of ionized gas.
29. ν—collision frequency of electrons.

$$30.\ \frac{1}{v_\xi^2} = \epsilon_0\mu_0\epsilon_\xi = \epsilon_0\mu_0\left[1 - \frac{\omega_c^2}{\omega(\omega - j\nu - \omega_0)}\right].$$

$$31.\ \frac{1}{v_\eta^2} = \epsilon_0\mu_0\epsilon_\eta = \epsilon_0\mu_0\left[1 - \frac{\omega_c^2}{\omega(\omega - j\nu + \omega_0)}\right].$$

$$32.\ \frac{1}{v_\zeta^2} = \epsilon_0\mu_0\epsilon_\zeta = \epsilon_0\mu_0\left[1 - \frac{\omega_c^2}{\omega(\omega - j\nu)}\right].$$

$$33.\ \frac{1}{v_4^2} = \frac{2}{v_\xi^2 + v_\eta^2} = \epsilon_0\mu_0\left[1 - \frac{\omega_c^2}{\omega(\omega - j\nu) - \dfrac{\omega^2\omega_0^2}{\omega(\omega - j\nu) - \omega_c^2}}\right].$$

REFERENCES

1. Bhar, J. N. Science and Culture (India), 2: 322. 1936–37.
2. Booker, H. G. Trans. Roy. Soc. (London), A, 237: 411. 1938.
3. Hartree, D. R. Proc. Cambridge Phil. Soc. 27: 143. 1930.
4. Hines, C. O. J. Geophys. Research, 56: 71. 1951.
5. Joos, G. Theoretical physics. Blackie & Sons, Ltd., Glasgow and London. 1934.
6. Lange-Hesse, G. Arch. Elektrotech. Ubertragung, 6: 149. 1952.
7. Madelung, E. Die mathematischen Hilfsmittel des Physikers. Springer-Verlag, Berlin. 1950.
8. Margenau, H. and Murphy, G. M. Mathematics of physics and chemistry. D. Van Nostrand Company, Inc., New York. 1943.
9. Page, L. and Adams, N. I. Electrodynamics. D. Van Nostrand Company, Inc., New York. 1945.
10. Proc. I. R. E. 38: 1266. 1950. Standards of wave propagation: definitions of terms.
11. Rydbeck, O. E. H. Trans. Chalmers Univ. Technol. Gothenburg, No. 34. 1944.
12. Saha, M. N. and Banerjea, B. K. Indian J. Phys. 19: 159. 1945.
13. Saha, M. N., Banerjea, B. K., and Guha, U. C. Indian J. Phys. 21: 180. 1947.
14. Stratton, J. A. Electromagnetic theory. McGraw-Hill Book Company, Inc., New York. 1941.
15. Valasek, J. Theoretical and experimental optics. John Wiley & Sons, Inc., New York. 1949.

COINCIDENCE STUDIES OF THE DECAY OF INDIUM 114[1]

By M. W. Johns, C. C. McMullen,[2] R. J. Donnelly,[3] and S. V. Nablo[4]

ABSTRACT

A coincidence circuit of resolving time 3×10^{-9} sec. has been used to examine the decay of In^{114}. Coincidence experiments are described to show that of the five gamma-rays which follow the K-capture process the 0.722 and 1.300 Mev. radiations are both in cascade with the 0.556 Mev. gamma-ray and that the spins and parities of the excited levels of energy 0.556, 1.278, and 1.856 Mev. in Cd^{114} are $2+$, $2+$, and $0+$, respectively. The observed beta–gamma coincidences may be ascribed to a combination of inner bremsstrahlung associated with the strong 2 Mev. β^- transition and a weak β^- group of intensity less than 1×10^{-3} beta per disintegration and end point about 0.8 Mev. The positron spectrum has a branching ratio of $4 \pm 1 \times 10^{-5}$ and an end point between 1.0 and 1.4 Mev.

INTRODUCTION

The 50-day activity of In^{114} has been studied by many workers. The main features of the strong β^- spectrum were established by Lawson and Cork (20) and confirmed by others. The 50-day activity is due to an isomeric transition in In^{114} from an excited state of energy 0.192 Mev. and spin 5 to the ground state of spin 1 (6). The β^- spectrum is due to an allowed transition from the ground state of In^{114} to that of Sn^{114}.

In addition to this dominant mode of decay, K-capture leading to an excited state of Cd^{114} was discovered by Maienschein and Meem (24) and their results confirmed and extended by Boehm and Preiswerk (4) and Mei, Mitchell, and Zaffarano (25). This process, of intensity 3 or 4% of the β^- intensity, leads to an excited state of Cd^{114} of energy 1.28 Mev. and de-excitation occurs through the emission of cascade gamma-rays of energies 0.722 and 0.556 Mev. The presence of a weak radiation of energy around 1.3 Mev. has also been established and its role as a crossover transition suggested. Boehm and Preiswerk (4) detected a weak β^+ component in the decay process and estimated its branching ratio as 0.01% and its end point as 0.650 Mev.

This work was originally undertaken to determine the spins of the excited states of Cd^{114} by angular correlation measurements. The difficulty in interpreting the results of the angular correlation measurements (14, 15) and the equivalent measurements of Steffen (28) led to a re-examination of the decay scheme. The discovery of Steffen and Zobel (29) that the 1.278 Mev. level of Cd^{114} is fed from the ground state of In^{114} has been of great assistance in interpreting the results. Precise measurements of the gamma-ray energies carried out in this laboratory (17) showed that the 1.300 Mev. radiation could not be the crossover transition originally proposed. In addition, these measurements indicated that this radiation was in cascade with the 0.556 Mev. radiation.

[1] *Manuscript received June 15, 1953.*
Contribution from the Department of Physics, McMaster University, Hamilton, Ontario.
[2] *Recipient of a Research Council of Ontario Scholarship 1951–52 and National Research Council Fellowship 1952–53.*
[3] *Recipient of a Research Council of Ontario Scholarship 1951–52. Present address, Department of Physics, Yale University, New Haven, Conn.*
[4] *Recipient of a Research Council of Ontario Scholarship, 1952–53.*

The coincidence experiments to be described in this paper support the decay scheme of Fig. 1 already proposed on the basis of energy measurements (16), set an upper limit to the number of negatrons proceeding to an excited state of Sn^{114}, assign spins to the excited states of Cd^{114}, and determine the yield and approximate end point of the positron component.

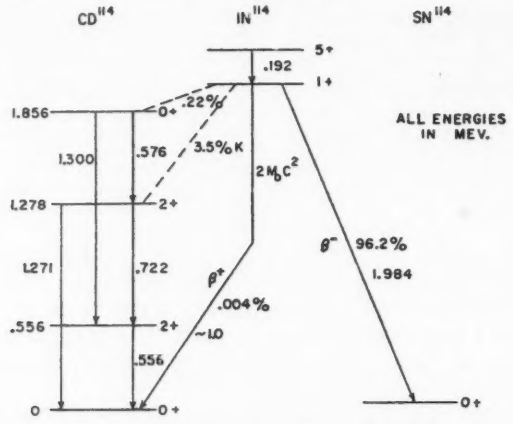

FIG. 1. Proposed decay scheme for In^{114}.

EXPERIMENTAL METHOD AND RESULTS

Apparatus

The coincidence measurements were carried out with a circuit of resolving time of three to five millimicroseconds similar in design to that described by Bell, Graham, and Petch (2) to which the reader is directed for a detailed account of its performance. The gamma-rays were detected with anthracene or stilbene scintillation counters. The crystals, of dimensions $\frac{1}{2}$ in. $\times$ $\frac{1}{2}$ in. $\times$ 1 in., were strapped to either 1P21 or 931A photomultiplier tubes. The entire tube and crystal was covered with an aluminum foil shield which was connected to the cathode of the photomultiplier. Further shielding of Scotch electrical tape was provided to ensure that the counters were light-tight. For gamma–gamma coincidence measurements the crystals were provided with lead shields 2 mm. thick to eliminate betas and attenuate the strong 0.192 Mev. gamma radiation from In^{114}. For beta counting the crystals were covered with 5 mgm./cm.^{2} aluminum foil. Each photomultiplier was mounted on a small portable copper box containing its resistor network and preamplifier. The photomultipliers were operated at 2000 v.

The performance of the circuit was tested by obtaining a resolution curve under the conditions of operation of the experiment. With a clipping cable 30 cm. long, the circuit gave efficient detection with resolution times of 5×10^{-9} sec. for anthracene and 3×10^{-9} sec. for stilbene in good agreement with the experience of Bell, Graham, and Petch. (Since the circuit possessed a resolution time of 0.8×10^{-9} sec. when operated from a square wave pulse generator (10)

whose rise time was 0.5×10^{-9} sec., it is clear that the largest contribution to the resolving time of the circuit is to be found in the properties of the phosphor used.) The resolution curve was obtained by measuring the coincidence rate as a function of the delay introduced between one of the scintillation counters and the fast coincidence detector. The following simplified version of the delay line described by Bell *et al.* was used to introduce this delay. The fast pulses from the two counters were fed through 100 ohm cable (RG/7U) to the two ends of a 100 ohm line 2.4 meters long formed with a solid central copper conductor and a copper shield of U-shaped cross section. The conductor was held in place with small pieces of lucite. The fast coincidence detector and its associated preamplifier (a Los Alamos model 500) rode on this line and the pulses entered the coincidence unit through a phosphor bronze spring which made good contact with the copper conductor. Since a shift of the contact point increased the length of the cable leading to one counter and reduced it for the other, a change in contact position of 15 cm. corresponded to a delay of 10^{-9} sec. Thus this variable delay line allowed a total delay of 1.6×10^{-8} sec. to be introduced. Larger delays were provided by changing the length of the cable from one of the counters to the variable delay line. The velocity of pulses in RG/7U cable as given by the manufacturer is 0.83 c while the velocity in the variable line is c, the velocity of light.

After checking the resolution, the contact was set at the point corresponding to the peak of the resolution curve and the experiment begun. Each measurement involved a determination of the difference between the coincidences in a short interval of time, 5 to 15 min., and the number of chance coincidences in an equal interval. The chance coincidences were obtained by switching a 5 meter length of cable to one or other of the leads from the counter to the coincidence detector. The chance rate was corrected for the small effects of attenuation in the delay cable. The proper correction factor was found by exciting each photomultiplier with a separate gamma source and examining the change of the chance coincidence rate with the length of the delay line used. For the 5 meters of cable used for measuring the chance rate the correction factor for attenuation was 1.15.

In general, it was not necessary to cool the photomultiplier. Although the noise contribution was very high at the high voltages used, the resolving time of the coincidence circuit was sufficiently short that the noise coincidence rate was completely negligible. In the study of the gamma–gamma coincidence rate as a function of lead absorber thickness, one crystal was exposed to the full intensity of the source while the other was shielded with a large amount of lead. In this case, it was found that coincidences between noise pulses from the shielded counter and the very large number of pulses from the unshielded counter were sufficiently frequent to be troublesome. For such experiments, the shielded photomultiplier and its crystal were cooled with liquid air with a consequent reduction in the noise coincidence rate by a factor of 10.

Coincidences between the 0.556 *and* 1.300 *Mev. Gamma-rays*

From the gamma energy measurements already reported (17), it appeared probable that the 0.556 Mev. radiation was in coincidence with both the 0.722

and 1.300 Mev. radiation as shown in Fig. 1. The following coincidence absorption experiment was carried out to test this part of the decay scheme.

Anthracene scintillation counters shielded with 2 mm. of lead were placed on opposite sides of the source at distances 1 and 12 cm., respectively, from the source. Lead was placed between the source and the distant counter and the coincidence rate measured as a function of the thickness of lead. The coincidence rate with a source of 100 mc. of In^{114} was about 200 c.p.m. with no absorber present and dropped by a factor of roughly 1000 with 12 cm. of absorber in place. The signal to chance ratio for zero absorber was six. With the shielded crystal and the photomultiplier immersed in liquid air, the signal to chance ratio was still two with 12 cm. of lead screening the cooled counter.

In order to minimize the effect of drifts in the electronic circuits, counts were taken alternately with and without the absorber in place and the measurements for no absorber normalized to the value of 1000.

Since the measurements were not made under conditions of "good" geometry, it was impossible to identify the energies of the gamma-ray components from the absorption curve by reference to the known absorption coefficients. As a method of identification, the experiment was repeated with a Co^{60} source in precisely the same geometric arrangement.

The experimental results are shown in Fig. 2. Curves A and B represent the In^{114} data while curve C represents the Co^{60} data. Curve A was taken with the side-channel discriminator of the shielded counter set at a low value while curve B was taken with this discriminator set to discriminate strongly against the 0.556 Mev. radiation. All data have been corrected for a background coincidence rate of 0.3 on the normalized scale. It is apparent that both curves show two distinct components, the softer of which, common to both, corresponds quite well with the theoretical curve for an equal mixture of 0.556 and 0.722 Mev. radiation and the harder of which seems to be of an energy slightly greater than that of the Co^{60} radiation of mean energy 1.2 Mev.

The decay of In^{114} is accompanied by six gamma-rays (16, 17) whose energies and relative intensities (given in brackets) follow: 0.192 Mev. (5.4), 0.556 Mev. (1), 0.722 Mev. (1), 0.576 Mev. (0.03), 1.300 Mev. (0.04), and 1.271 Mev. (0.009). An interpretation of the absorption curve must be based on these energies and intensities. The 0.192 Mev. radiation is due to an isomeric transition to the 72-sec. ground state of In^{114} so that it cannot be in coincidence with the other gamma-rays listed above. In order to decrease the chance coincidence rate, the effective relative intensity of this radiation was reduced to less than 0.2 by means of lead shielding and the discriminator settings of the coincidence circuit.

The strong component of the coincidence absorption curve has a slope consistent with an equal mixture of 0.556 and 0.722 Mev. radiation and accounts for almost all the gamma–gamma coincidences observed. It must therefore be identified as due to the 0.556–0.722 Mev. cascade observed by many workers (4, 24, 25).

The weak component must be ascribed to coincidences between either or both of the 1.271 and 1.300 Mev. radiations and one or more of the 0.556, 0.576, and 0.722 Mev. gamma-rays. In support of this assumption, discrimination against

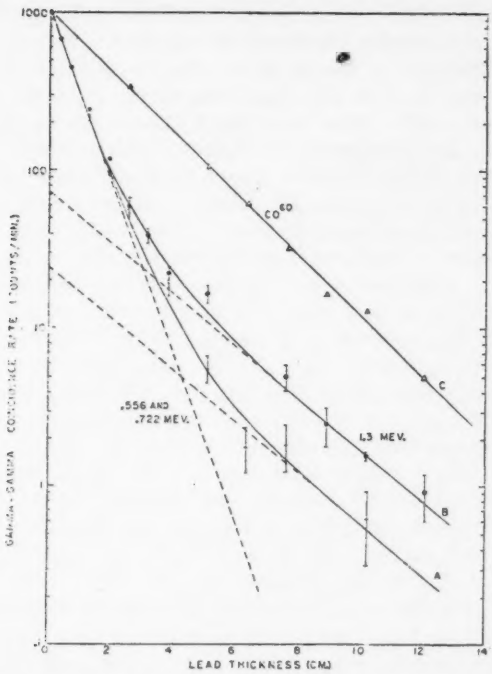

FIG. 2. Coincidence absorption of the gamma rays of In^{114} in lead.

the 0.556 and 0.722 Mev. gamma-rays in the shielded counter led to a large increase in the relative intensity of the high-energy component (curve B).

Since the relative detection efficiencies of the circuit as a function of gamma energy are known for the conditions under which curve A was taken, it is possible from the known gamma intensities to compute the relative intensity of the weak to the strong component in the absorption curve for all possible cascades. For the 1.300–0.556 or 1.300–0.722 Mev. cascades the relative intensity is expected to be about 3.5%; for the 1.271–0.556 or 1.271–0.722 Mev. cascades it should be about 0.5%; while for all other possibilities it should be less than 0.1%. The observed intensity under these conditions was 2.5% in good agreement with the calculated intensity for a 1.300–0.556 or 1.300–0.722 Mev. cascade and quite inconsistent with any of the other possibilities.

The results of these experiments confirm the fact reported by several workers (4, 25) that the 0.556 and 0.722 Mev. radiations are in cascade and in addition show that the 1.300 Mev. radiation is in cascade with either the 0.556 or 0.722 Mev. radiations. The existence of a level in Cd^{114} at 0.556 Mev. established by neutron-capture experiments (18, 30) and the presence of weak gamma-rays of energy 0.576 and 1.271 Mev. in the In^{114} decay spectrum (17) rule out the latter possibility.

Beta–Gamma Coincidences

Although the chief mode of decay of In^{114} involves a direct transition from the ground state of In^{114} to that of Sn^{114}, it has recently been pointed out by Nussbaum and van Lieshout (26) that transitions to the first excited state of Sn^{114} might be expected to occur in a small fraction of the disintegrations, and involve a β^- spectrum with an end point of about 0.8 Mev., followed by a gamma-ray of energy about 1.2 Mev. Their measurement sets an upper limit of 3×10^{-3} on the intensity of this transition. The following section describes a comparison of the beta–gamma coincidences obtained with sources of Co^{60}, Y^{90}, and In^{114} in an attempt to set an upper limit on the intensity of such a transition. Co^{60} was chosen as a comparison source because each disintegration consists of a β^- (end point 0.3 Mev.) followed by two cascade gamma quanta of energy about 1.2 Mev. Y^{90} was chosen because it possesses a simple β^- spectrum of end point (2.3 Mev.) slightly greater than In^{114} (2 Mev.) and with no known gamma-rays.

The coincidence circuit already described was used with two stilbene crystals ($\frac{1}{2}$ in. $\times$ $\frac{1}{2}$ in. $\times$ 1 in.), one of which was covered with 3 gm./cm.^{2} of lead to detect only gamma-rays and the other with a 4.0 mgm./cm.^{2} aluminum window to detect betas. The shielding on the gamma crystal had a negligible effect on the high-energy gamma-rays of interest here but reduced the contribution of the 0.192 Mev. gamma in indium and of the soft bremsstrahlung radiation accompanying both the In^{114} and Y^{90} decay. The beta crystal was covered with 1900 mgm./cm.^{2} of aluminum to determine its gamma counting rate. Each crystal subtended a solid angle of 0.02 of the total sphere at the source position. For each of the three sources the single counting rates, the gamma–gamma rate, and the beta–gamma rate were studied. The aluminum absorption curves for In^{114} and Y^{90} presented in Fig. 3 are very similar, indicating a beta end point in the region 0.8 to 1.0 Mev. Owing to the low coincidence rates and the presence of gamma–gamma coincidences in the case of In^{114}, it was impossible to follow these absorption curves for more than 1.5 decades.

Following the type of analysis described by Dunworth (9) and others, it is possible to compute the intensity of the low-energy β^- spectrum of In^{114} in three partially independent ways from a comparison of the single and coincidence rates recorded for In^{114} and Co^{60}. The values obtained by the three methods agree quite closely and give a mean of $1.0 \pm 0.5 \times 10^{-3}$ for the number of low-energy negatrons per disintegration of In^{114}.

Alternatively, the observed beta–gamma coincidence rate may be interpreted as due to bremsstrahlung. If one assumes that the beta–gamma coincidences observed in Y^{90} are due to a weak β^- group of energy about 1 Mev. followed by a 1.2 Mev. gamma-ray, a comparison of the $N(\beta\gamma)/N(\beta)$ ratio for Y^{90} with that for Co^{60} leads to an intensity for this group of 2×10^{-3}. On the other hand, a β^- group of this energy would have given a $N(\beta\gamma)/N(\gamma)$ ratio 10 times larger than the ratio actually observed. This suggests that the observed effect in Y^{90} is not due to true beta–gamma coincidences but to bremsstrahlung–beta coincidences. The magnitudes to be expected for such an effect were calculated for the β^- of In^{114} and Y^{90}, using the method outlined by Wu for P^{32} (31). The number of quanta per disintegration arising from inner bremsstrahlung

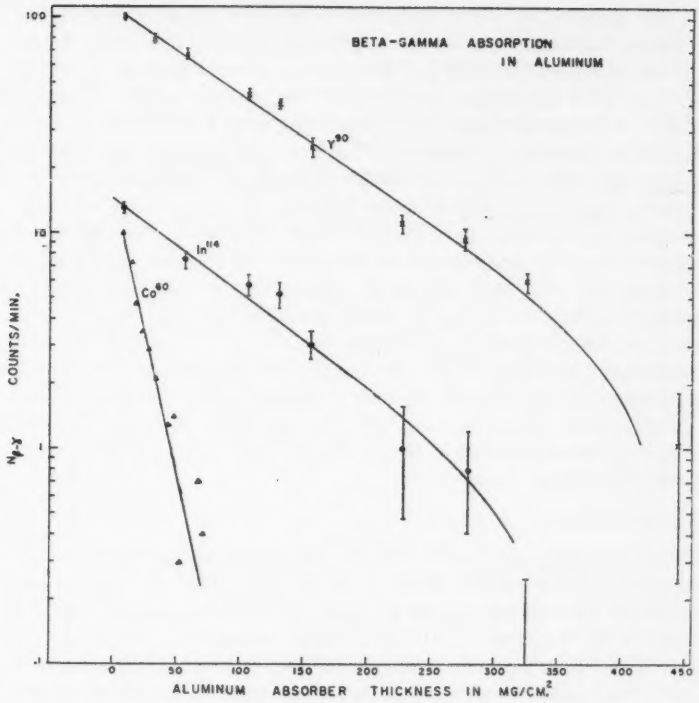

FIG. 3. Beta–gamma coincidence absorption in aluminum for Y^{90}, In^{114}, and Co^{60}. The gamma–gamma contributions have been subtracted from the In^{114} and Co^{60} coincidences. The curves have been arbitrarily normalized for clarity of presentation.

with energy sufficient to reach a stilbene crystal covered with a 3 gm./cm.^{2} lead shield was computed to be about 2×10^{-3} for In^{114} and 4×10^{-3} for Y^{90}, a number sufficient to account for all the beta–gamma coincidences observed in both sources. The 30 gm./cm.^{2} of lead shielding between the two crystals was sufficient to eliminate all bremsstrahlung coincidences arising from retardation of the betas in the beta crystal itself.

In the light of this evidence, it would appear that the intensity of any low-energy β^- group existing in In^{114} must be less than 1×10^{-3} of the high-energy β^- group.

Spins of the Excited States of Cd^{114}

(i) *Introduction*

Since Hamilton (13) showed that there was an expected correlation between the directions of emission of the first and second gamma-rays in a gamma cascade, the experimental determination of correlation functions has been used by Brady and Deutsch (5) and other workers as a powerful method of assigning spins to excited states of nuclei. Hamilton shows that the expected correlation function

is of the form $W(\theta) = 1 + a\cos^2\theta + b\cos^4\theta + \ldots$ and gives explicit expressions for the coefficients in the case of pure dipole and quadrupole transitions. The theory has been extended by Lloyd (22) to cover radiations of any multipole order. The series terminates with the $\cos^4\theta$ term unless both transitions are of multipole order greater than two. It has been pointed out by Ling and Falkoff (21) that the competition of electric 2^{l+1} and magnetic 2^l radiation in a transition may introduce interference effects which radically alter the correlation function expected on the pure multipole theory and they present explicit expressions for calculating the correlation functions for dipole–quadrupole mixtures. Lloyd (22) has shown that the interference terms introduced by Ling and Falkoff have physical reality only when the phase shift is 0, or π radians. On the basis of Weisskopf's theory (3) it appears that transitions of mixed character can only be expected for competition of $M1$ and $E2$ radiations, and that even here the $E2$ component should be much weaker than the $M1$ radiation. Expressions for correlation functions for triple cascades in which the first and third gamma-rays are detected have been given by Arfken, Biedenharn, and Rose (1). As would be expected, these correlation functions are much less anisotropic in general than for two gamma cascades.

(ii) *Experimental*

The following section reports the results of two separate determinations of the gamma–gamma correlation function for In^{114}. The two sources used had activities of 100 mc. and consisted of metallic indium irradiated to a specific activity of 0.5 mc./mgm. and 1 mc./mgm., respectively. Since the shielded detectors were sensitive only to the gamma-rays of energy greater than 200 kev., the effective source strength was about 3 mc. in each experiment. Despite this activity, the signal to chance ratio was better than four to one. The solid angles subtended by the scintillation detectors at the source were 0.027 and 0.045 steradians in the two experiments. Slight differences in the method of source mounting and in the precautions used to avoid Compton scattering existed but, since the individual points in the two runs agreed within the expected statistical errors, the weighted mean of the two sets of data was used.

Each source was mounted on the axis of a laboratory prism spectrometer table. The anthracene or stilbene crystals with their associated 1P21 photomultipliers were mounted on the fixed and movable arms of the spectrometer. Each source was centered carefully by observing the counting rate in the movable detector as a function of its angular setting. The crystal faces were covered with 2 mm. of lead to reduce the intensity of the strong 0.192 Mev. radiation and scattered radiation, while the sides of the crystals were covered with 3 mm. of lead for the same purpose. As a check on the suitability of the geometric arrangement, the correlation function for Co^{60} was determined and found to agree with that given by Brady and Deutsch (5) and others. Counting was carried on at the θ position, the 90° position, and on chance in turn until at least 10,000 true coincidences had been recorded for each selected value of θ.

The value of $[N(\theta) - N(\pi/2)]/[N(\pi/2) - N(\text{chance})]$ represents the value of the correlation function $[W(\theta) - 1]$ for the selected value of θ. A small correction

which was never greater than 0.007 was made to each value for the effect of the finite solid angles subtended by the crystals (7). The 180° position was also corrected for the presence of annihilation radiation from the weak positron component present in the decay. The effect of this correction was to lower the point at 180° from 0.203 ± 0.012 to 0.177 ± 0.030, the increase in the standard deviation being due to the uncertainty in the positron contribution. The experimental data, corrected as described above, are presented in Fig. 4. Since the upper level

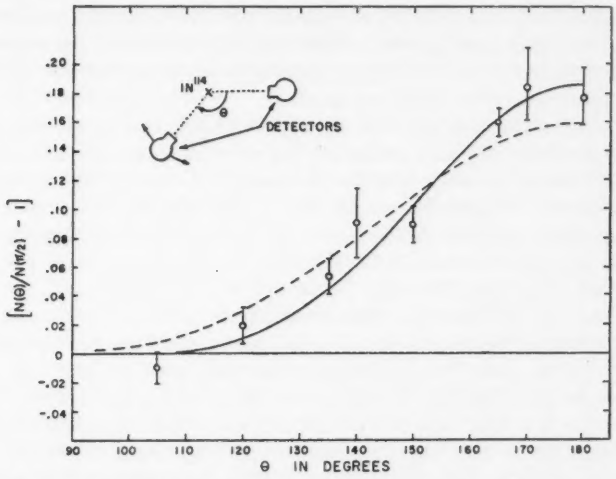

FIG. 4. The angular correlation function for the In^{114} cascade gamma-rays.
Solid line—the least squares fit to the experimental data and the theoretical correlation function for the 0.722–0.556 Mev. cascade modified by three weak cascades.
Dotted line—the theoretical curve for a 2–2–0 cascade with mixture *M*1 96.0%, *E*2 4.0%, and zero phase shift in the first transition.

of the 0.722–0.556 Mev. cascade is fed by *K*-capture from the In^{114} ground state of spin 1 (29), its spin is not greater than 3, while the lower level of the cascade is the ground state of an even–even nucleus with presumably zero spin. Hence it is difficult to conceive of many cascades in which both transitions could be octupole or higher order. The few which are possible give a much greater anisotropy than that shown by these data. It was therefore felt to be reasonable to fit the data to Hamilton's equation, retaining only terms to $\cos^4\theta$. If the points are given weights inversely proportional to the squares of their relative standard deviations, a least squares fit to the data yields the parameters $a = -0.0028$ and $b = +0.190$. The curve described by these parameters is shown as a solid line in Fig. 4. Although these parameters are somewhat different from those obtained from the correlation measurements of Steffen (28) and of Klema and McGowan (19), the resulting curves are very closely the same.

It is impossible to find any pure multipole cascade which will give good agreement with any of these data. The best choice is the 4–2–0 cascade which is ruled

out by the limitation on the spin of the upper level. Even when the possibility of $M1$–$E2$ interference is considered, the fit provided by any of the published sets of parameters is not very good. The best choice for the data presented here seems to be a 2–2–0 cascade in which the first transition is 96% $M1$ and 4% $E2$ with no phase shift and the second is pure quadrupole. This function is shown as the dotted curve in Fig. 4. It is very sensitive to the mixture of $M1$ and $E2$ radiation present. A 3.5% component of $E2$ fits well at angles near 180° but is considerably worse at angles below 150° while a 4.5% component fits well at small angles but gives too low a correlation value for large values of θ. When it is considered that there are three other cascades present in the decay process with intensities of 3 or 4% of the main 0.722–0.556 Mev. cascade, this measure of agreement is all that can be expected.

If it can be assumed that the discrepancy between the experimental and theoretical curves of Fig. 4 represents the distortion of the 0.722–0.556 Mev. cascade by the four weaker cascades, it is possible to use the difference to make an estimate of the spin of the 1.856 Mev. level. The four weak cascades and their intensities relative to the main cascade are (*a*) the 1.300–0.556 Mev. cascade (4%), (*b*) the 0.576–0.722–0.556 triple cascade in which the first and third gammas are detected (3%), (*c*) the 0.576–0.722 cascade (3%), and (*d*) the 0.576–1.271 cascade (0.01%). Since the main shape of the correlation function is determined by the strong cascade, the spins of the first three levels in Cd^{114} are 0, 2, 2. The 1.856 Mev. level may conceivably have a spin of 0, 1, 2, or 4 (if we allow the possibility of the upper level being fed from the 0.192 Mev. level of In^{114}). It is a relatively simple matter to consider the effect of the weak cascades, using the results of the theoretical papers referred to in the introduction to this section. Of the four possible choices, only the choice 0 gives any improvement in the agreement between the theoretical and experimental correlation curves. For this choice it is possible to fit the experimental curve exactly when the 0.722 Mev. transition is described as 96.2% $M1$ and 3.8% $E2$, with no phase shift. Qualitatively, it is possible to see this by considering that only in this case is there a strong correlation function in any of the weaker cascades which could introduce the measure of distortion required.

The fact that it is possible to get such agreement does not constitute very strong proof that the spin of the 1.856 Mev. level is zero. Supporting evidence exists in the absence of the gamma-ray corresponding to the 1.856 Mev. transition to the ground state of Cd^{114}. This radiation, if it exists, has an intensity of less than 4×10^{-4} quanta per disintegration (17), a value much less than would be expected were the spin of the 1.856 Mev. level 1 or 2.

Positron Spectrum in Indium^{114}

The existence of a very weak positron component in the decay of In^{114} was first suggested by Boehm and Preiswerk (4). Since their measurements were very tentative, it was felt worth while to determine the yield and end point by coincidence methods. Since the two 0.511 Mev. quanta accompanying positron annihilation are emitted in opposite directions, gamma–gamma coincidences due to annihilation radiation can be observed only when the angle θ formed by

the counters at the source is 180° and the positron yield can be determined directly by comparing the number of gamma–gamma coincidences when θ is not 180° with the number of annihilation quanta coincidences when $\theta = 180°$.

Let $\alpha(= 0.035)$ be the K-capture branching ratio for the cascade gamma rays (17) and f the positron yield. Then, if ϵ_1, ϵ_2, and ϵ_3 represent the intrinsic efficiencies of the anthracene crystals for 0.511, 0.556, and 0.722 Mev. radiation, it can be readily shown that $f = \alpha\delta(\epsilon_2\,\epsilon_3/\epsilon_1^2)N(\pi)/N(\gamma\gamma)_{180}\omega$. In this expression $\delta(= 1.14)$ is a correction factor made necessary because the cascade gammas are not emitted isotropically, while ω is the solid angle subtended by either counter at the source (in a symmetric arrangement). $N(\pi)/N(\gamma\gamma)_{180}$ is the ratio of the number of annihilation coincidences to the number of gamma–gamma coincidences in the 180° position.

The apparatus used for this experiment was the same as that employed for the previous coincidence work. In order to make $N(\pi)/N(\gamma\gamma)_{180}$ as large as possible consistent with reasonable coincidence rates, ω was kept small by placing the two crystals 23.6 cm. apart, with the source midway between them. The source was covered with sufficient brass to stop 1 Mev. positrons and the coincidence rate in the 180° position compared with that for an angle of 167° between the counters. The gamma–gamma rate at 167° was corrected to the 180° position by using the angular correlation function described above. The effect of positrons in the correlation experiment was much less marked since the counters were closer to the source and the source was uncovered. The ratio $(\epsilon_2\epsilon_3/\epsilon_1^2)$ was 1.56 from the known counter efficiencies, $\omega = 0.00186$, and $N(\pi)/N(\gamma\gamma)_{180} = 0.36 \pm 0.03$. Using these data the positron branching ratio is $4 \pm 1 \times 10^{-5}$. The standard deviation expressed in this result has been arbitrarily increased to take into account uncertainties in the branching ratio of the K-capture branch and in the counter efficiencies and solid angles. (The value previously given in Reference (15) should have read 5×10^{-5} while the value in Reference (16) was computed incorrectly using $[N(\pi) + N(\gamma\gamma)]_{180}/N(\gamma\gamma)_{180}$ instead of $[N(\pi)/N(\gamma\gamma)]_{180}$ and hence is roughly four times too large.)

In principle it should be possible to obtain a measure of the positron end point by using a thin source and observing the increase in the number of coincidences due to positron annihilation as the source is covered with successive layers of absorber. In essence this is the reverse of the common aluminum absorption method of determining a beta end point. Since the positron spectrum was too weak to study in the spectrometer available, an attempt has been made to estimate its energy by this method.

The source of indium metal was rolled into a foil 80 mgm./cm.^{2} in thickness and sandwiched between two mica shields 4 mgm./cm.^{2} thick. The movable detector was swung from the 180° position to the 155° position and the flat source oriented so that this detector looked at its surface from the same angle in both positions. This symmetry was necessary to prevent differences in gamma absorption from distorting the measurements. The aluminum absorbers used varied in thickness from 0 to 600 mgm./cm.^{2} though the positrons were all essentially absorbed when 130 mgm./cm.^{2} was placed on each side of the foil.

The data are presented in Fig. 5. The mean value of the annihilation contri-

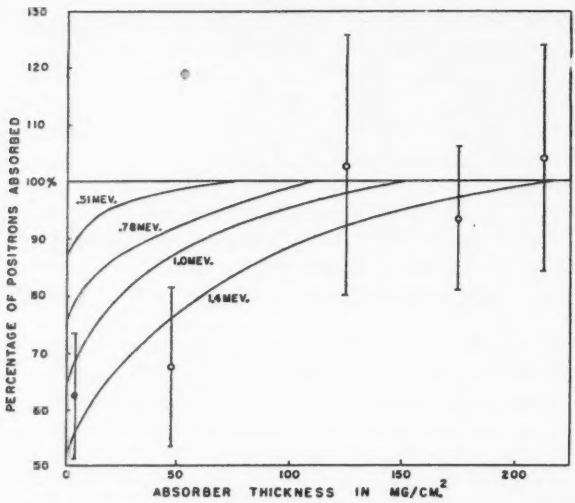

FIG. 5. Positron absorption in aluminum.

bution to the gamma–gamma rate in this geometry was 0.181 ± 0.014 for all absorbers of thickness over 130 mgm./cm.^{2} This value was taken as representing complete stoppage of all positrons in the absorbers and the ratios of the values obtained for each individual position to this value are expressed as percentages in the figure. It is lower than the value given above for a point source because of the large source area (0.5×2.0 cm.) which has a marked effect on the annihilation coincidence rate and very little on the gamma–gamma rate.

The theoretical curves shown were calculated for a plane sheet of active material of infinite extent and thickness 80 mgm./cm.^{2} covered with aluminum absorbers on both sides. First, the distribution of path lengths from all points within the source to the edge of the absorber was computed, and the fraction of betas of range R_0 escaping along such a path of length l taken as $(1 - l/R_0)$. By integration over all paths it was then possible to compute the fraction of homogeneous betas which would escape from the source as a function of their energy. A final integration over the complete positron spectrum calculated from the Fermi theory gave the curves shown in the figure.

It is seen that the experimental points are quite inconsistent with a positron end point near 0.65 Mev. and suggest that the end point lies between 1.0 and 1.4 Mev.

The low specific activity of the material at the time of the experiment and the restriction on the geometric area of the source imposed by the coincidence arrangement made it impossible to use a thinner source which might have given more clear-cut results.

The β^+ component observed in this experiment is presumably due to a transition from the ground state of In^{114} to the ground state of Cd^{114}. However, the

possibility cannot be excluded that some of the observed positrons are created by nuclear pair-production in the $0 \rightarrow 0$ transition from the 1.856 Mev. level of Cd^{114} to the ground state. A theoretical comparison of the lifetime for this transition (8, 27) with that of the competing $E2$ transitions from the 1.856 Mev. level (3) indicates that nuclear pair-production should not account for more than a few per cent of the positron yield. This does not conclusively eliminate this transition as a source of the observed positrons since calculations of this sort are known to be unreliable to several orders of magnitude.

Despite the limitations of this experiment, it does give support to the work of McGinnis (23) who has given the value 2.07 ± 0.2 Mev. for the In^{114}–Cd^{114} mass difference.

DISCUSSION

The four experiments described above provide strong support for the decay scheme shown in Fig. 1 which was originally proposed on the basis of energy and intensity measurements. Although these experiments suggest that the 1.856 Mev. level of Cd^{114} is fed by K-capture from the ground state of In^{114}, the possibility that it is due to a transition from the spin 5 state of In^{114} cannot be ruled out.

The log ft values for the transitions from the ground state of In^{114} to the 0.0, 0.556, 1.278, and 1.856 Mev. levels of Cd^{114} are, respectively, 6.5, > 5.3, 3.4, and 3.4 if one uses 2.07 Mev. for the In^{114}–Cd^{114} mass difference. The probable error of 0.2 in the 2.07 Mev. value introduces an uncertainty of 0.6 into the log ft value for the 1.856 Mev. level and somewhat smaller uncertainties into the others. The value for the β^- decay is 4.4. This means that the transition to the ground state of Cd^{114} is roughly 50 times less probable while that to the two upper levels is about 10 times more probable than the value expected for an allowed transition in indium. This unusual situation exists also in In^{110} where the 2.25 Mev. positron decay goes to a 0.656 level of Cd^{110} (log ft 5.5) while the energetically favored transition to the ground state is missing (12). An assumption that the missing transition is less than 10% of the intensity of the 2.25 Mev. positron group leads to a log $ft > 6.5$ for this transition in In^{110}.

It has been suggested by Dr. M. Goldhaber (11) that a wide variation in ft values between transitions which on the basis of spin and parity assignments are similar may be expected for nuclides containing an almost closed shell. The indium nuclei with 49 protons all fall into this category.

The parities of all the states in Fig. 1 may be expected to be even. This assignment is supported by the results of these and other experiments and is consistent with the proposed shell structure (12) for indium.

ACKNOWLEDGMENTS

The authors are indebted to Dr. R. H. Tomlinson of the Chemistry Department for the separation of Y^{90} from fission products and for his constant interest. They would also like to acknowledge profitable discussions held with Dr. R. M. Steffen, Dr. B. Kinsey, and Dr. M. Goldhaber.

The financial support received from the National Research Council of Canada and the Research Council of Ontario is gratefully acknowledged.

REFERENCES

1. ARFKEN, G. B., BIEDENHARN, L. C., and ROSE, M. E. Phys. Rev. 86: 761. 1952.
2. BELL, R. E., GRAHAM, R. L., and PETCH, H. E. Can. J. Phys. 30: 35. 1952.
3. BLATT, J. M. and WEISSKOPF, V. F. Theoretical nuclear physics. John Wiley & Sons, Inc., New York. 1952. p. 627.
4. BOEHM, F. and PREISWERK, P. Helv. Phys. Acta, 22: 331. 1949.
5. BRADY, E. L. and DEUTSCH, M. Phys. Rev. 78: 558. 1950.
6. CORK, J. M., SHREFFLER, R. G., and FOWLER, C. M. Phys. Rev. 74: 1657. 1948.
7. DEUTSCH, M. Repts. Progress Phys. 14: 196. 1951.
8. DRELL, S. D. Phys. Rev. 81: 656A. 1951, and Oak Ridge National Laboratory Report ORNL-792. 1950.
9. DUNWORTH, J. V. Rev. Sci. Instr. 11: 167. 1940.
10. GARWIN, R. L. Rev. Sci. Instr. 21: 903. 1950.
11. GOLDHABER, M. Private communication.
12. GOLDHABER, M. and HILL, R. D. Revs. Mod. Phys. 24: 179. 1952.
13. HAMILTON, D. R. Phys. Rev. 58: 122. 1940.
14. JOHNS, M. W., COX, C. D., and PETCH, H. E. Trans. Roy. Soc. Canada, III, 45: 174A. 1951.
15. JOHNS, M. W., COX, C. D., and MCMULLEN, C. C. Phys. Rev. 86: 632A, and Errata, 86: 581. 1952.
16. JOHNS, M. W., COX, C. D., DONNELLY, R. J., and MCMULLEN, C. C. Phys. Rev. 87: 1134L. 1952.
17. JOHNS, M. W., WATERMAN, H., MACASKILL, D., and COX, C. D. Can. J. Phys. 31: 225. 1953.
18. KINSEY, B. B. and BARTHOLOMEW, G. A. Phys. Rev. 90: 355A. 1953.
19. KLEMA, E. D. and MCGOWAN, F. K. Phys. Rev. 87: 524L. 1952.
20. LAWSON, J. L. and CORK, J. M. Phys. Rev. 57: 982. 1940.
21. LING, D. S. and FALKOFF, D. L. Phys. Rev. 76: 1639. 1949.
22. LLOYD, S. P. Phys. Rev. 81: 161L. 1951; 83: 716. 1951.
23. MCGINNIS, C. L. Phys. Rev. 81: 734. 1951.
24. MAIENSCHEIN, F. and MEEM, J. L. Phys. Rev. 76: 899. 1949.
25. MEI, J. Y., MITCHELL, A. C. G., and ZAFFARANO, D. J. Phys. Rev. 76: 1883L. 1949.
26. NUSSBAUM, R. H. and VAN LIESHOUT, R. Physica, 19: 451L. 1953.
27. OPPENHEIMER, J. R. and SCHWINGER, J. S. Phys. Rev. 56: 1066L. 1939.
28. STEFFEN, R. M. Phys. Rev. 83: 166L. 1951.
29. STEFFEN, R. M. and ZOBEL, W. Phys. Rev. 88: 170A. 1952.
30. THORNTON, W. A., DER MATEOSIAN, E., MOTZ, H. T., and GOLDHABER, M. Phys. Rev. 86: 604A. 1952.
31. WU, C. S. Phys. Rev. 59: 481. 1941.

PHOTONEUTRON CROSS SECTIONS OF SOME ELEMENTS[1]

By J. Goldemberg[2] and Leon Katz

ABSTRACT

The neutron yield from photo-reactions in nine elements has been measured as a function of the maximum energy of the University of Saskatchewan Betatron. Cross sections are given for each of the reactions as calculated from these data. The integrated cross sections are compared with theoretical sum-rule predictions of Levinger and Bethe and good agreement is obtained with $x = \frac{1}{2}$. The data support the conclusions reached in a preceding paper by Montalbetti, Katz, and Goldemberg. The competition between (γ, n) and (γ, p) reactions in chromium and in nickel is analyzed in the light of these experimental results. Good agreement with statistical theory is obtained in both cases.

INTRODUCTION

In a recent paper Montalbetti, Katz, and Goldemberg (21) have presented measurements of neutron yields and (γ, n) cross sections for some 22 elements, using a method which detected the neutrons emitted in these reactions. This work has been continued and some further measurements are here reported. These cover the elements lithium, chlorine, calcium, chromium, vanadium, nickel, bromine, lanthanum, and tantalum. Measurements by residual activity methods on some isotopes of chromium are also included.

Particular emphasis has been given to nickel, since the (γ, p) cross section for the element, as well as the (γ, n) cross section in the isotope Ni^{58}, has been measured previously. Using a subtraction procedure whose validity has been demonstrated (7), it is possible to obtain the (γ, n) cross section in Ni^{60}. A detailed computation of the competition between neutron and proton emission in Ni^{58} and Ni^{60} then gives the (γ, p) cross section of the natural element which is compared to the measured (γ, p) cross section.

APPARATUS AND EXPERIMENTAL PROCEDURE

The apparatus used in these measurements has been previously described in Reference (21). The same calibration procedure was also followed in the present measurements.

During our early tests on the sensitivity of the system to different neutron energies, some of the yield curves previously measured by residual activity were checked and found to have somewhat altered in shape. This problem was not pursued further at that time, but has now been more fully investigated, and is presented as an appendix to this paper.

Though the full implications of these changes in activation curve shape are not understood, their effect on our results (cross section curves) is expected to be within the accuracy of the present status of the experimental techniques used in this field.

A further indication of the reproducibility of activation curve shape is obtained by comparing measurements taken in different laboratories on the

[1] *Manuscript received August 14, 1953.*
Contribution from the Department of Physics, University of Saskatchewan, Saskatoon, Sask.
[2] *On leave of absence from the Departamento de Fisica, Universidade de Sao Paulo, Sao Paulo, Brazil.*

same element. Such a comparison has already been presented for phosphorus (21). A similar comparison of the activation curve of tantalum will be presented in the appendix.

Corrections for attenuation of the photon spectrum in the finite sized samples used were applied as outlined in Reference (21) and the cross section curves were calculated using the photon difference (18) method.

RESULTS

The measured neutron yield curves and the resulting cross sections are presented in the following diagrams and the pertinent photonuclear data are summarized in Table III. Results for each of the elements will be discussed separately, and for clarity, the isotopic abundance of each of the elements as well as their (γ, n) thresholds will be given at the beginning of each discussion. All thresholds were calculated using the most recent mass data.

Lithium (Li^7: 92.6%, 6.78; Li^6: 7.35%, 6.76) Fig. 1(*a*) and (*b*)

This is the lightest element in which we have studied the photo-reaction process. The cross section presents a broad peak indicating that even for such a light element, the usual picture of photonuclear processes applies (8).

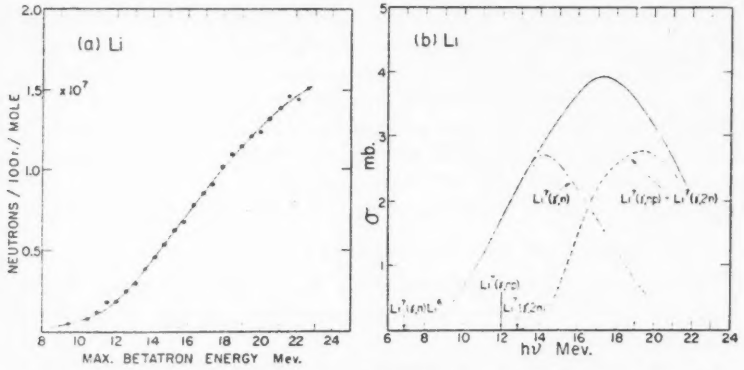

FIG. 1(*a*) and (*b*). Neutron yield and cross section of lithium.

Thresholds for the (γ, np) and $(\gamma, 2n)$ reactions are shown in Fig. 1(*b*). Probably a large part of the measured cross section is due to these reactions and a reasonable separation between them and $\sigma_{\gamma n}$ is indicated by the dotted lines. Since both the $(\gamma, 2n)$ and the $Li^7(\gamma, np)He^5 \rightarrow n + He^4$ reactions give rise to two neutrons each, the dashed curve of Fig. 1(*b*) shown for these two reactions needs to be divided by two to obtain their true combined cross section.

The reaction $Li^7(\gamma, p)He^6$ has recently been measured by residual activity in this laboratory (13). Since there is no Coulomb barrier to speak of in lithium, it should be expected that as many protons as neutrons would be emitted, allowing for the difference in thresholds. A comparison of the results shows that the (γ, n) and (γ, p) reactions in lithium are of the same order of magnitude.

Chlorine (Cl^{35}: 75.4%, 13.7; Cl^{37}: 24.6%, 11.6) Fig. 2(*a*) and (*b*)

This measurement gives only information on natural chlorine since it is not possible to separate the contributions from the two isotopes. Sodium chloride was used as the sample material, with the activation curve for chlorine being obtained by subtraction. The reliability of this procedure has been tested previously (7).

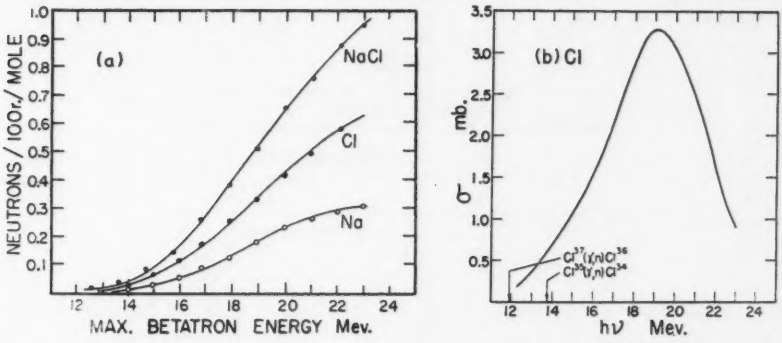

FIG. 2(*a*) and (*b*). Neutron yield and cross section of chlorine.

Calcium (Ca^{40}: 96.9%, 15.8; Ca^{42}: 0.64%, 12.7; Ca^{43}: 0.14%, 8.0; Ca^{44}: 2.1%, 11.4) Fig. 3(*a*) and (*b*)

The activation curve presents special features. An analysis of the thresholds of the different isotopes for the (γ, n) process together with isotopic abundance considerations shows that the initial bump below 17 Mev. must be attributed mainly to Ca^{44} and Ca^{42}, since Ca^{43} is an extremely low abundance isotope.

The cross section for the $Ca^{40}(\gamma, n)Ca^{39}$ reaction has been measured by detecting the activity of the residual nuclei by Summers-Gill *et al.* (23) and

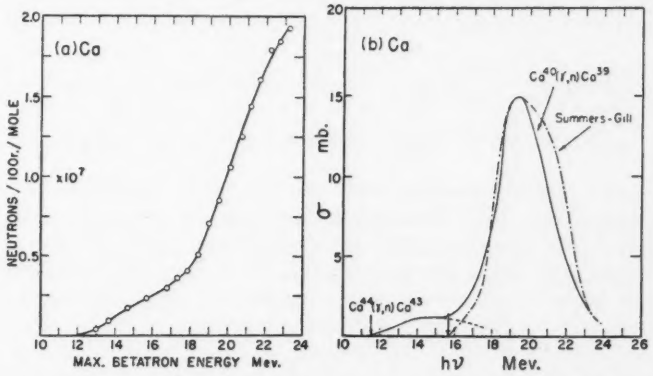

FIG. 3(*a*) and (*b*). Neutron yield and cross section of calcium. The cross section obtained for Ca^{40} by residual activity methods is indicated.

is shown in Fig. 3(*b*) by the dashed curve. The two measurements are in excellent agreement. Subtracting this curve from our results, we obtain what is essentially the (γ, n) cross section for the Ca^{44} isotope. It can be seen that this isotope has a peak (γ, n) cross section out of all proportion relative to the main isotope Ca^{40}. The abundance ratio is $\simeq 1/50$ whereas the peak cross section ratio is 1/13. This discrepancy may be explained on the basis of (γ, n) versus (γ, p) thresholds in the isotopes involved. These thresholds are given in Table I.

TABLE I

THRESHOLDS FOR (γ, n) AND (γ, p) REACTIONS IN THE ISOTOPES OF CALCIUM

Isotope	Threshold (Mev.)	
	(γ, n)	(γ, p)
Ca^{40}	15.8	8.1
Ca^{44}	11.4	11.6

Chromium (Cr^{50}: 4.4%, 13.4; Cr^{52}: 83.7%, 11.54; Cr^{53}: 9.5%, 7.75; Cr^{54}: 2.4%, 10.20) Fig. 4(*a*) and (*b*)

The cross section for chromium presents a peculiar shape owing to contributions of small percentage isotopes.

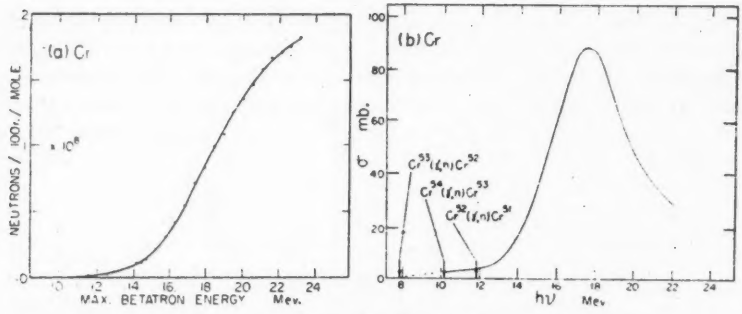

FIG. 4(*a*) and (*b*). Neutron yield and cross section of chromium.

In Fig. 5(*a*) and (*b*) are shown the activation and cross section curves for the reaction $Cr^{53}(\gamma, p)V^{52}$ obtained by detecting the residual activity. The same data on the reaction $Cr^{50}(\gamma, n)Cr^{49}$ also obtained by residual activity methods are presented in Fig. 6(*a*) and (*b*). The absolute determination of the yields was made by comparison to copper using our usual procedures (7).

A comparison of our results with statistical theory (1, 2, 3) and with the results of Wäffler and Hirzel (24) is shown in Table II. All calculations refer to 16.6 Mev. excitation energy; this energy was chosen as representing the average energy of the γ-rays used in the experiment of Wäffler and Hirzel.

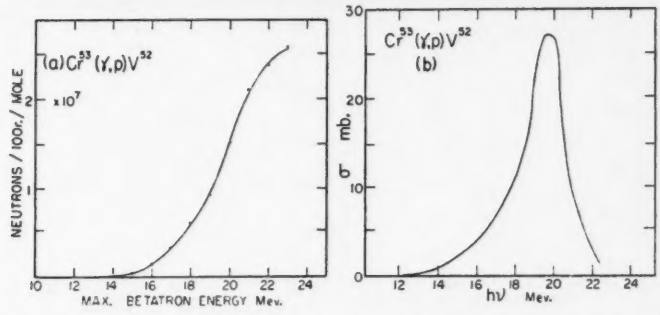

FIG. 5(*a*) and (*b*). Activation curve and cross section of the reaction $Cr^{53}(\gamma, p)V^{52}$ as obtained by residual activity methods.

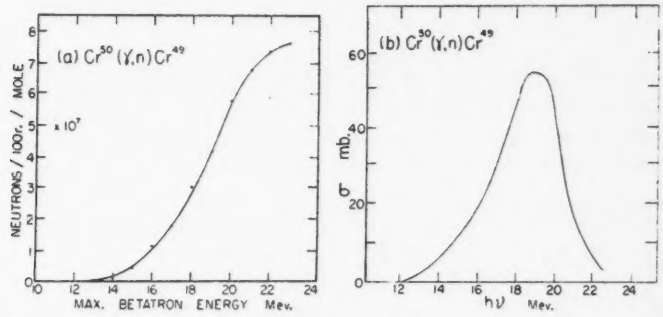

FIG. 6(*a*) and (*b*). Activation curve and cross section of the reaction $Cr^{50}(\gamma, n)Cr^{49}$ as obtained by residual activity methods.

TABLE II

COMPARISON OF EXPERIMENTS IN CHROMIUM WITH STATISTICAL THEORY, AT 16.6 MEV.

Reaction	Ratio to $Cr^{53}(\gamma, p)V^{52}$		
	Experiment	Theory	Wäffler and Hirzel
$Cr^{50}(\gamma, n)Cr^{49}$	.216	.380	.324
$Cr^{52}(\gamma, n)Cr^{51}$	.070	.083	—

All thresholds for the reactions involved have been calculated using masses from Collins, Nier, and Johnson (4) and Duckworth (6). The theoretical ratio obtained by Wäffler and Hirzel for Cr^{50} is lower than ours, owing probably to the use of wrong thresholds.

The theoretical ratio for Cr^{53} is low by a factor of 10.

Vanadium (V^{50}: 0.24%, 7.9; V^{51}: 99.76%, 10.8) Fig. 7(*a*) and (*b*)

This is practically a 100% isotope; the activation curve and cross section present the usual features.

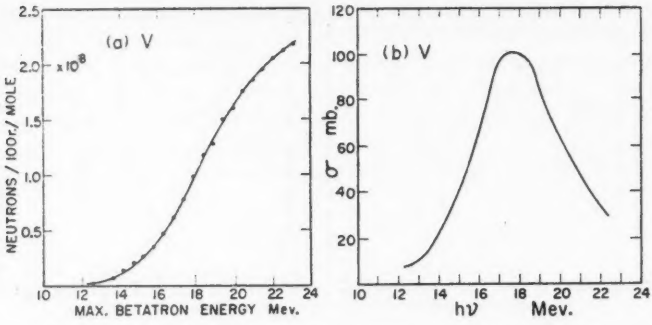

FIG. 7(*a*) and (*b*). Neutron yield and cross section of vanadium.

Nickel (Ni^{58}: 67.9%, 11.7; Ni^{60}: 26.2%, 11.6; Ni^{61}: 1.2%, 7.8; and Ni^{62}: 3.7% 10.86) Fig. 8(*a*) and (*b*)

As shown in Fig. 8(*b*), the cross section for nickel very clearly indicates contributions from the main isotopes. Subtracting the contribution from Ni^{58} measured by Katz *et al.* (17), the remaining part must be attributed almost exclusively to Ni^{60}. The contribution of the small percentage isotopes cannot be separated here.

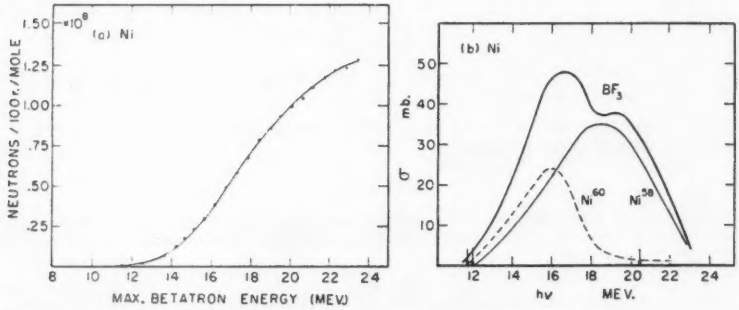

FIG. 8(*a*) and (*b*). Neutron yield and cross section of nickel. The cross section of the reaction $Ni^{58}(\gamma, n)Ni^{57}$ obtained by residual activity methods is indicated.

The cross section for the emission of protons has been measured for the natural element by Halpern and Mann (9). We calculated the number of protons emitted by nickel, at all energies of interest, assuming the validity of the statistical theory and using the same procedure as Heidmann and Bethe (14). The thresholds for (γ, n) reactions used were as above and for (γ, p) are those given by Heidmann and Bethe (14) in their paper. This computation was done separately for Ni^{58} and Ni^{60} and the results combined according to isotopic abundance to give that of the natural element.

The results are shown in Fig. 9; the curve of Halpern and Mann seems to be displaced to the right by about 2 Mev.; we do not attribute much signifi-

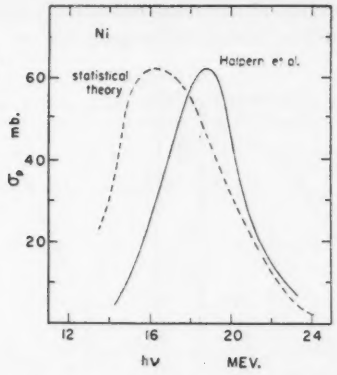

FIG. 9. Cross section for the (γ, p) reaction in nickel as obtained by Halpern et al. (9) and as calculated from statistical theory using the data of his work.

cance to this because of the results discussed in the appendix. Aside from this displacement, the two curves are in good agreement in absolute value.

Bromine (Br^{79}: 50.6%, 10; Br^{81}: 49.4%, 10.2) Fig. 10(*a*) and (*b*)

The thresholds for both isotopes are quite close in this case and no obvious separation of the contributions of each is possible. The (γ, n) cross section for the reaction Br^{81} has been measured by residual activity methods (19) and is plotted in Fig. 10(*b*); subtracting this from the total, we get the (γ, n) cross section for the isotope Br^{79}.

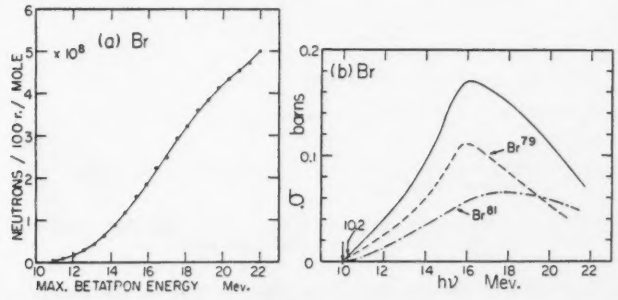

FIG. 10(*a*) and (*b*). Neutron yield and cross section of bromine. The cross section of the (γ, n) reaction in Br^{81} as obtained by residual activity is indicated.

Lanthanum (La^{138}: 0.089%; La^{139}: 99.9%, 8) Fig. 11(*a*) and (*b*)

Lanthanum is practically a 100% isotope, so only the characteristics of La^{139} are shown in Fig. 11(*a*) and (*b*). The presence of a contribution of a $(\gamma, 2n)$ reaction is quite obvious in the cross section curve. Knowledge of the cross section for the reaction $La^{139}(\gamma, n)La^{138}$ would make it possible to separate out this contribution.

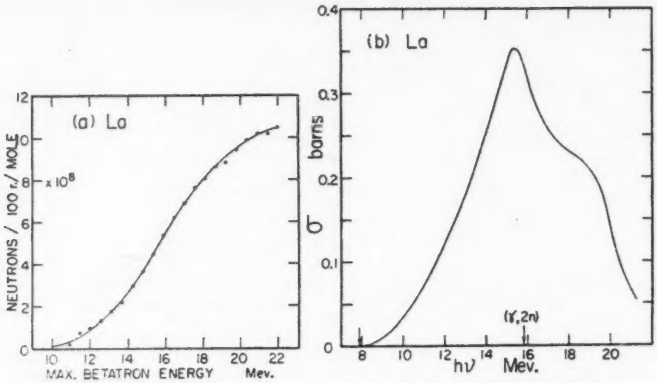

FIG. 11(*a*) and (*b*). Neutron yield and cross section of lanthanum.

Tantalum (Ta^{181}; 100%; 7.7) Fig. 12(*a*) and (*b*)

This is a 100% isotope element for which the (γ, n) reaction has been measured by residual activity (16). Subtracting this (γ, n) cross section from

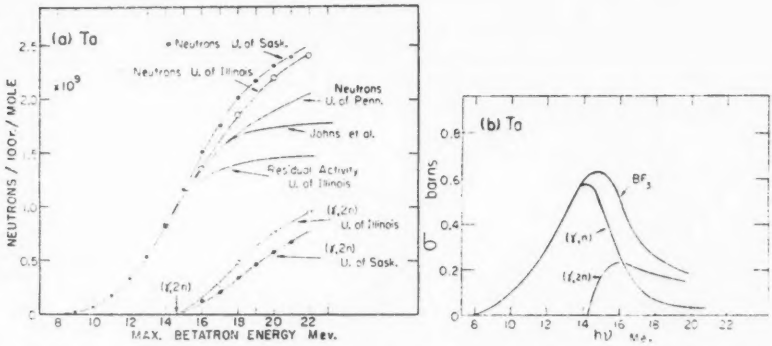

FIG. 12(*a*) and (*b*). Neutron yield and cross section of tantalum. Data obtained by residual activity and neutron detection by other investigators are shown.

the present curve the contribution from the (γ, $2n$) process, starting at 14 Mev., is obtained. These results substantiate those obtained by Hanson and Whalin (11).

DISCUSSION OF RESULTS

The relevant characteristics of the cross sections obtained in this work are listed in Table III. In Fig. 13 are plotted the integrated cross sections, together with results reported previously for a number of elements (21). The present results reinforce the conclusions obtained previously about the validity of the sum rules, namely that for high Z the emission of neutrons

accounts for most of the integrated cross section for absorption of photons and that $x = 0.5$ seems to be a reasonable choice for the fraction of exchange-

TABLE III

CHARACTERISTICS OF PHOTONUCLEAR CROSS SECTIONS

Element	Half-width		E_m (Mev.)	σ_m (barns)	Integrated σ (Mev.-barn)			
	(γ, n)	For element			(γ, n)	(γ, p)	$(\gamma, 2n)$	$(\gamma, n) + (\gamma, np) + 2(\gamma, 2n)$
Li		9.8	17.5	.004				0.020*
Cl		5.8	19.0	.033	0.21			
Ca^{40}	3.2		19.5	.015	0.06			
Cr		5.8	17.5	.105	0.60			
Cr^{53}		2.3(γ,p)	19.7	.027		0.09		
Cr^{50}	3.6		19.0	.056	0.25			
V^{51}	5.4		17.7	.100	0.59			
Ni		6.5	16.5	.050	0.34			
Ni^{60}	4		16.0	.095	0.42			
Br		7.0	16.0	.175	1.3			
Br^{79}	6		16.0	.220	1.3			
La^{138}	5		15.5	.350	2.2			
Ta	4.6	6.0	15	.63	2.8		0.6	4.1

All cross sections corrected for isotopic abundance.
**Integrated cross section to peak position.*

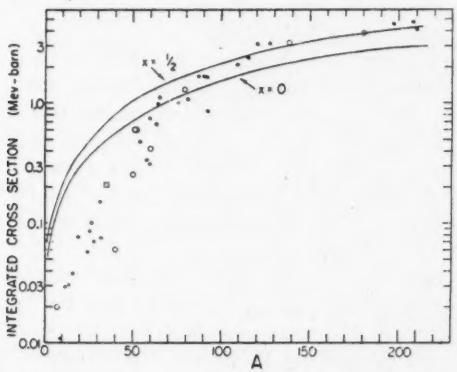

FIG. 13. Experimental values of the integrated cross sections given in Table III. Data contained in Reference (21) are included. The solid lines represent theoretical predictions.

force in the interaction of neutrons and protons. For low Z besides the contribution to $\int \sigma . dE$ from the (γ, p) process, a substantial absorption of photons must occur at higher or lower energies than those covered in this experiment.

The results obtained for Ni^{60} and the comparison with the (γ, p) cross section obtained by Halpern and Mann constitute a direct comparison between competition for emission of neutrons and protons in the same nucleus.

The agreement obtained in this comparison, in a medium-weight nucleus,

for which some hope exists for the applicability of the statistical model, is quite contrary to the results published by Wäffler and Hirzel. Further work on the same problem with many other elements is necessary before any definite conclusion may be reached.

APPENDIX

During the course of some experiments performed recently we noticed that the shape of the activation curve for the reaction $C^{12}(\gamma, n)C^{11}$ was different from that obtained previously in this laboratory (12, 15). All these experiments were made measuring the 20 min. activity induced in carbon from this reaction. We also found that activation curves for the same elements measured in different laboratories showed similar discrepancies in shape.

In Fig. 12(*a*) we show the results for tantalum from the University of Illinois (11) and the University of Saskatchewan measurements. Measurements on the neutron yield of tantalum made at the University of Pennsylvania (10) are also included on the same graph. All results have been normalized to ours at 14 Mev. It will be seen that the three neutron yield curves taken at the three laboratories are in disagreement above 14 Mev. Similarly the residual activity curves obtained at Illinois and Saskatchewan (11, 16) are in disagreement. However, the differences between the neutron yield curve and the residual activity curve as plotted in the lower part of the diagram are in fair agreement. A similar though smaller discrepancy is found in the case of Cu^{63}, when we compare the measurements at Illinois (5), Case Institute of Technology (20), and Saskatchewan (16).

It would be very tempting to attribute the difference between the results taken in different laboratories to small changes in the monitoring procedure of the γ-ray flux. This explanation is, however, partially ruled out since similar differences have been found between measurements taken months apart in this laboratory using the same monitoring procedure. For this reason it was felt that some more fundamental point was in question and measurements were undertaken to find what characteristics of the betatron could give rise to changes in the activation curves.

We suspected that the explanation for the observed effect might result from changes in bremsstrahlung spectrum and for this reason it was felt that the high threshold of carbon should accentuate the observed effects. Activation curves for the reaction $C^{12}(\gamma, n)C^{11}$ were measured under different conditions, such as changes in stable orbit size and slight displacements of the donut.

The only noticeable effect was found when different donuts were used. This result is not altogether unexpected, considering the rather "odd" shape of the conventional "targets" used in betatrons. As shown in a recent article by workers at the National Bureau of Standards (22) a "target" consisting of a wire 60 mils in diameter behaves as far as bremsstrahlung radiation is concerned as a target of thickness between 10 and 20 mils. Thus it is not unlikely that small differences between the donuts in different laboratories and differences in expander pulse have the effect of producing radiation of

different composition. It should be mentioned incidentally that a thick target increases the number of soft photons relative to the number of high-energy photons. This effect depresses the high-energy portion of the activation curve since for a given radiation dose there are fewer high-energy photons and thus less activity is induced.

We should remark that the University of Saskatchewan curves as shown in Fig. 12 are the steepest of all the measured curves; this would seem to indicate that the spectrum of our machine is closer to a thin target spectrum. Moreover, owing to the lack of our knowledge of the spectrum of each betatron at different times, cross sections cannot be considered as known to better than 15 or 20% in absolute value; to this we have to add the uncertainty of the method of measuring activities.

In conclusion, we should emphasize that considerable care has to be taken when comparing data of different laboratories, particularly if differences between activation curves are to be used to evaluate higher processes, such as $(\gamma, 2n)$, as outlined in our "subtraction" method (7).

Fortunately cross section shapes are not extremely sensitive to changes in activation curve shape. We estimate that in spite of the difficulties presented above the peak position of the cross section curve and its width at half-maximum are known to better than 1 Mev.

REFERENCES

1. ALMY, G. M. and BUTLER, W. A. Phys. Rev. 91: 58. 1953.
2. BLATT, J. M. and WEISSKOPF, V. F. Technical Report No. 42. M.I.T. May, 1950.
3. BLATT, J. M. and WEISSKOPF, V. F. Theoretical nuclear physics. John Wiley and Sons, Inc., New York. 1952. p. 373.
4. COLLINS, T. L., NIER, A. O., and JOHNSON, W. H., JR. Phys. Rev. 86: 408. 1951.
5. DIVEN, B. C. and ALMY, G. M. Phys. Rev. 80: 407. 1950.
6. DUCKWORTH, H. E. Private communication.
7. GOLDEMBERG, J. and KATZ, L. Phys. Rev. 89: 1300. 1953.
8. GOLDHABER, M. and TELLER, E. Phys. Rev. 74: 1046. 1948.
9. HALPERN, J. and MANN, A. K. Phys. Rev. 83: 370. 1951.
10. HALPERN, J., NATHANS, R., and MANN, A. K. Phys. Rev. 88: 679. 1952.
11. HANSON, A. O. and WHALIN, E. A. Phys. Rev. 89: 324. 1953.
12. HASLAM, R. N. H., JOHNS, H. E., and HORSLEY, R. J. Phys. Rev. 82: 270. 1951.
13. HASLAM, R. N. H. and ROBB, D. S. Private communication.
14. HEIDMANN, J. and BETHE, H. A. Phys. Rev. 84: 274. 1951.
15. HORSLEY, R. J. Ph.D. Thesis, University of Saskatchewan, Saskatoon, Sask. 1953. (Unpublished.)
16. JOHNS, H. E., KATZ, L., DOUGLAS, R. A., and HASLAM, R. N. H. Phys. Rev. 80: 1062. 1950.
17. KATZ, L., BAKER, R. G., HASLAM, R. N. H., and DOUGLAS, R. A. Phys. Rev. 82: 271. 1951.
18. KATZ, L. and CAMERON, A. G. W. Can. J. Phys. 29: 578. 1951.
19. KATZ, L., PEASE, L., and MOODY, H. Can. J. Phys. 30: 476. 1952.
20. KRON, V. E. and SHRADER, E. F. Phys. Rev. 87: 685. 1952.
21. MONTALBETTI, R., KATZ, L., and GOLDEMBERG, J. Phys. Rev. 91: 659. 1953.
22. MOTZ, J. W., MILLER, W., and WYCKOFF, H. O. Phys. Rev. 89: 968. 1953.
23. SUMMERS-GILL, R. G., HASLAM, R. N. H., and KATZ, L. Can. J. Phys. 31: 70. 1953.
24. WÄFFLER, H., and HIRZEL, O. Helv. Phys. Acta, 21: 200. 1948.

ELECTRON CAPTURE BY SLOW SINGLY CHARGED HELIUM IONS IN HELIUM[1]

By J. David Jackson

ABSTRACT

The capture of electrons by slow singly charged helium ions passing through helium gas is discussed theoretically. Calculations of the capture cross section for incident ion energies from 200 ev. to 100 kev. are made using an impact parameter method due to Kohn. In this energy interval the computed cross section is found to be fitted very closely by the empirical expression $(\sigma/\pi a_0^2) = 7.94 - 2.35 \log_{10} E(\text{kev.})$. The results are compared with recent experimental data. The agreement between theory and experiment is good, except for the data of Keene.

1. INTRODUCTION

In recent years considerable precise experimental work has been done on the process of charge exchange or electron capture between atoms moving with relative kinetic energies from a few electron volts up to hundreds of kilovolts (6, 8, 9, 14, 17).* As a result, renewed interest has been aroused in the theoretical calculation of the cross sections for electron capture, with a view to the improvement of the earlier work of Brinkman and Kramers (3), Massey and Smith (12), and others. New calculations for electron capture by protons in hydrogen in the energy range above 25 kv. have been made independently by Jackson and Schiff (7), and Bates and Dalgarno (1); good agreement with experiment (9, 14, 17) was obtained. At lower energies different methods of calculation are necessary owing to the adiabatic nature of the collisions. Recently the electron capture by protons from hydrogen atoms at low energies has been treated by Dalgarno and Yadav (4), using the method of "perturbed stationary states", and by Kohn (10) who employed a simple "impact parameter" method. Independently Bates, Massey, and Stewart (2), in a general paper on inelastic and charge transfer collisions at low energies, have discussed an impact parameter method similar to that of Kohn. They also showed that the impact parameter method is essentially equivalent to the method of perturbed stationary states, a result which was obtained independently by the author (unpublished).

The present paper is concerned with the application of Kohn's impact parameter method to the simplest adiabatic electron capture problem for which there are experimental data, the capture of electrons by singly-charged helium ions passing through helium. (The calculations for the simpler problem of protons in hydrogen at low energies cannot be compared with experiment because they ignore molecular effects in the target material, effects which are crucial at low energies.) Massey and Smith (12) and Dallaporta and Bonfiglioli (5) gave a theoretical discussion of the electron capture by helium ions in helium by means of the perturbed stationary state method. In spite of this earlier work it was felt

[1] *Manuscript received June 24, 1953.*
Contribution from the Department of Mathematics, McGill University, Montreal, Quebec.
A preliminary report of this work was presented before the Royal Society of Canada, June 1–3, 1953, at London, Ontario.

*For references to earlier work on electron capture see the book by Massey and Burhop (11).

worth while to re-examine this particular problem by a simpler method, especially since there were new experiments at energies not covered by the earlier calculations, and since Massey and Smith had made some rough approximations whose accuracy is hard to assess.*

2. CROSS SECTION FOR RESONANCE ELECTRON CAPTURE

For the resonance charge exchange between two like atoms (e.g. He^+ in He) moving at relative velocities small compared to the orbital velocities of the electrons, the cross section can be written as:

$$\sigma = 2\pi \int_0^\infty P(p)\, p\, dp \tag{1}$$

where $P(p)$ is the probability of charge exchange for the two atoms passing each other at an impact parameter p. $P(p)$ is given by equation [134] of Bates, Massey, and Stewart (2), or in a somewhat simplified form by Kohn (10):

$$P(p) = \sin^2 \tfrac{1}{2}(\eta_+ - \eta_-) \tag{2}$$

where

$$\frac{\eta_+ - \eta_-}{2} = \frac{v_0}{v} \int_p^\infty \frac{R}{(R^2 - p^2)^{\frac{1}{2}}} [E_+(R) - E_-(R)]\, dR.$$

Here v is the relative velocity of the two atoms, v_0 is the Bohr orbit velocity ($v_0 = e^2/\hbar = c/137$), p is the impact parameter in units of the Bohr radius a_0, R is the internuclear separation in the same units, $E_\pm(R)$ are the two lowest molecular potential energy curves for the appropriate molecular ion in units of (e^2/a_0). (In the present case it is the helium molecular ion He_2^+.)

The differences between the present equation [2] and equation [134] of Bates, Massey, and Stewart (2) are not significant in the present problem provided the velocity is such that $v \gg (m/M)v_0$ (i.e. for all energies above 1 ev.).

A characteristic result appears from equations [1] and [2]. The integral in [2] is of order unity for small p, so that for $v \ll v_0$, $\frac{1}{2}(\eta_+ - \eta_-)$ is very large. This means that $P(p)$ oscillates very rapidly between zero and unity for small values of p. In computation it is often adequate to break the range of integration involved in [1] into two regions, $0 \leqslant p \leqslant p^*$ and $p^* \leqslant p < \infty$, where p^* is chosen so that $\frac{1}{2}(\eta_+ - \eta_-)$ is equal to 2π or 4π, for example. The integration between 0 and p^* is approximated by using the average value of $P(p)$, while the integration beyond p^* is done numerically. Thus

$$\frac{\sigma}{\pi a_0^2} \simeq \tfrac{1}{2}(p^*)^2 + 2\int_{p^*}^\infty P(p)\, p\, dp \tag{3}$$

where p is in units of a_0. For $v \backsim v_0$, it is necessary to do the complete integration in [1] numerically.

Two comments may be made in passing. The first is that it is characteristic

* *Note added in proof: A paper by O. B. Fursov, "Resonance exchange of ions in slow collisions", Zhur. Eksptl. i. Teoret. Fiz. 21: 1001. 1951, has recently come to the author's attention. Fursov develops the same results as Kohn, and by crude estimation of the molecular potential energy curves at large nuclear separations obtains rough values for the charge exchange cross sections. For helium ions in helium he gets a cross section in the energy range 100 ev. to 1 kev. which is about one and one half times that found in the present paper.*

of the adiabatic resonance electron capture process that all that is needed is the molecular potential energy curves for the lowest symmetric and antisymmetric states of the appropriate molecular ion. Once these are available the calculation is relatively simple. The other comment is that in addition to the resonance electron capture there are other, nonresonance, captures which leave the captured electron in an excited state. These nonresonance captures are small in comparison with the resonance capture, and will be neglected in subsequent comparison with experiment.

3. ELECTRON CAPTURE BY SLOW HELIUM IONS IN HELIUM

The capture of electrons by singly charged helium ions in helium gas has been investigated experimentally by Hasted (6) and others (11) at energies below one kilovolt, and by Keene (9) and others (11) in the kilovolt region. The most recent experimental data are shown in Fig. 2 (a graph of the often contradictory early experiments is given on p. 519 of Reference (11)). The theoretical curve computed on the basis of the perturbed stationary state method by Massey and Smith (12) and Dallaporta and Bonfiglioli (5) is also shown in Fig. 2.

Using the impact parameter method given in section 2 we have calculated this cross section for incident ion energies from about 200 ev. to 100 kev. (where $v = v_0$). In order to evaluate $P(p)$ we need to know the molecular energies $E_\pm(R)$ of the helium molecular ion. These have been evaluated approximately by Pauling (13) many years ago. The results given in his paper are adequate for our purposes, especially as all we need are differences between the two energies. By making use of the values of $E_\pm$ given by Pauling, and the values of $E_\pm(0)$ which can be obtained by symmetry arguments from the atomic energy levels

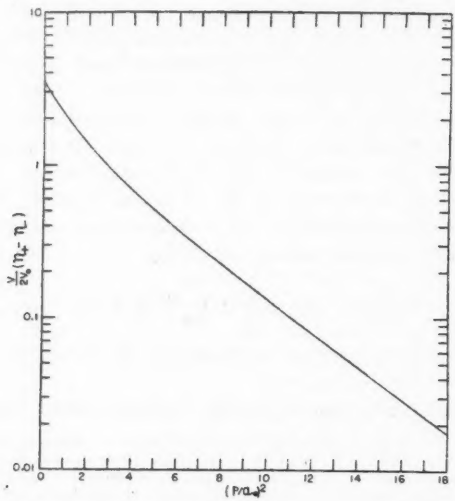

FIG. 1. $v(\eta_+ - \eta_-)/2v_0$ for helium ions in helium as a function of the square of the impact parameter $(p/a_0)^2$.

of the beryllium atom, it was possible to evaluate the integral appearing in [2] for impact parameters from 0 to $4a_0$. This function is plotted versus $(p/a_0)^2$ in Fig. 1. The values for $(p/a_0)^2$ greater than about 12 are somewhat uncertain owing to lack of knowledge of $E_{\pm}(R)$, and so limit the cross section calculations to energies greater than about 200 ev. For a given value of (v/v_0) the values of $(\eta_+ - \eta_-)/2$ versus p can be easily found from Fig. 1, and so $P(p)$ evaluated. Then the integration indicated in [1] (or [3]) is performed to give the cross section σ. In the interval between 200 ev. and 100 kev. the cross section was found empirically to fit very closely the formula, $(\sigma/\pi a_0^2) = 7.94 - 2.35 \log_{10} E$ (kev.).

The resulting curve for the charge exchange cross section is compared with recent experiment and earlier theoretical work in Fig. 2. The agreement with the

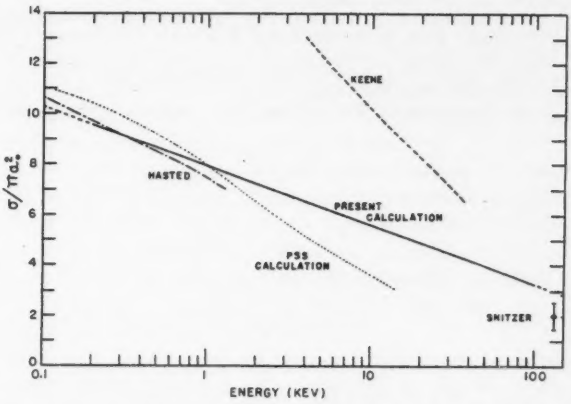

FIG. 2. Cross section for electron capture by singly charged helium ions passing through helium in units of πa_0^2 (0.88×10^{-16} cm.^{2}) as a function of the incident ion energy in kev.

work of Hasted (6) below 1 kev. is seen to be good. The disagreement between theory and the data of Keene (9) is marked. It could be argued that the impact parameter method must begin to fail above a few thousand electron volts energy since the velocity is approaching v_0. However, Keene's data obviously do not join on to Hasted's data at lower energies, while the theoretical curve is in good agreement there. In addition, a preliminary measurement at 131 kev. by Snitzer (16) gives a value of $(2 \pm 0.5)\pi a_0^2$, in good enough agreement with the extrapolated value of $3.0\ \pi a_0^2$ from the present calculations. A further argument for the approximate validity of the present calculation in the region from 10 to 100 kev. is that a rough Born approximation estimate (valid above 100 kev.) by Schiff (15) gives a value of $3.5\ \pi a_0^2$ at 100 kev., very close to the value of $3.2\ \pi a_0^2$ obtained here. The differences between the perturbed stationary state calculations and the present work, with its somewhat better agreement with Hasted's data, can probably be attributed to the approximations made by Massey and Smith (12) in the course of their calculations.

The author wishes to thank Dr. W. Kohn for making known to him the adiabatic impact parameter method before publication.

REFERENCES

1. BATES, D. R. and DALGARNO, A. Proc. Phys. Soc. (London), A, 65: 919. 1952.
2. BATES, D. R., MASSEY, H. S. W., and STEWART, A. L. Proc. Roy. Soc. (London), A, 216: 437. 1953.
3. BRINKMAN, H. C. and KRAMERS, H. A. Proc. Acad. Sci. (Amsterdam), 33: 973. 1930.
4. DALGARNO, A. and YADAV, H. N. Proc. Phys. Soc. (London), A, 66: 173. 1953.
5. DALLAPORTA, N. and BONFIGLIOLI., P. Commentationes Pontif. Acad. Sci. 7: 141. 1943.
6. HASTED, J. B. Proc. Roy. Soc. (London), A, 205: 421. 1951.
7. JACKSON, J. D. and SCHIFF, H. Phys. Rev. 89: 359. 1953.
8. KANNER, H. Phys. Rev. 84: 1211. 1951.
9. KEENE, J. P. Phil. Mag. 40: 369. 1949.
10. KOHN, W. Phys. Rev. 90: 383A. 1953.
11. MASSEY, H. S. W. and BURHOP, E. H. S. Electronic and ionic impact phenomena. Oxford University Press, New York. 1952.
12. MASSEY, H. S. W. and SMITH, R. A. Proc. Roy. Soc. (London), A, 142: 142. 1933.
13. PAULING, L. J. Chem. Phys. 1: 56. 1933.
14. RIBE, F. Phys. Rev. 83: 1217. 1951.
15. SCHIFF, H. Ph.D. Thesis, McGill University, Montreal, Quebec. 1953.
16. SNITZER, E. Phys. Rev. 89: 1237. 1953.
17. WHITTIER, A. C. Ph.D. Thesis, McGill University, Montreal, Quebec. 1952.

AN ATOMIC MASS STUDY OF NUCLEAR SHELL STRUCTURE IN THE REGION $82 < n < 126$[1]

By Benjamin G. Hogg[2] and Henry E. Duckworth

ABSTRACT

A number of new atomic masses are reported in the region $82 < n < 126$ and are used to study nuclear stability in this region. No stability effects associated with a particular neutron number are noticed but rather there is a broad general increase in stability between the 82 and 126 neutron shells.

I. INTRODUCTION

In a previous paper (12), the mass region $28 \leqslant n \leqslant 50$ and $28 \leqslant Z \leqslant 40$ was investigated for nuclear shell effects. In particular, the possible existence of subshell effects between 28 and 50 nucleons was looked for, but none was found. Only the large effects due to the wide splitting of the nuclear energy levels by spin–orbit coupling were clearly shown.

The region of the mass table which is discussed in this paper is that in which $82 \leqslant n \leqslant 126$; 82 and 126 neutrons represent very stable nuclear configurations which are attributed, on the one-particle picture (10, 16, 17), to wide splitting of the nuclear energy levels $h_{11/2}$–$h_{9/2}$ and $i_{13/2}$–$i_{11/2}$, respectively. Between 82 and 126 neutrons five subshells are filled, namely $h_{9/2}$, $f_{7/2}$, $f_{5/2}$, $p_{3/2}$, and $p_{1/2}$. These fill at 92, 100, 106, 110, and 112 neutrons, respectively, if the levels fill in regularly.

In the sections to follow new atomic mass values are presented, principally for rare earth nuclides, and nuclear stability in the $82 \leqslant n \leqslant 126$ region is investigated.

II. EXPERIMENTAL

The new atomic mass measurements upon which this paper is based were made with a Dempster-type double focusing mass spectrograph. Both the instrument (3) and the method (11) have been previously described in some detail.

The mass differences obtained in the present work are given in Table I.

III. COMPUTATION OF ATOMIC MASSES

The data in Table I have been combined with existing data to compile the list of masses shown in Table II, where the source of each or its method of computation is described by footnotes. Some of the rare earth elements, namely, europium, terbium, thulium, ytterbium, and lutetium, were not studied in this work since they were not available to us in metallic form.

[1] *Manuscript received August 4, 1953.*
Contribution from the Department of Physics, Hamilton College, McMaster University, Hamilton, Ontario. This work was supported by the Office of Scientific Research, Air Research and Development Command, U.S. Air Force, the National Research Council of Canada, and the Research Council of Ontario.

[2] *Holder of a National Research Council of Canada Fellowship.*

TABLE I*

LIST OF NEW ATOMIC MASS DIFFERENCES

Nuclides	Mass difference in m.m.u.	Previous measurements
$Pb^{207} - 1.5Ba^{138}$	116.9 ± 4	
$Ce^{140} - 2Ge^{70}$	56.8 ± 6	59.5 ± 4^a
$Pr^{141} - 3Ti^{47}$	50.9 ± 3	51.3 ± 4^a
$Nd^{144} - 3Ti^{48}$	66.7 ± 3	
$Nd^{146} - 2Ge^{73}$	65.8 ± 4	67.8 ± 12^a
$Nd^{148} - 2Ge^{74}$	74.8 ± 2	
$Nd^{148} - 2Se^{74}$	72.3 ± 4	
$Nd^{150} - 3Ti^{50}$	85.2 ± 5	77.4 ± 20^b
$Nd^{150} - 2As^{75}$	77.4 ± 4	
$Sm^{144} - 2Ge^{72}$	66.9 ± 8	
$Sm^{148} - 2Ge^{74}$	71.9 ± 4	
$Sm^{148} - 2Se^{74}$	70.0 ± 5	
$Sm^{150} - 2As^{75}$	72.5 ± 8	
$Sm^{152} - 2Ge^{76}$	76.2 ± 2	
$Sm^{152} - 2Se^{76}$	81.4 ± 6	
$Sm^{154} - 2Se^{77}$	81.8 ± 3	
$Gd^{154} - 2Se^{77}$	81.0 ± 2	
$Gd^{156} - 3Cr^{52}$	100.4 ± 4	99.4 ± 18^b
$Gd^{158} - 2Br^{79}$	86.6 ± 2	
$Gd^{160} - 2Se^{80}$	94.3 ± 2	
$Dy^{160} - 2Se^{80}$	91.0 ± 8	
$Dy^{162} - 2Br^{81}$	92.9 ± 5	
$Dy^{164} - 2Se^{82}$	95.2 ± 8	
$Ho^{165} - 3Mn^{55}$	84.8 ± 8	
$Er^{164} - 2Se^{82}$	96.5 ± 4	
$Er^{168} - 3Fe^{56}$	126.0 ± 3	
$Er^{170} - 2Rb^{85}$	111.7 ± 8	
$Hf^{176} - 2Sr^{88}$	128.7 ± 6	125.1 ± 8^a
$Hf^{178} - 2Y^{89}$	131.6 ± 6	125.8 ± 10^a
$Hf^{180} - 2Zr^{90}$	137.1 ± 3	138.6 ± 6^a
$W^{182} - 2Zr^{91}$	135.5 ± 3	135.6 ± 8^a 142.9 ± 36^c
$Os^{190} - 2Mo^{95}$	146.0 ± 4	147 ± 6^c

*Some of the mass differences listed in this table have appeared in Table I of Reference 12. They are included here since they are required for some of the calculations to follow.

[a] *Reference* (4).

[b] *Reference* (8).

[c] *Dempster, A. J. Phys. Rev. 53: 64. 1938.*

IV. DISCUSSION

(a) *Representation of the Data*

Table II contains a large number of isotopic masses in the region $82 \leqslant n \leqslant 126$. The procedure for analyzing for stability effects is the same as that employed in an earlier paper (12). This consists of plotting neutron number against the difference between the masses calculated from the semiempirical mass formula by Metropolis and Reitweisner (18) and the experimental masses of Table II, as shown in Fig. 1. A proton number plot in this region gives no new information since there are insufficient isotonic masses available.

Since the semiempirical mass formula has no compensating factors which allow for shell structure, we should expect to find large mass differences at regions of higher stability.

A second method of representing the data, shown in Fig. 2, which is more

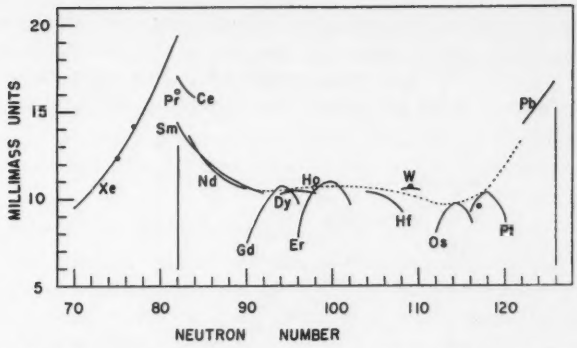

FIG. 1. A plot of experimental deviation from the semiempirical masses versus neutron number. The solid curves are the best fit for points belonging to even A, even Z nuclei. The closed circles represent odd A, even Z nuclei, and the open circles represent odd Z, odd A nuclei.

TABLE II

ATOMIC MASSES ADOPTED IN THIS PAPER

$Xe^{132} = 131.94618 \pm 8^a$	$Gd^{154} = 153.9694 \pm 4^c$	$W^{183} = 183.0066 \pm 7^k$
$Xe^{134} = 133.94804 \pm 10^a$	$Gd^{156} = 155.9715 \pm 4^c$	$W^{184} = 184.0074 \pm 7^l$
$Xe^{136} = 135.95046 \pm 8^a$	$Gd^{158} = 157.9736 \pm 8^c$	$Os^{188} = 188.0157 \pm 5^l$
$Ba^{138} = 137.9498 \pm 5^b$	$Gd^{160} = 159.9785 \pm 12^c$	$Os^{190} = 190.0174 \pm 6^m$
$Ce^{140} = 139.9488 \pm 10^c$	$Dy^{160} = 159.9752 \pm 14^c$	$Os^{192} = 192.0225 \pm 6^l$
$Ce^{142} = 141.9528 \pm 4^d$	$Dy^{162} = 161.9779 \pm 11^c$	$Pt^{194} = 194.0241 \pm 6^n$
$Pr^{141} = 140.9509 \pm 4^e$	$Dy^{164} = 163.9814 \pm 14^c$	$Pt^{195} = 195.0265 \pm 6^n$
$Nd^{144} = 143.9562 \pm 3^f$	$Ho^{165} = 164.9822 \pm 8^e$	$Pt^{196} = 196.0267 \pm 6^n$
$Nd^{148} = 147.9642 \pm 6^g$	$Er^{164} = 163.9827 \pm 12^c$	$Pt^{198} = 198.0327 \pm 6^n$
$Nd^{150} = 149.9676 \pm 3^h$	$Er^{168} = 167.9849 \pm 4^c$	$Pb^{204} = 204.0363 \pm 10^o$
$Sm^{144} = 143.9567 \pm 9^c$	$(Er^{170} = 169.9907)^i$	$Pb^{206} = 206.0388 \pm 10^o$
$Sm^{148} = 147.9616 \pm 7^c$	$Hf^{176} = 175.9957 \pm 7^j$	$Pb^{207} = 207.0405 \pm 10^o$
$Sm^{150} = 149.9632 \pm 10^c$	$Hf^{178} = 177.9988 \pm 9^c$	$Pb^{208} = 208.0416 \pm 10^o$
$Sm^{152} = 151.9677 \pm 5^c$	$Hf^{180} = 180.0031 \pm 8^c$	$Bi^{209} = 209.0446 \pm 10^o$
$Sm^{154} = 153.9712 \pm 5^c$	$W^{182} = 182.0041 \pm 7^c$	

[a] *Reference 9.*

[b] *The weighted mean for the Ba^{138} mass of the Ba^{138}–Zr^{92} comparison (see Reference 4) and the Pb^{207}–Ba^{138} comparison from Table I. The masses of Zr^{92} and Pb^{207} are taken from References 12 and 23, respectively.*

[c] *Derived from Table I and the comparison mass of Reference 12.*

[d] *Based on the Pr^{141} mass in conjunction with the $Ce^{142}(\gamma,n)Ce^{141}$ threshold, Reference 22, and the decay of Ce^{141}, Reference 13.*

[e] *Derived from Table I using the comparison mass of Reference 1.*

[f] *Weighted mean of the value derived from Table I and the value from Reference 4.*

[g] *Weighted mean of values obtained from the Nd^{148}–Ge^{74} and the Nd^{148}–Se^{74} comparisons of Table I. The comparison masses are taken from Reference 12.*

[h] *Weighted mean of values derived from the Nd^{150}–Ti^{50} and the Nd^{150}–As^{75} comparisons of Table I using the Ti^{50} mass of Reference 1 and the As^{75} mass of Reference 12.*

[i] *Derived from Table I and an estimated mass of $Rb^{85} = 84.9385$ a.m.u. This estimate is made from Fig. 1 of Reference 12.*

[j] *Based on a remeasurement of old plates, Reference 4, and the new mass of Sr^{88}, Reference 12.*

[k] *Based on the mass of W^{182} given above and the $W^{183}(\gamma,n)W^{182}$ threshold, Reference 22.*

[l] *Reference 7.*

[m] *Derived from Table I and the mass of Mo^{95}. The mass of $Mo^{95} = 94.9357 \pm 5$ a.m.u. was obtained from the known mass of Mo^{94}, Reference 12, and the $Mo^{95}(\gamma,n)Mo^{94}$ threshold, Reference 22.*

[n] *A remeasurement of the old plates of References 5 and 6.*

[o] *References 23 and 24.*

conventional in nature, is to plot the binding energy per nucleon versus mass number. Stability effects appear on this plot as changes in the slope of the curve. Incidentally, the new masses reported in this paper make it possible to fill in the only large gap which has existed in the binding energy per nucleon curve.

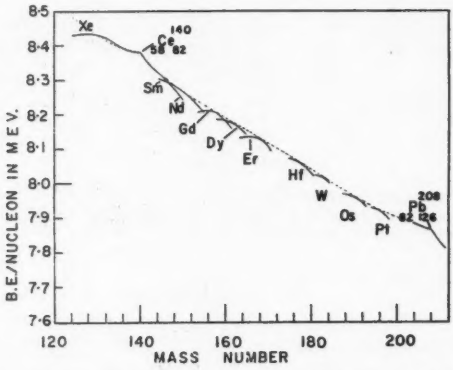

FIG. 2. The binding energy per nucleon curve in the region $82 \leqslant n \leqslant 126$.

(b) Analysis of Fig. 1 for Stability Effects

Sharp peaks at 82 and 126 neutrons are immediately evident from Fig. 1. These are attributed to the spin–orbit splitting of the $h_{11/2}$–$h_{9/2}$ and $i_{13/2}$–$i_{11/2}$ neutron levels. In addition, at 126 neutrons the 82 proton shell is completed, and both factors contribute to the stability of the lead region.

If one adheres to the strict one-particle model of the nucleus with strong spin–orbit coupling, subshells are expected at 92, 100, 106, 110, and 112 neutrons. These are labelled $h_{9/2}$, $f_{7/2}$, $f_{5/2}$, $p_{3/2}$, and $p_{1/2}$ respectively.

92 Neutrons—The sweep downward in Fig. 1 from the highly stable 82 neutron configuration seems to reach its lowest point in the vicinity of 92 neutrons. A slight rise appears after 92 neutrons, but this seems to be part of a general rise and not associated with the filling of any single subshell.

100 Neutrons—At 100 neutrons the increase in stability approaches its maximum. However, as mentioned above, this is a gradual increase and not of the type associated with shell structure, as at 82 or 126 neutrons.

106 Neutrons—In the region of 106 neutrons the stability is slowly decreasing.

110 and 112 Neutrons—At 110 and 112 neutrons the mass difference continues to decrease. This indicates that no extra stability is associated with these neutron numbers. As the neutron numbers increase up to 126, the stability increases greatly, as expected.

90 Neutrons—If the $h_{11/2}$–$h_{9/2}$ levels are widely split, the $h_{9/2}$ levels may fill in after the $f_{7/2}$ group. In this case 90 neutrons would constitute a subshell. No extra stability is found at 90 neutrons; in fact, it is a particularly unfavored place in terms of stability.

(*c*) *Analysis of Fig. 2 for Stability Effects*

Fig. 2 shows sharp discontinuities at Ce^{140} and Pb^{208} which have previously been attributed (4, 5) to the filling of shells at these two nuclides. The effects, however, do not show up as markedly as in Fig. 1 since they are reduced by division by the mass number, which ranges from 130 to 208. This insensitive nature of the binding energy per nucleon curve almost completely obscures the small stability effect found between the 82 and 126 neutron shells in Fig. 1.

(*d*) *Discussion of the Mid-shell Stability Effect*

The extra stability in the heavier rare earth region is not adequately explained on a strict one-particle picture. The smooth increase and decrease in stability, shown in Fig. 1, is not of the type which characterizes the completion of nuclear shells.

Recently, a modification of the strict one-particle model has been suggested by de Shalit and Goldhaber (21). In this modification the structure of the core is taken into account instead of regarding the core as simply setting up a potential in which the odd particle moves. They assume that only towards the closing of nuclear shells do "pure states" exist, that is, states which one would expect on a strict one-particle model. Between shells they predict a mixing of configurations, which leads to a higher stability than that associated with the "pure" state of the shell theory.

It is an experimental fact (25) that large electric quadrupole moments exist between shells. These large quadrupole moments indicate a highly distorted nucleus. The region of the rare earths is that region in which the quadrupole moments are the largest of all (approximately ten times the quadrupole moments between other shells), and hence we may expect a large distortion of the nuclear core. It has been pointed out by Davidson and Feenberg (2) that a distortion of the core leads to mixing of configurations. If mixed configurations lead to higher stability, as postulated by de Shalit and Goldhaber, this may account for the stability effect which we have found experimentally.

Scharff-Goldhaber (20) has plotted the first excited states of even–even nuclei against atomic number, and finds that between shells the first excited states are depressed. This depression of the first excited states has also been qualitatively explained (21) on the basis of mixed configurations, which have pushed the first excited state to a lower level. Experimentally, the depression of the first excited states shows up clearly (20) in the region $82 < n < 126$. This is in keeping with our present results, which indicate that the ground states are also depressed, although not as much as the first excited state.

It has been noted (12) that no extra stability occurs between the 28 and 50 neutron shells. In terms of the mixing of states hypothesis, we should expect mixing to be much less in this region since the number of possible configurations is greatly reduced.

The lack of evidence for subshells can also be explained in the same manner.

This mixing of configurations to form a state would "wash out" the strict one-particle representation of a state and, hence, subshells would not exist. Only where the states are pure, near magic numbers, would we expect shell structure effects.

(*e*) *The δ-Term in the Semiempirical Mass Formula*

In Fig. 1 the even A isotopes of the even Z elements are represented by the solid curve. The odd A isotopes of these elements are represented by closed circles. The position of these closed circles relative to the solid lines indicates the correctness of the δ-term used by Metropolis and Reitweisner (18) in their calculations based on the semiempirical mass formula. There is a random distribution of the odd-A isotopes indicating that the δ-term used in these calculations is a good approximation.

(*f*) *The Nd^{150}–Sm^{150} Mass Difference and Possible Radioactivity of Nd^{150}*

This mass difference is of interest because of its large magnitude, seen from Table I to be Nd^{150}–$Sm^{150} = 4.6 \pm 0.8$ Mev. If the total decay energy of Pm^{150} be less than this figure, then Nd^{150} should be unstable. Kohman (14) has suggested that Nd^{150} may be radioactive but he and Mulholland have been unable to detect an activity and have set a half-life on the event of greater than 2×10^{15} years (19).

It is possible that the decay energy in the negatron branch of Pm^{150} exceeds 4 Mev. (15), in which case Nd^{150} would be lower than Pm^{150} and single beta emission would not be possible. Even if this is the case Nd^{150}, because of the large Nd^{150}–Sm^{150} mass difference, is a potential double-beta emitter.

(*g*) *Summary*

A small mass effect, which represents extra stability, has been found between the 82 and 126 neutron shells. This effect is a broad general increase in stability which occurs in the same region as the recently observed increase in the stability of the first excited states. It does not seem possible to explain this phenomenon on a strict one-particle picture of the nucleus. Reference is made to a plausible explanation involving the mixing of configurations in mid-shell regions.

V. ACKNOWLEDGMENTS

This atomic mass investigation of the rare earth region was made possible by the use of samples of pure metallic neodymium, gadolinium, dysprosium, holmium, and erbium which were kindly made available to us by Dr. F. H. Spedding.

The authors are greatly indebted to Dr. M. Goldhaber for helpful suggestions concerning the interpretation of the data and to Dr. Truman Kohman for occasional information concerning the radioactivity of Nd^{150}.

REFERENCES

1. Collins, T. L., Nier, A. O., and Johnson, W. H., Jr. Phys. Rev. 86: 408. 1952.
2. Davidson, J. P. and Feenberg, E. Phys. Rev. 89: 856. 1953.
3. Duckworth, H. E. Rev. Sci. Instr. 21: 54. 1950.
4. Duckworth, H. E., Kegley, C. L., Olson, J. M., and Stanford, G. S. Phys. Rev. 83: 1114. 1951.

5. DUCKWORTH, H. E. and PRESTON, R. S. Phys. Rev. 82: 468. 1951.
6. DUCKWORTH, H. E., WOODCOCK, K. S., and PRESTON, R. S. Phys. Rev. 78: 479. 1950.
7. GEIGER, J. S., HOGG, B. G., DUCKWORTH, H. E., and DEWDNEY, J. W. Phys. Rev. 89: 627. 1953.
8. GRAVES, A. C. Phys. Rev. 55: 863. 1939.
9. HALSTED, R. E. Phys. Rev. 88: 666. 1952.
10. HAXEL, O., JENSEN, J. H. D., and SUESS, H. E. Phys. Rev. 75: 1766. 1949.
11. HOGG, B. G. and DUCKWORTH, H. E. Can. J. Phys. 30: 637. 1952.
12. HOGG, B. G. and DUCKWORTH, H. E. Can. J. Phys. 31: 942. 1953.
13. HOLLANDER, J. M., PERLMAN, I., and SEABORG, G. T. Revs. Mod. Phys. 25: 469. 1953.
14. KOHMAN, T. P. Phys. Rev. 73: 16. 1948.
15. KOHMAN, T. P. Private communication. May 1953.
16. MAYER, M. G. Phys. Rev. 75: 1969. 1949.
17. MAYER, M. G. Phys. Rev. 78: 16. 1950.
18. METROPOLIS, N. and REITWEISNER, G. Table of atomic masses. Unpublished. 1950.
19. MULHOLLAND, G. I. and KOHMAN, T. P. Phys. Rev. 85: 144. 1952.
20. SCHARFF-GOLDHABER, G. Phys. Rev. 90: 587. 1953.
21. DE SHALIT, A. and GOLDHABER, M. To be published.
22. SHER, R., HALPERN, J., and MANN, A. K. Phys. Rev. 84: 387. 1951.
23. STANFORD, G. S., DUCKWORTH, H. E., HOGG, B. G., and GEIGER, J. S. Phys. Rev. 85: 1039. 1952.
24. STERN, M. D. The masses of the heavy isotopes. U.C.R.L. 1728. 1952.
25. TOWNES, C. H., FOLEY, H. M., and LOW, W. Phys. Rev. 76: 1415. 1949.

ON INVERTING LAPLACE TRANSFORMS OF THE FORM $h(s)/(p(s) + q(s)e^{-\tau s})$[1]

By T. E. Hull[2] and W. A. Wolfe[3]

ABSTRACT

Some appeal is made to the theory of integral equations to construct a general and practical successive approximation procedure for inverting transforms of the form given in the title, where $p(s)$ and $q(s)$ are polynomials in s, the degree of $p(s)$ being greater than the degree of $q(s)$, and $h(s)$ is any function which does not greatly complicate the transform. The approximations converge rapidly when τ is relatively small. In some cases upper and lower bounds and asymptotic expressions for the inverse are produced. Problems from the theory of counters and the theory of heat transfer are used to illustrate the method.

INTRODUCTION

A number of physical problems can be reduced to the mathematical one of inverting the Laplace transform

$$[1] \qquad \int_0^\infty e^{-st}\, U(t)\, dt = \frac{h(s)}{p(s) + q(s)e^{-\tau s}},$$

where $p(s)$ is a polynomial of degree n in s and $q(s)$ is a polynomial of degree less than n, while $h(s)$ is some simple function of s which need not concern us for the moment.

The image $U(t)$ of such a transform can usually be found explicitly by expanding in powers of $e^{-\tau s}$ and inverting term by term. The result, however, is rarely of any practical value since τ is usually much smaller than the values of t in which one is interested and there is consequently a large number of terms in the expansion.

We propose to construct a method of successive approximations for the inversion of such a transform. When the method applies it often leads in a natural way to simple expressions for upper and lower bounds and for an asymptotic form of the desired solution. The method applies to those cases where τ is relatively small. Such cases are important in physical applications because τ can be interpreted, for example, as the resolving time of a Geiger-Müller counter or the time for the passage of an element of liquid through a surface heat exchanger.

Since in many cases $p(s)$ and $q(s)$ contain only one or two terms, we shall begin by illustrating the procedure with two simple applications. Then we explain, with the aid of one theorem and a few remarks, how the underlying ideas can be applied to the general case.

A number of authors have dealt with transforms like [1]. A method proposed by Feller (2) provides practical bounds to the inverse in some cases, but otherwise little attention seems to have been paid to this aspect of the problem. Hayes (4) and Sherman (8) consider such transforms when investigating stability problems for systems governed by differential-difference equations.

[1] *Manuscript received September 18, 1953.*
Contribution from the University of British Columbia, Vancouver, B.C.
[2] *Department of Mathematics.*
[3] *Department of Mechanical Engineering.*

Location of the poles of [1] and the resulting direct evaluation of the inverse have been considered for a problem in econometrics by James and Belz (5) and for a problem in servomechanism theory by Wolfe (10).

COUNTER THEORY

A certain problem in the theory of counters provides a simple example to which the method can be applied. Since physical considerations motivate the method, we shall first sketch the derivation of the problem.

We assume that a counter is subjected to a random events per unit time; not all the events are registered because of the counter's finite resolving time τ. The problem is to calculate the expected number $U(t)$ of registrations in time t.

Laplace transform methods are especially suited to this type of probability problem (1, 2) and we adopt Feller's approach (2) to derive an expression for the Laplace transform

$$u(s) \equiv L\{U(t)\} \equiv \int_0^\infty e^{-st}\, U(t)\, dt \tag{2}$$

of $U(t)$. The result (equation [6]) is obtained after we first consider the probability distribution of the time between succeeding registrations, and then of the time from one registration to the kth succeeding one.

The randomness of the events means: the probability that the first event, after any fixed instant, will occur between times t and $t + dt$ after that instant is

$$ae^{-at}\, dt.$$

We assume the resolving time to be "nonextended"; that is, we assume that the counter registers an event if and only if no *registration* has taken place during a time interval τ preceding the event. (When the resolving time is "extended" the problem possesses a simple solution (2).)

If T is the time between succeeding registrations, the distribution of T is given by

$$J(t)\, dt \equiv \Pr\{t \leqslant T \leqslant t + dt\}$$

$$= \begin{cases} 0, & t < \tau \\ ae^{-a(t-\tau)}\, dt, & t > \tau \end{cases}$$

so that

$$L\{J(t)\} \equiv j(s) = ae^{-\tau s}/(s + a). \tag{3}$$

If T_k is the time between one registration and the kth succeeding registration (Fig. 1), we define

$$J_k(t)\, dt \equiv \Pr\{t \leqslant T_k \leqslant t + dt\}$$

so that

$$L\{J_k(t)\} = j^k(s)$$

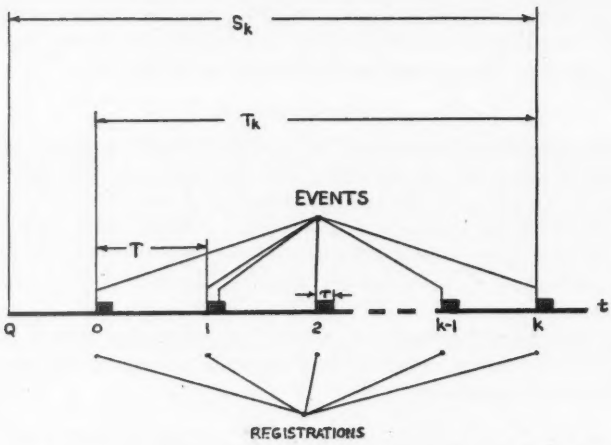

FIG. 1. Schematic diagram showing events and registrations distributed along the time axis. Each solid block has length τ and covers an inactive period of the counter—the one event shown taking place in such a period is therefore not registered.

from the convolution property of Laplace transforms (1, p. 27). If S_k is the time from any instant Q, *not* in a registration period, up to the $(k+1)$th succeeding registration,

$$H_k(t)\,dt \equiv Pr\{t \leqslant S_k \leqslant t + dt\}$$

$$= (J_k(t)^* ae^{-at})\,dt$$

where (*) is the convolution operator. Then, if

$$I_k(t) \equiv \Pr\{S_k \leqslant t\},$$

we have

$$[4] \qquad i_k(s) \equiv L\{I_k(t)\} = L\left\{\int_0^t H_k(t)\,dt\right\} = aj^k(s)/s(s+a).$$

Now the probability of exactly k registrations during time t, after Q, is

$$I_{k-1}(t) - I_k(t).$$

Therefore

$$[5] \qquad U(t) = \sum_{k=1}^{\infty} k\{I_{k-1}(t) - I_k(t)\} = \sum_{k=0}^{\infty} I_k(t)$$

so that, from equations [2–5], we finally obtain

$$[6] \qquad u(s) = \sum_{k=0}^{\infty} i_k(s) = \frac{a}{s(s + a - ae^{-\tau s})}.$$

The inverse of [6] can be obtained in the explicit and finite form

$$[7] \qquad U(t) = 1 - e^{-at} + \sum_{k=1}^{[t/\tau]} \left\{ 1 - e^{-a(t-k\tau)} \sum_{m=0}^{k} \frac{a^m (t - k\tau)^m}{m!} \right\}$$

([x] is the greatest integer not exceeding x) by expanding $u(s)$ in powers of $e^{-\tau s}$ and inverting term by term. Equation [7] is in fact the explicit form of [5] but it is relatively unmanageable except when t is small, i.e. when t is of the order of magnitude of τ.

For values of t in which one is usually interested a different expansion of [6] is evidently needed. In a later section we shall give a procedure for choosing the expansion in any particular case. For the moment it is sufficient to note that $1 - e^{-\tau s}$ goes to zero with τ; an expansion in powers of this expression will therefore converge rapidly when τ is small. The resulting series can then be inverted term by term.

This procedure can be interpreted in terms of the theory of integral equations and we shall see that, in many cases, this interpretation leads in a natural way to upper and lower bounds for the desired solution. Inverting the proposed series term by term is equivalent (7) to solving by successive substitutions the integral equation

$$[8]^* \qquad U(t) = at - \int_0^{\min(t,\tau)} aU(t - u)\, du$$

as can easily be verified.

The first term on the right side of [8] is simply the unperturbed solution—i.e. the solution for $\tau = 0$—and the integral term is the correction for nonzero τ. The successive approximations can therefore be expected to converge rapidly when the effect of τ is small. Moreover since, for $t > 0$, $U(t)$ and at are positive so that the integral term is negative, the approximations are alternately upper and lower bounds for $U(t)$; one therefore knows in practice exactly when to terminate the series.

Expanding [6] in powers of $1 - e^{-\tau s}$ and inverting term by term leads to the following new form of the solution:

$$[9] \qquad U(t) = at - \sum_{k=1}^{\infty} \frac{(-a)^{k+1}}{k+1} \sum_{m=0}^{[t/\tau]} \frac{(-1)^m (t - m\tau)^{k+1}}{m!(k-m)!}.$$

This series converges rapidly and its terms alternate in sign. Simple but still useful approximations can be obtained, however, directly from the integral equation [8] if we restrict our attention to values of $t > n\tau$ for the nth approximation. It is a straightforward matter to show that this nth approximation is

$$[10] \quad U_n(t) = \frac{at(1-(-a\tau)^{n+1})}{1+a\tau} + \frac{a^2\tau^2(1+n(-a\tau)^{n+1}-(n+1)(-a\tau)^n)}{2(1+a\tau)^2}, \qquad t > n\tau,$$

where $U_n(t)$ is an upper bound for even n and a lower one for odd n.

Since usually $a\tau < 1$, we can let $n \to \infty$ and obtain immediately the asymptotic formula

The integral equation corresponding to the form [7] is

$$U(t) = 1 - e^{-at} + \int_{\tau}^{\max(t,\tau)} ae^{-a(u-\tau)}\, U(u)\, du.$$

[11] $$U(t) \sim \frac{at}{1 + a\tau} + \frac{a^2\tau^2}{2(1 + a\tau)^2}.$$

Feller (2) showed that this expression is itself an upper bound for all t. Examination of the bounds given by equation [10] will show that, except for very small t, [11] is a much better approximation to $U(t)$ than is

$$at/(1 + a\tau)$$

which is the lower bound given by Feller.

HEAT TRANSFER THEORY

As a second example let us consider the following typical problem in the theory of heat exchangers. Suppose that the liquid in a tank is heated by being passed with a velocity v through an externally connected heat exchanger of the surface type. Then, neglecting conductivity and transverse variations in temperature, the temperature $U(x, t)$ of the liquid in the exchanger is governed by

[12] $$\frac{\partial U}{\partial t} + v\frac{\partial U}{\partial x} = \lambda(T - U)$$

where T is the (constant) temperature of the heating fluid in the exchanger and λ is a parameter depending on the over-all heat transfer coefficient, the geometry of the exchanger, and the density and specific heat of the liquid.

If the liquid enters the exchanger at $x = 0$ and leaves at $x = L$, the assumptions of perfect mixing in the tank and no losses to the surroundings lead to the boundary condition

[13] $$dU(0, t)/dt = \beta\{U(L, t) - U(0, t)\}$$

where β is the fraction of tank liquid circulated per unit time.

We shall assume that the liquid is initially at the temperature U_0.

For most practical purposes v and λ are so large that the first term in [12] can be neglected. It is then a straightforward matter to obtain $u_A(0, s)$, the Laplace transform of the corresponding *approximate* tank temperature $U_A(0, t)$. The result is

$$u_A(0, s) = \frac{T}{s} - \frac{T - U_0}{s + \beta - \beta e^{-\overline{\lambda}L/v}},$$

so that (cf. Ref. 3)

[14] $$U_A(0, t) = T - (T - U_0)\, e^{-(\beta - \beta e^{-\lambda L/v})t}.$$

In the more general case considered here we obtain

[15] $$u(0, s) \equiv L\{U(0, t)\}$$

$$= \frac{T}{s} - \frac{(T - U_0)(s + \lambda + \beta - \beta e^{-(s+\lambda)L/v})}{(s + \lambda)(s + \beta - \beta e^{-(s+\lambda)L/v})}.$$

Let us define

$$u(s) \equiv \frac{s + \lambda + \beta - \beta e^{-(s+\lambda)L/v}}{(s + \lambda)(s + \beta - \beta e^{-(s+\lambda)L/v})}.$$

We proceed to handle $u(s)$ as in the counter theory problem except that we now add and subtract γ in the last term of the denominator and expand in powers of

$$\gamma - \beta e^{-(s+\lambda)L/v}.$$

The constant γ is taken to be the one real root of

[16] $$\gamma = \beta e^{-(\lambda-\beta+\gamma)L/v}.$$

The reason for choosing this particular expansion will again follow from the general results of the next section. For the present it is sufficient to show that this expansion preserves all the desirable features of our solution for the counter theory problem.

Expanding as indicated and inverting term by term is equivalent to solving by successive approximations the integral equation

[17] $$U(t) = F(t) - \int_0^{\min(t,\, L/v)} G(u)\, U(t-u)\, du,$$

where F, G can easily be found. We need only:

$$F(t) = \frac{\lambda e^{-(\beta-\gamma)t}}{\lambda + \gamma - \beta}, \quad t > L/v,$$

$$G(t) = \gamma e^{-(\beta-\gamma)t}, \qquad t < L/v.$$

The upper limit in [17] is $\leqslant L/v$ because, as can be readily verified, our choice of γ ensures that $G(t) = 0$ when $t > L/v$.

In practice L/v, the 'passage time' of the liquid through the exchanger, and γ are both small; the integral term in [17] is then a small correction term. As with the counter problem, the successive approximations can therefore be expected to converge rapidly. The approximations are again alternately upper and lower bounds.

The nth approximation to $U(t)$ is now

[18] $$U_n(t) = \frac{\lambda e^{-(\beta-\gamma)t}(1-(-\gamma L/v)^{n+1})}{(\lambda + \gamma - \beta)(1 + \gamma L/v)}, \quad t > (n+1)L/v,$$

which is an upper bound for n even and a lower bound for n odd.

The required tank temperature is of course

$$U(0, t) = T - (T - U_0)\, U(t).$$

Usually $\gamma L/v < 1$ so that we can let $n \to \infty$ and obtain finally an asymptotic formula for the tank temperature

[19] $$U(0, t) \sim T - \frac{(T - U_0)\lambda e^{-(\beta-\gamma)t}}{(\lambda + \gamma - \beta)(1 + \gamma L/v)}.$$

Using Feller's (2) method it can be shown that, when $T - U_0 > 0$, the expression in [19] is a lower bound for $U(0, t)$ for all t, whereas by [12] $U_A(0, t)$ in [14] is an upper bound. The bounds are interchanged when $T - U_0 < 0$.

GENERAL THEORY

In each of the above problems we were confronted with Laplace transforms of a certain type. These transforms could be inverted explicitly and in finite terms, but the results were too complicated to be of practical use. We have used another procedure, one which generates rapidly converging successive approximations to the solution. We shall show now that the procedure can be applied to any transform of the form

$$u(s) = \frac{h(s)}{p(s) + q(s)e^{-\tau s}}$$

where $p(s)$ is a polynomial of degree n in s (we shall assume the coefficient of s^n to be 1), and $q(s)$ is a polynomial of degree less than n, while $h(s)$ is some function of s which does not greatly complicate the transform. Rapid convergence of the method depends on τ being small, as is often the case, but it is just when τ is small that the "finite" solution (equation [7] for the counter) is of so little use.

We rewrite the Laplace transform in the form

$$u(s) = \frac{f(s)}{1 + g(s)}$$

so that expanding in powers of $g(s)$ and inverting term by term is equivalent (7) to solving the integral equation

$$[20] \qquad U(t) = F(t) - \int_0^t G(u)\, U(t-u)\, du$$

by successive approximations; $U(t)$, $F(t)$, $G(t)$ are of course the inverses of $u(s)$, $f(s)$, $g(s)$ respectively. The essential feature of our choice of $g(s)$ is the vanishing of $G(t)$ for $t > \tau$. Properly arranged this will mean that, as $\tau \to 0$, $F(t)$ goes over into the solution of the problem for $\tau = 0$; the integral term is then merely a "correction" term and the successive approximations can be expected to converge rapidly for small τ. Moreover, when, as in the examples considered earlier, we know that the integral is positive we can conclude that the approximations are alternately upper and lower bounds for the solution.

Our purpose now is to show that $g(s)$ can always be chosen so that $G(t) = 0$ when $t > \tau$. If we add and subtract

$$\prod_{k=1}^{n} (s - \alpha_k)$$

in the denominator of the given transform and then divide numerator and denominator by this same expression we can write

$$f(s) = h(s) \Big/ \prod_{k=1}^{n} (s - \alpha_k),$$

$$g(s) = \left[- \prod_{k=1}^{n} (s - \alpha_k) + p(s) + q(s)e^{-\tau s} \right] \Big/ \prod_{k=1}^{n} (s - \alpha_k).$$

Assuming the α_k's to be distinct we can expand in partial fractions to obtain

$$g(s) = \sum_{m=0}^{n} \left\{ \frac{A_m}{s - \alpha_m} + \frac{B_m e^{-\tau s}}{s - \alpha_m} \right\},$$

where

$$A_m = p(\alpha_m) \Big/ \prod_{k=1}^{n}{}'(\alpha_m - \alpha_k), \quad B_m = q(\alpha_m) \Big/ \prod_{k=1}^{n}{}'(\alpha_m - \alpha_k),$$

the $'$ meaning that the product is to be taken over all k except $k = m$.

We now have

$$G(t) = \sum_{m=1}^{n} \{A_m + B_m e^{-\alpha_m \tau}\} e^{\alpha_m t}, \quad t > \tau,$$

and if $G(t)$ is to vanish when $t > \tau$ we must have

$$A_m + B_m e^{-\alpha_m \tau} = 0,$$

i.e.

$$p(\alpha_m) + q(\alpha_m) e^{-\alpha_m \tau} = 0.$$

Thus $G(t) = 0$ when $t > \tau$ if $\alpha_1, \alpha_2, \ldots, \alpha_n$ are any n distinct zeros of the denominator of the original transform. With appropriate changes in the partial fractions expansion of $g(s)$, and correspondingly in $G(t)$, one can show that up to r of the α_k's can be taken equal to α if α is a zero of order r.

If, when $\tau \to 0$, $F(t)$ is to go over into the solution of the problem with $\tau = 0$, it is clear from the form of $f(s)$ that $\alpha_1, \alpha_2, \ldots, \alpha_n$ must go over into the n zeros of $p(s) + q(s)$. This condition uniquely determines which zeros must be chosen. (For the counter problem we can take $h(s) = a/s$ and only one zero, the one at the origin, is chosen from the denominator of $u(s)$; similarly for the heat exchanger problem the only zero chosen is $\beta - \gamma$ where γ is the real root of [16].) Standard integral equation theory guarantees the convergence of the approximation procedure for a choice of *any* n zeros. However, a choice other than the one required here would lead to an $F(t)$ which could not be considered a satisfactory zero order approximation to the solution, and to a $G(t)$ which did not remain finite as $\tau \to 0$.

Finally, let us consider the circumstances under which bounds for the solution appear in the course of the calculations. The integral in [20] must be positive so that the integral term is a negative correction to $F(t)$. Whether or not this condition is satisfied in a given problem can be decided without difficulty only when $p(s)$ and $q(s)$ are particularly simple polynomials in s. When the condition is not satisfied some other procedure, such as that given by Feller and referred to above, must be used.

For example, an interesting but not uncommon situation arises in the counter theory problem for "extended" resolving time. Feller (2, p. 114) derives the expression

[21]
$$u(s) = \frac{ae^{-(s+a)\tau}}{s + ae^{-(s+a)\tau}}$$

for the transform of the frequency function which governs the distribution of the time between the registrations. That is, $U(t)dt$ is here the probability that the time between consecutive registrations is between t and $t + dt$.

We obtain

$$f(s) = \frac{ae^{-(s+a)\tau}}{s+a}, \quad g(s) = \frac{-a + ae^{-(s+a)\tau}}{s+a},$$

so that

$$F(t) = \begin{cases} 0, & t < \tau, \\ ae^{-at}, & t > \tau, \end{cases}$$

$$G(t) = -ae^{-at}, \; t < \tau.$$

The integral in [20] is now negative so that the integral term is a *positive* correction to the approximation $F(t)$. Further approximations generate only successively better *lower* bounds which for $t > (n+1)\tau$ become

$$U_n(t) = \frac{ae^{-at}(1-(a\tau)^{n+1})}{1-a\tau}.$$

In this case the asymptotic form of the solution, when $a\tau < 1$, is

$$U(t) \sim ae^{-at}/(1-a\tau)$$

which, using Feller's method, can be shown to be an upper bound for all t.

Transforms like [21] also arise in the theory of automatic controllers (6, p. 112ff) and in econometrics (5, 9). In these applications the time constant τ is usually too large for efficient use of our method.

REFERENCES

1. ELMORE, W. C. Nucleonics, 6 (No. 1): 26. 1950.
2. FELLER, W. Courant anniversary volume. Interscience Publishers, Inc., New York. 1948. p. 105.
3. FISHER, R. C. Ind. Eng. Chem. 36: 939. 1944.
4. HAYES, N. D. J. London Math. Soc. 25: 226. 1950.
5. JAMES, R. W. and BELZ, M. H. Econometrica, 4: 157. 1936.
6. OLDENBOURG, R. C. and SARTORIUS, H. The dynamics of automatic controls. The American Society of Mechanical Engineers, New York. 1948.
7. ROBINSON, L. B. J. Appl. Phys. 19: 237. 1948.
8. SHERMAN, S. J. London Math. Soc. 27: 364. 1952.
9. SIMON, HERBERT A. Econometrica, 20: 247. 1952.
10. WOLFE, W. A. Trans. Am. Soc. Mech. Engrs. 73: 413. 1951.

ON θ VALUES IN METALS. II[1]

By F. M. Kelly[2]

ABSTRACT

The four methods of calculating Θ_D, the Debye characteristic temperature for specific heats, and Θ_R, the characteristic temperature which appears in the quantum theory of electrical resistance, discussed in a previous paper, are applied to copper, silver, and gold. An allowance has also now been made for the variation of electrical resistance with volume to take into account the effects of thermal expansion before Θ_R is calculated and compared with Θ_D. Revised values of Θ_R for lithium and sodium are given.

I. INTRODUCTION

In a previous paper (9), which we shall refer to as (I), theories of specific heat and electrical resistance of metals were discussed. Four methods of calculating the Debye characteristic temperature (Θ_D) and the characteristic temperature (Θ_R) which appears in the quantum theory of electrical resistance were compared. For convenience the tables given previously are reprinted below as Tables I and II, in which the references to equation and table numbers are to those of paper (I).

TABLE I

Methods of evaluating Θ_D

No.	Method of obtaining Θ_D	Mathematical assumption of behavior of Θ_D
1	C_V: Equation [3]	Constant
2	U: Equation [2]	Variable parameter
3	$\Sigma(T) = C_V/(U/T)$: Table I	Constant
4	$\Sigma(T) = C_V/(U/T)$: Equation [4]	Variable parameter

TABLE II

Methods of evaluating Θ_R

No.	Method of obtaining Θ_R	Mathematical assumption of behavior of Θ_R
1	From resistance ratio using reference temperature, Equation 6	Constant
2	From resistance ratio using reference temperature, Equation 7	Variable parameter
3	$(dR/dT)/(R/T)$, Equation 8	Constant
4	$(dR/dT)/(R/T)$, Equation 9	Variable parameter

II. VARIATION OF ELECTRICAL RESISTANCE WITH VOLUME

Before Θ_D and Θ_R can be strictly compared an allowance may have to be made for the effect of thermal expansion. In Appendix I of (I) it was shown

[1] *Manuscript received September 21, 1953.*
Contribution from the Division of Physics, National Research Laboratories, Ottawa. Issued as N.R.C. No. 3128.
[2] *Present address: Department of Physics, University of Manitoba, Winnipeg, Canada.*

that $\int_0^T C_v\,dT$ (as computed) is very closely equal to $U(T, V_0)$ (where V_0 is the volume at absolute zero), and consequently the values of Θ_D given in (I) apply essentially to a constant volume of metal.

Now, turning to Θ_R, the volume expansion-coefficient of a metal is given by Grüneisen's formula (7)

$$\alpha = \gamma C_v \chi / V \tag{1}$$

$$= A C_v \tag{2}$$

where γ is (Grüneisen's) constant, χ is the compressibility, and A may then be taken as approximately independent of temperature, and hence may be deduced from available room temperature data. Then

$$\Delta V / V_0 = A\,U(T) \tag{3}$$

where $\Delta V = V_T - V_0$. If we assume that the change of resistance with volume is due solely to the change in Θ with volume (cf. Mott and Jones, p. 271 (15)), we have

$$\frac{\Delta R}{R} = 2\gamma \frac{\Delta V}{V_0} \tag{4}$$

where ΔR is the change in electrical resistance due to the expansion of the metal. However, equation [4] neglects any change which may occur in the electron-lattice interaction constant κ (cf. equation [5] of (I)) during expansion. We have as yet no sound theoretical knowledge of κ (cf., e.g., MacDonald and Pearson (11)). Consequently, we shall assume in general

$$\frac{\Delta R}{R} \propto \frac{\Delta V}{V_0} \tag{5}$$

and determine the constant of proportionality from Bridgman's (1) experimental measurements at room temperature of compressibility and change of resistance with pressure. The calculation of $(\partial R/\partial T)_V$ has also been discussed previously by Meixner (13).

The calculation of ΔR in this way has been carried through for lithium and sodium to revise the data presented in (I), and also for copper, silver, and gold.

III. RESULTS

(i) *Lithium*

In contrast to that of most metals (cf. (1)), the electrical resistance of lithium *increases* as the volume *decreases*. The magnitude of the change due to the thermal expansion from the volume V_0, however, is small compared to that of the other alkalies and, in all, amounts to only 3% at 300°K. Below 100°K. there is no appreciable change in the Θ_R values. However, at 300°K., the corrected values of the resistance lead by method 4 to a Θ_R of 360°K. in place of 340°K. It was pointed out previously that the observed Θ_D was greater than Θ_R, while theory predicts $\Theta_D < \Theta_R$. The correction to Θ_R does not alter this conclusion.

(ii) *Sodium*

The change of the electrical resistance due to thermal expansion is considerably larger for sodium than for lithium and amounts to some 18% at room temperature. The values of Θ_R computed from the revised resistance data are given in Fig. 1 and differ noticeably from those given in Fig. 7 of (I).

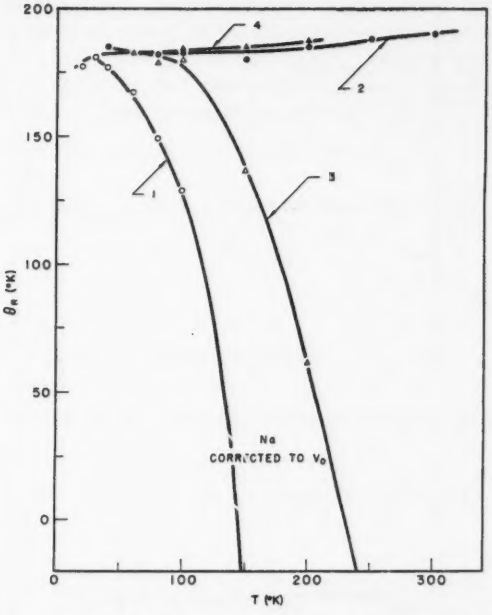

FIG. 1. Θ_R for sodium after allowance for thermal expansion.

Methods 1 and 3 give a Θ_R which falls rapidly and becomes zero at approximately 150° and 250°K. respectively. This is similar to the behavior of Θ_D (see Fig. 8 in (I)). The curves of Θ_R using methods 2 and 4 are computed assuming that Θ_R is constant in the region of 60°K., and give a value of Θ_R which increases slowly with temperature. Thus, Θ_R is about 12% larger than Θ_D in the lower temperature range, but at higher temperature Θ_R increases while Θ_D decreases.

(iii) *Potassium*

Since the electrical resistance of potassium shows anomalies of the type observed in rubidium above 150°K. (cf. MacDonald (10)) and the major change in the resistance due to thermal expansion takes place at temperatures above this, we have not revised the calculations for potassium.

(iv) *Copper*

I am indebted to Dr. T. M. Dauphinee for supplying accurate measurements of the temperature variation of the electrical resistance of copper. The resis-

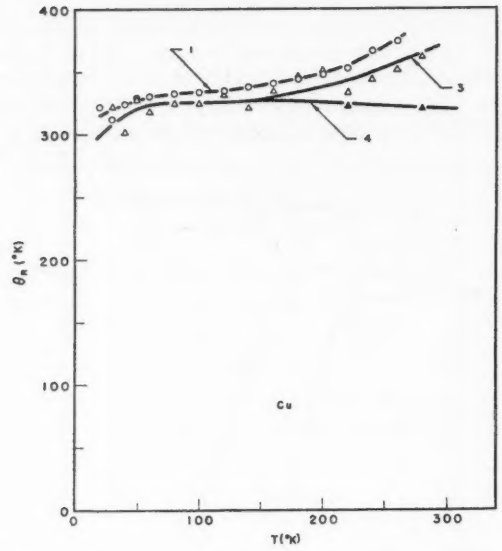

FIG. 2. Θ_R for copper before allowance for thermal expansion.

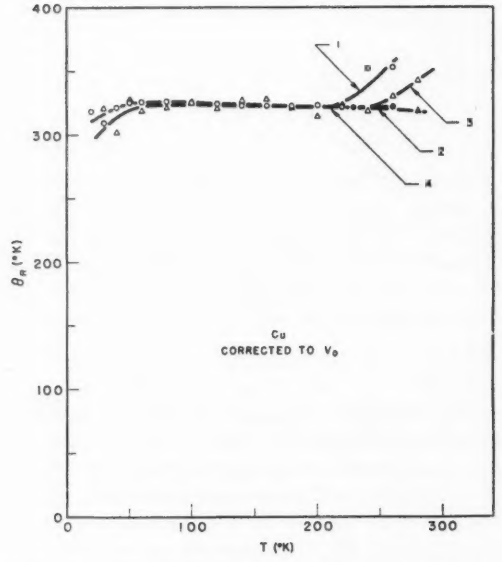

FIG. 3. Θ_R for copper after allowance for thermal expansion.

tance vs. temperature graph shows no anomalies below the ice point. The resistance-rise at higher temperatures is however more rapid than linear with temperature. This behavior is similar to that of sodium mentioned in (I).

Values of Θ_R computed from the measured resistance are given in Fig. 2 while the results of the calculations after an allowance has been made for the change of resistance due to thermal expansion are given in Fig. 3. The allowance for expansion of the metal in the case of copper results in a Θ_R which remains constant over a wider temperature range. The results of methods 2 and 4 are the same suggesting that the electron-lattice interaction parameter κ does remain constant in the temperature interval studied.

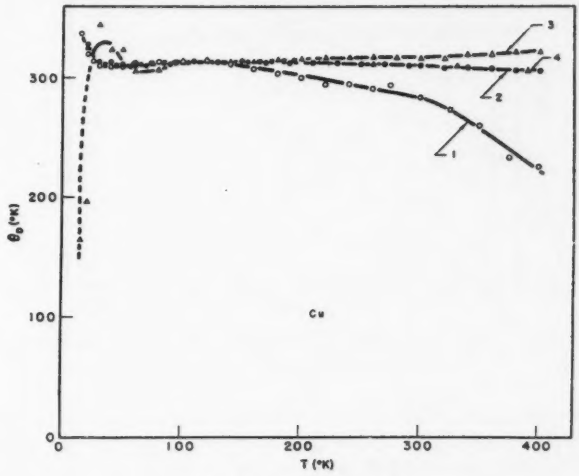

FIG. 4. Θ_D for copper.

The specific heat of copper was taken from the measurements of Mendelssohn and Closs (14), Eucken and Werth (4), Dockerty (2), and Giauque and Meads (6). The variation of Θ_D with temperature is illustrated in Fig. 4. As in the case of the alkalies (see (I)) most of the apparent variation of Θ_D is due to the neglect of terms involving $d\Theta/dT$ in the numerical evaluations. The agreement of Θ_D calculated by methods 2 and 4 indicates that the numerical parameter (assumed to be $3R$) does indeed remain constant (cf. (I)).

The discussion given in (I) shows that the results of method 4 should be best for direct comparison of Θ_R and Θ_D. In the case of copper Θ_R is nearly equal to Θ_D and their temperature variation is similar.

(v) *Silver*

The electrical resistance of a vacuum annealed strip of silver was measured in a bath of isopentane from room temperature down to approximately 130°K., and in our Collins helium cryostat to helium temperature. The ratio $R_{4.0°K.}/R_{237°K.}$ equals 9×10^{-4}.

Values of Θ_R computed from the observed resistance are given in Fig. 5. When allowance is made for the change of resistance due to thermal expansion, methods 1 and 3 show a Θ_R which is approximately constant in the region of 150 to 200°K. as shown in Fig. 6.

Method 4 has been applied on the assumption that $d\Theta/dT$ is zero between 150° and 200°K. The position of the maximum of Θ_R from method 3 is shifted

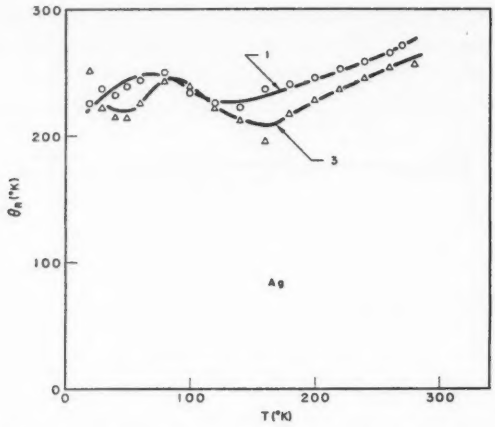

FIG. 5. Θ_R for silver before allowance for thermal expansion.

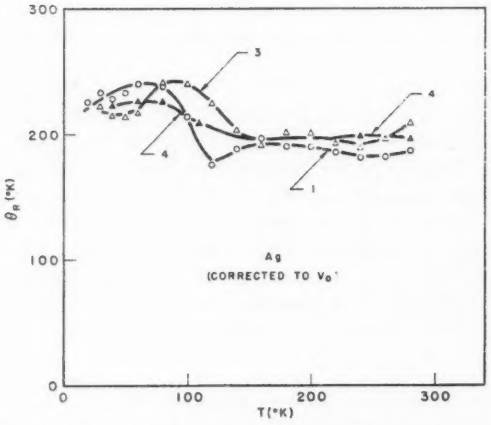

FIG. 6. Θ_R for silver after allowance for thermal expansion.

to approximately 60°K. when method 4 is applied. A similar maximum appeared in Θ_R for lithium (cf. (1)) and was associated with a change in crystal structure. The behavior of Θ_R below 120°K. might possibly suggest that a similar change occurs in silver.

Specific heat data for silver were taken from the work of Keesom and Kok (8), Eucken, Clusius, and Woitinek (3), and Meads, Forsythe, and Giauque (12). The values of Θ_D computed using the four methods are shown in Fig. 7.

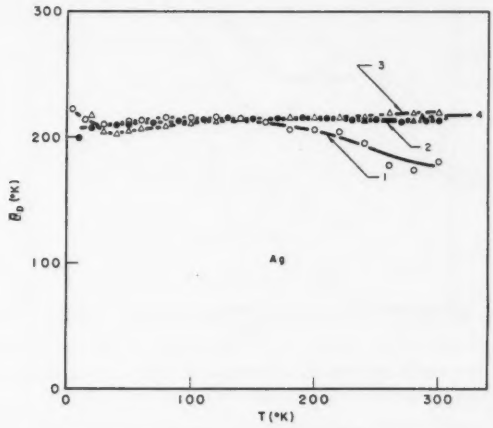

FIG. 7. Θ_D for silver.

A comparison of Figs. 6 and 7 shows that below 80°K. Θ_R is slightly greater than Θ_D. However, at higher temperatures $\Theta_D > \Theta_R$ contrary to the predictions of theory. The maximum in Θ_R is not reflected in Θ_D. This behavior is similar to that of lithium.

(vi) *Gold*

Two specimens of "pure" vacuum annealed gold wire were measured. The specimen with the lower residual resistance (1.8×10^{-2} of the ice point resistance) was used for the calculation.

Fig. 8 shows Θ_R for gold as a function of temperature from the measured resistance. Since Θ_R shows no portion where $d\Theta/dT$ is zero for an extended region, methods 2 and 4 cannot be applied. When an allowance is made for the change of resistance due to thermal expansion of the metal the over-all variation of Θ_R is reduced as shown in Fig. 9.

A maximum in Θ_R occurs below 100°K. and, as in the case of silver, might suggest some change in structure.

The specific heat measurements of Geballe and Giauque (5) were used for the calculations of Θ_D given in Fig. 10. In contrast to Θ_R, Θ_D shows very little variation with temperature. Method 4 was applied assuming that the results

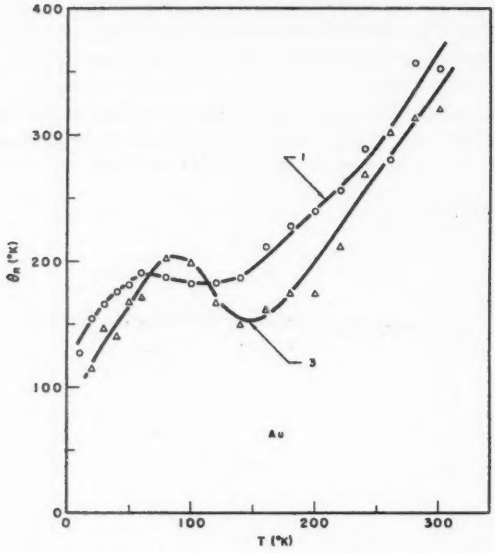

FIG. 8. Θ_R for gold before allowance for thermal expansion.

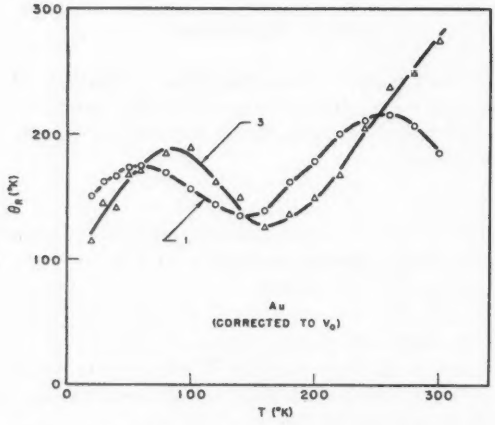

FIG. 9. Θ_R for gold after allowance for thermal expansion.

of method 3 give a constant Θ_D above 200°K., although, in fact, Θ_D from method 3 is increasing slowly throughout the range of temperature.

Since method 4 could not be applied to Θ_R no accurate comparison can be made between Θ_D and Θ_R. However, it appears that Θ_D is equal to or slightly greater than Θ_R except at temperatures above 300°K.

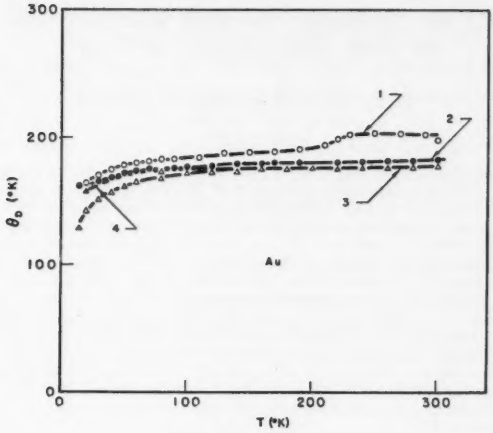

FIG. 10. Θ_D for gold.

IV. SUMMARY

For the highly compressible alkali metals the values of Θ_R calculated by methods 1 and 3 are significantly altered if an allowance is made for the variation of electrical resistance with thermal expansion. However, none of the conclusions given in (I) is changed. The values of Θ_R for copper, silver, and gold, computed after an allowance has been made for thermal expansion, are more nearly constant than those obtained directly from the measured values of the electrical resistance. For these three metals it turns out that Θ_R is equal to or somewhat less than Θ_D contrary to the predictions of theory.

ACKNOWLEDGMENTS

The author thanks Dr. D. K. C. MacDonald for many helpful suggestions and discussions which have been incorporated in this paper, and Dr. J. S. Dugdale for reading the manuscript.

REFERENCES

1. BRIDGMAN P. W. The physics of high pressures. Bell & Sons, Ltd., London. 1949.
2. DOCKERTY, S. M. Can. J. Research, 9: 84. 1933.
3. EUCKEN, A., CLUSIUS, K., and WOITINEK, H. Z. anorg. u. allgem. Chem. 202: 39. 1931–32.
4. EUCKEN, A. and WERTH, H. Z. anorg. u. allgem. Chem. 188: 152. 1930.
5. GEBALLE, T. H. and GIAUQUE, W. F. J. Am. Chem. Soc. 74: 2368. 1952.
6. GIAUQUE, W. F. and MEADS, P. F. J. Am. Chem. Soc. 63: 1897. 1941.
7. GRÜNEISEN, E. Handb. Physik, 10: 1. 1926.
8. KEESOM, W. H. and KOK, J. A. Physica, 1: 770. 1934.
9. KELLY, F. M. and MACDONALD, D. K. C. Can. J. Phys. 31: 147. 1953.
10. MACDONALD, D. K. C. Phil. Mag. 43: 479. 1952.
11. MACDONALD, D. K. C. and PEARSON, W. B. Proc. Roy. Soc. (London), A, 219: 373. 1953.
12. MEADS, P. F., FORSYTHE W. R., and GIAUQUE, W. F. J. Am. Chem. Soc. 63: 1902. 1941.
13. MEIXNER, J. Ann. Physik, 38: 609. 1940.
14. MENDELSSOHN, K. and CLOSS, J. O. Z. physik. Chem. B, 19: 291. 1932.
15. MOTT, N. F. and JONES, H. The theory of the properties of metals and alloys. Oxford University Press, London. 1936.

THE EFFECT OF SUNRISE ON THE REFLECTION HEIGHT OF LOW FREQUENCY WAVES[1]

By S. B. Brown[2] and W. Petrie[3]

ABSTRACT

It has been found that when radio waves of frequency 16 kc./s. and somewhat higher are transmitted over distances of 540 km., the phase and amplitude of the received signal change suddenly about one hour before ground sunrise at the mid-point of the transmission path. This effect results from a lowering of the nighttime reflection height of 95 km. to the daytime value of 70 km.

By considering the geometry of the situation, it is apparent that the process of photo-ionization of atmospheric molecules cannot produce the observed effect since the relevant wave lengths are absorbed before reaching the 95 km. height. On the other hand, electrons may be removed from negative oxygen ions by visible and near infrared radiation which does reach the 95 km. level prior to sunrise. The problem is then to determine the intensities of the relevant wave lengths at the 95 km. level, and to compute the rate at which electrons are released from negative ions. It is shown that the pre-sunrise effect at 95 km. is readily explained as a negative ion phenomenon, and the rate of fall of reflection height is discussed.

INTRODUCTION

It has been found that when radio waves of frequencies 16 kc./s. and somewhat higher are transmitted over distances of between 500 and 900 km., both the phase and amplitude of the received signal change suddenly about one hour before ground sunrise when the sun's zenith distance at the mid-point of the transmission path is near 98° (1, 4). It can be shown that for this position of the sun a solar ray which is incident on the 95 km. level (the nighttime reflection height) is tangent to the surface of a sphere about 35 km. above the earth's surface. The geometry of the situation is illustrated in Fig. 1, T and R being the positions of transmitter and receiver.

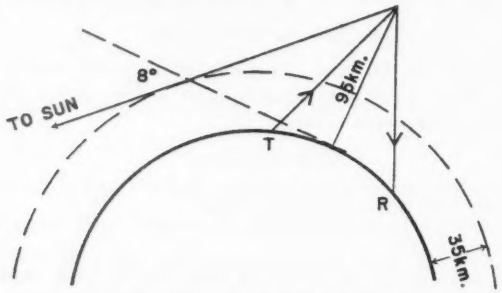

Fig. 1. Sunrise in the ionosphere.

The interpretation of the phase change before sunrise is that the reflection height is being lowered from the nighttime value of 95 km. (1). It is apparent

[1] *Manuscript received September 28, 1953.*
Contribution from Defence Research Telecommunications Establishment, Radio Physics Laboratory, Defence Research Board, Ottawa, Ont.
Research performed under Defence Research Board Project No. D48-95-11-17.
[2] *Queen's University, Kingston, Ont.*
[3] *Defence Research Telecommunications Establishment, Radio Physics Laboratory.*

as will be shown later that photoionization of atoms and molecules will be negligible at the time concerned, and other processes which can produce electrons must be examined. It has been suggested, apparently first by Ratcliffe and later by others, that the pre-sunrise effect is due to the release of electrons from negative ions. In what follows this problem will be examined. It is necessary to determine the number of particles along the solar ray path to the 95 km. level, the residual intensity of the radiation in the relevant wave-length range after it has traversed the same path, and the rate of release of electrons from negative ions.

THE NUMBER OF PARTICLES ALONG THE PATH CONCERNED

There is considerable uncertainty as to the particle density distribution in the earth's upper atmosphere. Possibly the best approach is to adopt the values suggested by the "Rocket Panel" (10). The total number of particles along the path through the atmosphere may be expressed as,

$$N = 10^5 \int_P^\infty n \, dy, \qquad [1]$$

where n is the number of particles /cm.^{3}; dy is in km.; P is one end of the path at the 95 km. level and ∞ is the end of the path towards the sun. One may substitute for n an expression which gives the variation of particle density with height. According to Nicolet (9)

$$n_0 = n^* \left(\frac{H_0}{H^*} \right)^{-(1+\beta)/\beta} \qquad [2]$$

and

$$H_0 = H^* + \beta Z \qquad [3]$$

where n^* and n_0 are the particle densities at some reference level and at a height Z above this level respectively, H^* and H_0 are the scale heights at the reference level and distance Z above the reference level respectively, and β is the scale height gradient. The path with which we are concerned penetrates the atmosphere to the 35 km. level and proceeds upwards to a height of 95 km. Taking the former height as the reference level, computing H^*, H_0, and β from the rocket data, and combining equations 1 to 3, one may integrate the resulting equation to give N. It is necessary to divide the path into segments, such that in each segment β is approximately constant. From the computed β values it appeared that five segments and hence five integrals were required. The value of N is of the order of 4.6×10^{24} in a 1 cm.^{2} column along the path. The same method of computation has been used and outlined in some detail by Lindquist (6). As a check on the value of N, the path was divided into a number of small segments and the total number of particles obtained by addition.

THE INTENSITY OF SOLAR RADIATION AT THE PRE-SUNRISE REFLECTION HEIGHT

We need to know the number of solar quanta in a certain wave-length interval incident on the earth's atmosphere, and to determine the residual intensity in this same interval after the radiation has passed along the path

we are considering and has reached the reflection level of 95 km. From Planck's law it can be shown that the number of solar quanta in the frequency interval ν_1 to ν_2 entering 1 cm.^{2} of the earth's atmosphere per second is

$$[4] \qquad N_q = \frac{2\pi}{c^2}\frac{r^2}{R^2}\int_{\nu_1}^{\nu_2}\frac{\nu^2}{(e^{h\nu/kT}-1)}\,d\nu$$

where r and R are the solar radius and the distance from the sun to the earth. This equation has been integrated with $T = 6000°$ K. for quanta of energy between 1 and 4 ev. and with $T = 5000°$ K. for quanta of energy between 4 and 6 ev., the temperature distribution recommended by several authors including Bates and Massey (2). The results of the integration are given in Table I, expressed as the number of quanta/cm.^{2}/sec. in an energy interval of 1 ev. The interval given in the table is chosen, since it includes the wave lengths which are important in the process of the removal of electrons from oxygen negative ions.

TABLE I

SOLAR RADIATION INCIDENT ON THE ATMOSPHERE

Energy range (ev.)	Number of quanta/cm.^{2}/sec./ev.
1–2	2.7×10^{17}
2–3	1.1×10^{17}
3–4	3.2×10^{16}
4–5	1.8×10^{15}
5–6	2.6×10^{14}

The residual intensity of solar radiation at any depth in the atmosphere will be determined by the processes of absorption and scattering. It is apparent that the intensity of the ultraviolet radiation which is responsible for the daytime production of the ionosphere must be negligible after the radiation has traversed the path we are considering. The total number of particles along the path is 4.6×10^{24}, which is equivalent to 1.7 km. of air at N.T.P. This thickness of air reduces the intensity of ultraviolet radiation to near zero, hence the photo-ionization of atoms and molecules need not be considered.

The pre-sunrise effect takes place near 95 km. and the reflection height drops to some 70 km. At the former level the relative importance of atomic and molecular negative ions depends upon the particular atmospheric model chosen. At the 70 km. level the dominating negative ion is formed from molecular oxygen. Although the wave-length interval most effective in removing electrons from oxygen negative ions is somewhat uncertain, it appears to include the range 12000–2000Å (2). However, since practically all radiation below 3000Å is absorbed along the path we are considering, we need not include radiation below this wave length. In the relevant wave-length interval there are no continuous absorption regions such as are found at shorter wave lengths owing to the processes of dissociation and ionization. There are discrete absorption bands of oxygen, water vapor, and ozone, but by applying Beer's law and using data on the total numbers of the above particles and the ab-

sorption coefficients, it can readily be shown that these bands have negligible effect.

We must also consider the weakening of the radiation due to Rayleigh scattering. When the scattering back into the beam is neglected, the intensity of the radiation at the end of the path in question will be

[5] $$I = I_0 e^{-\beta l}$$

where β is the scattering coefficient. As we have indicated above the value of l is of the order of 1.7×10^5 cm. Using β values as given by Van de Hulst (11), I/I_0 may be calculated as a function of wave length. The results are given in Table II.

TABLE II

RAYLEIGH SCATTERING FACTORS

Wave length (Å)	β	I/I_0
3000	14.8×10^{-7}	0.78
4000	4.4×10^{-7}	0.93
5000	1.7×10^{-7}	0.97
6000	0.8×10^{-7}	0.99
7000	0.4×10^{-7}	0.99

ELECTRON DENSITIES AT NIGHT

In order to solve this problem, data are required on the rates at which several processes proceed including attachment, detachment, and recombination. The attachment rate/electron/cm.^{3}/sec. to oxygen molecules is

[6] $$\alpha_3 n(O_2).$$

The value of the attachment coefficient α_2 is not known with certainty, but we will adopt the figure of 1.4×10^{-15} cm.^{3}/sec. given by Biondi (3). $n(O_2)$ is the number density of oxygen molecules. Following the notation of Bates and Massey (2), the rate of photodetachment/negative ion/cm.^{3}/sec. is

[7] $$\sum_{\epsilon=1}^{\infty} I_\epsilon A_\epsilon.$$

I_ϵ is the number of incident quanta of energy ϵ/cm.^{2}/sec., and A_ϵ the cross section for quanta of energy ϵ. It is convenient to divide the relevant energy range into intervals of 1 ev. as has been done in Table I. If we adopt the minimum values of A_ϵ as given by Bates and Massey (2), and the number of incident quanta from Tables I and II, the rate of photodetachment is of the order of 0.0175/cm.^{3}/sec. There are few experimental data on electron and negative ion densities at 95 and 70 km. prior to the pre-sunrise effect, hence we must attempt to calculate the values. The rate of change of electron and negative ion densities at night may be expressed by the following equations,

[8] $$\frac{dn_e}{dt} = \text{N.I.} + \alpha_1 n(O_2^-)\, n(A) + \alpha_2 n(O^-)\, n(B) - \alpha_3 n(O_2)\, n_e - \alpha_4 n(O)\, n_e - \alpha_5 n(C^+) n_e,$$

$$[9] \qquad \frac{dn(O_2^-)}{dt} = \alpha_3 n(O_2)\, n_e - \alpha_1 n(O_2^-)\, n(A) - \alpha_6 n(O_2^-)\, n(D^+),$$

$$[10] \qquad \frac{dn(O^-)}{dt} = \alpha_4 n(O)\, n_e - \alpha_2 n(O^-)\, n(B) - \alpha_7 n(O^-)\, n(E^+).$$

N.I. is the nocturnal ionization rate, the α values are the rate coefficients of the various processes, and the n values the densities of the relevant particles. Since the particles involved in the processes of recombination and collisional removal of electrons from negative ions are not known with certainty, we have called these particles A, B, D^+, and E^+. The total density of positive ions is $n(C^+)$. In equation [8] the second and third terms are the rates of removal of electrons from negative ions by collision, the remaining terms the electron attachment and recombination rates. In [9] and [10] the terms are the rates of attachment, detachment, and recombination. Adding the three equations we have

$$[11] \quad \frac{dn_e}{dt} + \frac{d}{dt}[n(O_2^-) + n(O^-)] = \text{N.I.} - [\alpha_5 n(C^+)\, n_e + \alpha_6 n(O_2^-)\, n(D^+) + \alpha_7 n(O^-)\, n(E^+)].$$

In view of the lack of concrete information on the distribution of O and O_2 and consequently of O^- and O_2^- in the height range concerned, the second term on the left side of [11] may be replaced by $d[n^-]/dt$ where n^- is the total concentration of negative ions. In what follows we assume that all the negative ions are molecular, and although this assumption will be a poor one if the atmospheric model of Moses and Wu (8) is correct, the error will not invalidate the type of analysis used or the conclusions reached. On the right side of [11] the last two terms are replaced by a single term, $\alpha n^-\, n(C^+)$, which is equivalent to the effective recombination rate of negative ions. Furthermore, on replacing n^- by λn_e where λ is the ratio of negative ion and electron densities, and $n(C^+)$ by $(n_e + n^-)$, we find

$$[12] \qquad \frac{dn_e}{dt} = \frac{\text{N.I.}}{1+\lambda} - (\alpha_5 + \lambda\alpha) n_e^2.$$

Integration with constant N.I. and λ values yields the following equation,

$$[13] \qquad n_e = \left(\frac{Q}{P}\right)^{\frac{1}{2}} \left[\frac{e^{2(PQ)^{1/2}(t+c)} - 1}{e^{2(PQ)^{1/2}(t+c)} + 1}\right],$$

where $Q = \text{N.I.}/(\lambda + 1)$, $P = (\alpha_5 + \lambda\alpha)$, and c is a constant of integration. The constant c may be determined by inserting the daytime value of n_e and a time $t = 0$. It turns out that for reasonable values of Q and P the constant may be neglected if we are concerned with the nighttime value of n_e when t will be large. In fact for large t equation [13] becomes

$$[14] \qquad n_e = \left[\frac{\text{N.I.}}{(\lambda+1)(\alpha_5 + \lambda\alpha)}\right]^{\frac{1}{2}}.$$

In order to evaluate this equation we need information on nighttime ionization rates and values of λ. An expression for the latter value may be obtained from

equation [9] or [10]. When a state of equilibrium is reached, i.e., when negative ions are formed and destroyed at the same rate, we have

$$\lambda = \frac{n(O_2)\,\alpha_3}{n(A)\,\alpha_1 + n_e\alpha_6(1+\lambda)}. \qquad [15]$$

Bates and Massey (2) have discussed the collisional processes which can remove electrons from negative ions. Using their data, it appears that the nighttime values of λ at 95 and 70 km. are of the order of 1 and 35. More recently Mitra and Jones (7) have examined the problem of the nighttime value of λ and have summarized the available data. The λ values given above are comparable to those suggested by Mitra and Jones.

There is little concrete information on nighttime ionization rates, and since the value of λ is also subject to some uncertainty, equation [14] has been evaluated over a range of values of N.I. and λ. An α value of 10^{-6} cm.^{3}/sec. has been used, and α_6 the electronic recombination coefficient neglected. The results are given in Table III.

TABLE III

NIGHTTIME ELECTRON DENSITIES

N.I.	$\lambda = 0.1$	$\lambda = 1$	$\lambda = 10$	$\lambda = 20$	$\lambda = 30$	$\lambda = 40$	$\lambda = 50$
5	6740	1580	213	112	75	56	45
10	9530	2240	301	158	105	79	63
15	11660	2740	368	194	129	97	78
20	13440	3160	425	224	149	112	89
25	15070	3530	477	250	166	125	100

THE PRE-SUNRISE EFFECT ON 16 KC./S. WAVES

According to Budden (5) the electron density required to reflect 16 kc./s. waves over distances in the range 400 to 4000 km. is between 135 and 400/cm.^{3}; on the other hand a somewhat higher electron density is needed to reflect waves sent up at vertical incidence. Since 16 kc./s. waves transmitted over long distances are reflected at night from a height of some 95 km., we can say that the lower limit to the electron density at this height is within the range of values given by Budden (5), and that the electron density falls to less than these values a short distance below 95 km. Referring to Table III, it is noticed that with $\lambda = 1$, a reasonable value for the height of 95 km., an electron density sufficient to reflect 16 kc/s. waves may be maintained with a relatively low nighttime ionization rate.

If the pre-sunrise effect is due to the release of electrons from negative ions, the change in electron density will be given by equation [8] with an added term to account for the photodetachment process. Then,

$$dn_e/dt = \text{N.I.} + \alpha_1 n^- n(A) + \rho n^- - \alpha_3 n(O_2) n_e. \qquad [16]$$

In this equation ρ is the detachment rate per negative ion. It has been assumed that the dominating negative ion is molecular, and electronic recombination which is a relatively slow process has been neglected. Now the sum of the

numbers of electrons and negative ions must equal the number of positive ions, and if we consider a sufficiently small interval of time during which the ionization will remain constant, then

[17] $$n^- = n^+ - n_e.$$

Substituting this in the previous equation gives

[18] $$dn_e/dt = \text{N.I.} - [\alpha_1 n(\text{A}) + \rho + \alpha_3 n(\text{O}_2)]\, n_e + n^+ \alpha_1 n(\text{A}) + \rho n^+.$$

This is of the form

[19] $$dn_e/dt + Pn_e = Q.$$

The solution is

[20] $$n_e = \frac{Q}{P} + \left(n_0 - \frac{Q}{P}\right) e^{-Pt}.$$

At time $t = 0$ the constant of integration n_0 is equal to n_e. Hence n_0 may be assigned a reasonable value from Table III. As an example, suppose that the electron density necessary to reflect 16 kc./s. waves is 200/cm.^{3} If $\lambda = 30$ at 70 km. and the nighttime ionization rate is 15/cm.^{3}/sec., then from Table III n_e is 129/cm.^{3} and hence n^+ is of the order of 4000/cm.^{3} Substituting these figures in [20] along with the value of ρ calculated previously and reasonable values of the other quantities, it can be shown that the electron density would rise to 200/cm.^{3} with the resulting reflection of 16 kc./s. waves in a small time of the order of one second. This will be so with any reasonable range of values of the relevant parameters.

There is no difficulty then in explaining the lowering of reflection height as the result of the release of electrons from negative ions. However, we must also consider the rate of lowering. It is apparent from the geometry of the situation that when the pre-sunrise effect commences, a ray which is incident on the 70 km. level has passed through a considerable thickness of atmosphere, and the value of ρ for this ray will be less than the figure we have used in referring to a ray which is incident on the 95 km. level. By adding up the particles along the path of the former ray it appears that the path length is of the order of 156 km. of air at N.T.P. If we substitute this path length and the appropriate Rayleigh scattering coefficients in Beer's law, it can be seen that the intensity of all wave lengths shorter than about 4960Å is effectively reduced to zero. Under these circumstances the value of ρ is much reduced and is in fact of the order of 0.0016.

As a result of the foregoing, we can say that when the value of ρ at 95 km. is 0.0175 and electrons are being rapidly released from negative ions, ρ is much smaller and electrons are being removed from negative ions more slowly at the 70 km. level. We need to know what time elapses before the value of ρ at 70 km. increases to 0.0175, since under these circumstances as we have seen, the process of electron release is rapid. It can be shown from simple geometry that the zenith distance of the sun must decrease by approximately 2.5° before the ray which is incident on the 70 km. level is tangent to a sphere 35 km. above the ground. Since the zenith distance of the sun changes by

about 8° per hour (1) at the location where the sunrise experiments were performed, the time delay involved is some nineteen minutes. Hence, since this is evidently the maximum period during which ρ can vary appreciably, it does not seem that the fall of reflection height during the period of one hour is entirely due to the effect discussed above.

In the foregoing analysis, it was assumed that the total ionization remained constant during the period of the sunrise effect. This may not be a sufficiently accurate approximation. For example, if the nighttime negative and positive ion densities at 70 km. are of the order of 4×10^3/cm.^{3} and the recombination coefficient some 10^{-6} cm.^{3}/sec., then the recombination rate is 16/cm.^{3} sec., which could more than offset the ionization rate with a resulting decrease in total ionization. This would have the effect of reducing the rate at which the electron density builds up owing to the release of these particles from negative ions.

One may attempt to find a suitable empirical equation which gives the required variation of electron density. Such an equation appears to be

$$[21] \qquad n_e = A - \frac{B}{(t + t_0)^P}$$

where A, B, t_0, and P are constants. Then,

$$[22] \qquad \frac{dn_e}{dt} = \frac{BP}{(t + t_0)^{P+1}} = \text{N.I.} + \rho n^- - \alpha_3 n(\text{O}_2)\, n_e.$$

We have neglected the term which expresses the rate of collisional removal of electrons from negative ions. Solving for the term ρn^- and replacing n^- by $(n^+ - n_e)$, we find

$$[23] \quad n^+ = \frac{1}{\rho}\left\{\frac{B}{(t + t_0)^P}\left[\frac{P}{t + t_0} - \alpha_3 n(\text{O}_2) - \rho\right] - \text{N.I.} + A\alpha_3 n(\text{O}_2) + A\rho\right\}.$$

If we consider the 70 km. level at the time $t = 0$, and take the electron and positive ion densities from Table III to be of the order of 130 and 4000/cm.^{3}, and say that n_e must reach a limiting value of 200/cm.^{3} in a period of one hour, then equation [23] yields a relationship between P and t_0 for some assumption regarding the final value of n^+. If this relationship is substituted in [21] along with the limiting values of the electron density at $t = 0$ and $t = \infty$, then it can be shown that n_e will vary appreciably over a period of one hour.

It seems likely that the slow rate of fall of reflection height from 95 to 70 km. is the result of at least two effects, one being a variable ρ factor as the zenith distance of the sun decreases, the other a reduction of total ionization during the one-hour period of the pre-sunrise phenomenon.

REMARKS ON OTHER SUNRISE EFFECTS

We have discussed the sunrise effect on waves of frequency 16 kc./s. propagated over long distances. When these same waves are transmitted at vertical incidence the amplitude begins to decrease one hour before ground sunrise, while the reflection height does not drop until some ten minutes after ground

sunrise (1). The explanation is likely as follows. The electron density produced at ground sunrise by the release of electrons from negative ions is not sufficient to reflect 16 kc./s. waves transmitted at vertical incidence, hence reflection does not take place until after sunrise. However, the number of electrons produced is sufficient to increase the absorption and the wave is returned with reduced amplitude.

Weekes and Stuart (12) have investigated sunrise phenomena on waves near a frequency of 100 kc./s. at both vertical and oblique incidence. The results are generally the same as those observed at the lower frequency of 16 kc./s., with apparently one difference. When the higher frequency wave is transmitted at vertical incidence, the amplitude decreases and the reflection height remains constant during the one hour before ground sunrise. For one hour after ground sunrise the height of reflection falls some 8 km.; and in this period the amplitude remains nearly constant. A possible explanation follows. As we have indicated, while electrons are being released from negative ions at a certain level and the electron density is building up, the amplitude of a passing wave will be reduced even if reflection takes place at some distance above this level. However, once this process operates at a constant rate which may occur near ground sunrise, presumably the electron density can decrease again owing to recombination. This effect alone would increase the amplitude of the returned signal, but if at the same time the reflection height is dropping and the amplitude decreasing, the combined effects may result in a nearly constant amplitude.

CONCLUDING REMARKS

From the foregoing discussion it appears that the sunrise effects on the reflection of low frequency waves can be explained in terms of the release of electrons from negative ions. Although there are uncertainties in the analysis, these are likely due to lack of concrete information on nighttime ionization values and the rates of certain reactions.

ACKNOWLEDGMENTS

The authors wish to thank Dr. T. W. Straker for his helpful remarks regarding details of the pre-sunrise radio observations.

REFERENCES

1. Bain, W. C., Bracewell, R. N., Straker, T. W., and Westcott, C. H. Proc. Inst. Elec. Engrs. (London), Pt. 4, 99: 1. 1952.
2. Bates, D. R. and Massey, H. S. W. J. Atm. and Terrest. Phys. 2: 1. 1951.
3. Biondi, M. A. Phys. Rev. 84: 1072. 1951.
4. Bracewell, R. N., Budden, K. G., Ratcliffe, J. A., Straker, T. W., and Weekes, K. Proc. Inst. Elec. Engrs. (London), Pt. 3, 98: 221. 1951.
5. Budden, K. G. Phil. Mag. 44: 504. 1953.
6. Lindquist, R. J. Geophys. Research, 57: 439. 1952.
7. Mitra, A. P. and Jones, R. E. Scientific Report No. 44, Contract No. AF 19 (122)-144. Penn. State College. 1953.
8. Moses, H. E. and Wu, Ta-You. Phys. Rev. 87: 627. 1952.
9. Nicolet, M. and Bossy, L. Ann. géophys. 5: 275. 1949.
10. Rocket Panel. Phys. Rev. 88: 1027. 1952.
11. Van de Hulst, H. C. *In* The atmospheres of the earth and planets. *Edited by* G. P. Kuiper. University of Chicago Press, Chicago. 1949. p. 49.
12. Weekes, K. and Stuart, R. D. Proc. Inst. Elec. Engrs. (London), Pt. 4, 99: 29, 38. 1952.

LETTERS TO THE EDITOR

Under this heading brief reports of important discoveries in physics may be published. These reports should not exceed 600 words and, for any issue, should be submitted not later than six weeks previous to the first day of the month of issue. No proof will be sent to the authors.

The Effect of a Steady Transverse Electric Field on the Viscosity of Polar Liquid Dielectrics

It is well established that the viscosity of a polar organic liquid which conducts appreciably may apparently be increased by the application of a steady electric field across the channel in which the liquid flows. Andrade and Dodd (1) suggested that this increase is caused by an effective reduction in channel depth resulting from the formation of concentrations of polar molecules around ions in the vicinity of the conducting walls of the channel.

Whitehead (3) ascribed an electrical effect to a similar cause; he showed that the direct current between two electrodes immersed in stationary transformer oil decreases over a period of about one hour to a steady low value. There is independent evidence to show that the electric field intensity within the liquid becomes nonlinear as space charges build up, with a corresponding reduction in electric current (2).

It has now been found that the fall in current occurs at the same rate when the liquid is flowing between the electrodes as when it is stationary. As the current falls, the viscosity (which increases when the field is applied) returns to normal; the general nature of the rate of fall of viscosity is similar to that of the current decrease, though the two curves are of appreciably different shape. At the lowest current value, the viscosity has the same value as that which it had before the field was applied.

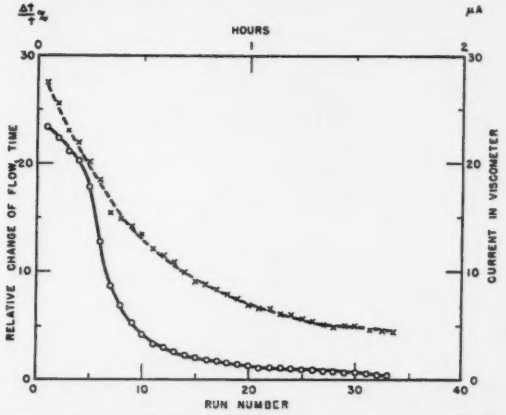

FIG. 1. Change of viscosity (full line) of amyl acetate with time for a direct potential of 600 v. across the channel of 0.1 mm. Successive runs are at three-minute intervals. The current is indicated by the dashed line.

These facts are illustrated in the figure, which is a record of the change in the relative time of flow of a succession of runs with amyl acetate taken in a capillary viscometer of the same general description as that used by Andrade and Dodd.

At the final asymptotic values, the removal of the field for an interval of about three minutes (while a viscosity measurement is made) results in no significant change in either viscosity or current when the same field is reapplied.

These experimental results are some evidence that the space charges, if indeed they exist, accumulate much closer to the conducting walls of the channel than has been suggested by other workers. In the present case, measurements on the rate of flow indicate that if these ionic layers exist, they have a mean depth of less than 0.1 μ at each wall, and they are not removed by motion of the liquid. It also appears that the apparent increase in viscosity is strictly a function of the electric current, and can not be a spurious effect caused by the presence of space charges.

Corroboration for this point of view was obtained by modifying Andrade and Dodd's experiments. With the application of steady fields of different intensities, the viscosity increase rises approximately linearly with the intensity of the applied field, to a saturation value at about 20 kv. cm.$^{-1}$, and above that value there is no further increase in viscosity; this confirms the results of Andrade and Dodd. There is, of course, the time-dependent decrease at these saturation fields. When a square wave form of 1 c.p.s. is substituted for the steady field, however, the viscosity increase continues to rise linearly with the intensity of the applied electric field up to a value of 75 kv. cm.$^{-1}$ for a channel depth of 0.1 mm. This behavior is inconsistent with the theory of a reduction in the effective channel depth, which would lead to saturation effects at frequencies up to a few hundred cycles per second.

It is hoped to carry out further experiments to investigate the mechanism of the viscosity increase.

1. ANDRADE, E. N. DA C. and DODD, C. Proc. Roy. Soc. (London), A, 187: 296. 1946.
2. GEMANT, A. Elektrotech. Z. 54: 108. 1933.
3. WHITEHEAD, J. B. Trans. Am. Inst. Elec. Engrs. 50: 692. 1931.

RECEIVED NOVEMBER 5, 1953.

JOHN HART*

*Formerly at the Davy Faraday Laboratory of the Royal Institution of Great Britain; now at the Division of Physics, National Research Council, Ottawa, Canada.

CANADIAN JOURNAL OF PHYSICS

Notes to Contributors

Manuscripts

(i) ***General.*** Manuscripts should be typewritten, double spaced, on paper 8½×11 in. **The original and one copy are to be submitted.** Tables (each typed on a separate sheet) and captions for the figures should be placed at the end of the manuscript. Every sheet of the manuscript should be numbered.

Style, arrangement, spelling, and abbreviations should conform to the usage of this journal. Names of all simple compounds, rather than their formulas, should be used in the text. Greek letters or unusual signs should be written plainly or explained by marginal notes. Superscripts and subscripts must be legible and carefully placed.

Manuscripts should be carefully checked before they are submitted; authors will be charged for changes made in the proof that are considered excessive.

(ii) ***Abstract.*** An abstract of not more than about 200 words, indicating the scope of the work and the principal findings, is required, except in Notes.

(iii) ***References.*** References should be listed **alphabetically by authors' names,** numbered, and typed after the text. The form of the citations should be that used in this journal; in references to papers in periodicals, titles should not be given and only initial page numbers are required. All citations should be checked with the original articles and each one referred to in the text by the key number.

(iv) ***Tables.*** Tables should be numbered in roman numerals and each table referred to in the text. Titles should always be given but should be brief; column headings should be brief and descriptive matter in the tables confined to a minimum. Numerous small tables should be avoided.

Illustrations

(i) ***General.*** All figures (including each figure of the plates) should be numbered consecutively from 1 up, in arabic numerals, and each figure referred to in the text. The author's name, title of the paper, and figure number should be written in the lower left corner of the sheets on which the illustrations appear. Captions should not be written on the illustrations (see Manuscript (i)).

(ii) ***Line Drawings.*** Drawings should be carefully made with India ink on white drawing paper, blue tracing linen, or co-ordinate paper ruled in blue only; any co-ordinate lines that are to appear in the reproduction should be ruled in black ink. Paper ruled in green, yellow, or red should not be used unless it is desired to have all the co-ordinate lines show. All lines should be of sufficient thickness to reproduce well. Decimal points, periods, and stippled dots should be solid black circles large enough to be reduced if necessary. Letters and numerals should be neatly made, preferably with a stencil (**do NOT use typewriting**), and be of such size that the smallest lettering will be not less than 1 mm. high when reproduced in a cut 3 in. wide.

Many drawings are made too large; originals should not be more than 2 or 3 times the size of the desired reproduction. In large drawings or groups of drawings the ratio of height to width should conform to that of a journal page but the height should be adjusted to make allowance for the caption.

The original drawings and one set of clear copies (e.g. small photographs) are to be submitted.

(iii) ***Photographs.*** Prints should be made on glossy paper, with strong contrasts. They should be trimmed so that essential features only are shown and mounted carefully, with rubber cement, on white cardboard.

As many photographs as possible should be mounted together (with a **very** small space between each photo) to reduce the number of cuts required. Full use of the space available should be made and the ratio of height to width should correspond to that of a journal page; however, allowance must be made for the captions. Photographs or groups of photographs should not be more than 2 or 3 times the size of the desired reproduction.

Photographs are to be submitted in duplicate; if they are to be reproduced in groups one set should be mounted, the duplicate set unmounted.

Reprints

A total of 50 reprints of each paper, without covers, are supplied free. Additional reprints, with or without covers, may be purchased.

Charges for reprints are based on the number of printed pages, which may be calculated approximately by multiplying by 0.6 the number of manuscript pages (double-spaced typewritten sheets, 8½ × 11 in.) and making allowance for illustrations (not inserts). The cost per page is given on the reprint requisition which accompanies the galley.

Any reprints required in addition to those requested on the author's reprint requisition form must be ordered officially as soon as the paper has been accepted for publication.

Contents

Page

Clausius-Mosotti Equation for Certain Types of Anisotropic Crystals—*H. E. J. Neugebauer* - - - - - - - - - - - - 1

Spectrum of the AlC Molecule—*P. B. Zeeman* - - - - - - - - 9

Birefringence in Crystals and in the Ionosphere—*C. H. M. Turner* 16

Coincidence Studies of the Decay of Indium 114—*M. W. Johns, C. C. McMullen, R. J. Donnelly, and S. V. Nablo* - - - - 35

Photoneutron Cross Sections of Some Elements—*J. Goldemberg and Leon Katz* - - - - - - - - - - - - - - - - - - 49

Electron Capture by Slow Singly Charged Helium Ions in Helium—*J. David Jackson* - - - - - - - - - - - - - - - - 60

An Atomic Mass Study of Nuclear Shell Structure in the Region $82 < n < 126$—*Benjamin G. Hogg and Henry E. Duckworth* - 65

On Inverting Laplace Transforms of the Form $h(s)/(p(s) + q(s)e^{-\tau s})$ —*T. E. Hull and W. A. Wolfe* - - - - - - - - - - - - - 72

On Θ Values in Metals. II—*F. M. Kelly* - - - - - - - - - - 81

The Effect of Sunrise on the Reflection Height of Low Frequency Waves—*S. B. Brown and W. Petrie* - - - - - - - - - - 90

Letter to the Editor:

The Effect of a Steady Transverse Electric Field on the Viscosity of Polar Liquid Dielectrics—*John Hart* - - - - - - 99

Printed in Canada *by* University of Toronto Press